THE DEVELOPMENT OF COSMIC RAY SHOWERS (10^{15}-10^{17}eV)

By

GREGORY J. THORNTON, B.Sc.(Hons)

A thesis
presented for the degree of
DOCTOR OF PHILOSOPHY
at the
UNIVERSITY OF ADELAIDE
(Department of Physics)

June, 1984

To my long-suffering parents.

CONTENTS

SUMMARY

Cosmic rays with energies above 10^{14}eV have only been studied indirectly via the cascades (extensive air showers) they initiate in the atmosphere. The astrophysical interpretation of high energy cosmic rays is hampered by the subsequent lack of knowledge of the composition of the primary beam. The way in which the showers develop should provide some insight into the primary composition, although the unknown nature of particle interactions at such energies complicates the interpretation.

This thesis describes an experiment to determine a shower development parameter, the depth of maximum, from the width of the Cerenkov light pulse produced by the extensive air shower. The data and the conversion from pulse width to depth of maximum are examined for sources of error or bias. Possible interpretations of the results are considered, mainly from a primary composition viewpoint but also with reference to possible changes in the nature of the particle interactions.

The experimental data are also used to examine a technique of determining the shower size from the measurements of a single Cerenkov light pulse. The possible extension of the technique to provide a large collecting area for showers with $E_p \sim 10^{19}$eV is briefly considered.

This thesis contains neither material which has been accepted for the award of any other degree or diploma, nor, to the best of the author's knowledge and belief, any material previously published or written by any other person, except where due reference is made.

Signed:

G.J. Thornton

Adelaide

June, 1984

ACKNOWLEDGEMENTS

I would like to thank my supervisor, Dr. Roger Clay, for his help, guidance, enthusiasm and his uncharacteristic patience. I also thank Professor J.R. Prescott for his overall support of my work and for some useful discussions.

I wish to express my gratitude to Don McDonald who, as a prior and contemporary user of the transient digitizer, had the recording system working before I started. The contributions of Dr. John Patterson and Peter Gerhardy, who were responsible for the particle system and its data analysis, are also acknowledged, as is Dr. Alan Gregory's general interest in the interpretation of Cerenkov pulse widths.

I am grateful to Phil Crouch, Jim Kuhlmann, Dave Liebing, Bruce Dawson and Steve Gibson for their friendship and support and for all the little things they have done to help me over the years.

Finally, I thank Pattie Owen for typing this thesis and Jack Szeszycki for preparing the diagrams.

CHAPTER ONE

COSMIC RAYS

1.1 INTRODUCTION

Cosmic rays are high energy nuclei, electrons and photons mainly from sources outside the solar system. For the cosmic rays considered in this thesis (energy $\gtrsim 10^{10}$eV) only the extra solar nuclear component is believed to be important.

It is natural to ask where and how these particles are accelerated to such high energies (as high as 10^{20}eV). On the other hand, the existence of these energetic nuclei provide an opportunity to study some aspects of particle interactions at energies much greater than those attainable with current accelerators. However, these fundamental matters are complicated by other uncertainities. For example, one would wish to know to what extent the observed energy spectrum of cosmic rays is determined by their acceleration mechanism and the characteristics of their propagation in galactic or extra-galactic space. In order to properly interpret the observations in terms of either the propagation or interaction physics one needs a knowledge of the composition of the beam.

It is clear, then, that any non-trivial interpretation of a cosmic ray experiment may be rather speculative but it will be constrained by the need to be

consistent with the results of other experiments in often quite different areas. Considering our lack of detailed knowledge in many areas of cosmic ray physics, this is not always a serious constraint although, often, no consistent interpretation is apparent.

Cosmic rays interact in the atmosphere to produce extensive air showers. The development of a cosmic ray extensive air shower is influenced by both high energy particle interactions and the composition of the initiating cosmic ray. The research on which this thesis is based was undertaken with the (naive) intention of studying the composition of cosmic rays with energies $\sim 10^{16}$eV. In view of the above, one should perhaps say that the results relate to the, as yet, inseparable problem of the composition and particle physics at that energy.

This chapter contains a brief examination of cosmic radiation in general, but with a particular emphasis on those matters that may have a more direct bearing on the composition/interaction problem at cosmic ray energies of about 10^{16}eV.

1.2 EXTENSIVE AIR SHOWERS (EAS)

Because of the low flux of the highest energy cosmic rays, it is not practicable to measure them directly with satellite or balloon-borne detectors as is the case for particles with energies $\lesssim 10^{14}$eV. Instead, these cosmic rays are detected via the products of their

interactions in the earth's atmosphere. The cascade of secondary particles produced by these atmospheric interactions is known as an extensive air shower (EAS). These showers will be examined in more detail in chapter two. The EAS consists of three major components: (1) a hadronic core whose lateral extent is a few metres; (2) a penetrating muon component extending out to distances of the order of a hundred metres; and (3) a 'soft' electromagnetic component with a lateral extent similar to that of the muons. The number of muons progressively builds up in the cascade, while the numbers of particles in the hadronic and soft components grow to a maximum and then decay in the atmosphere. For showers initiated by cosmic rays of energy $\lesssim 10^{13}$eV, only the muon component reaches sea level. At primary energies $\sim 10^{16}$eV, the soft component is (numerically) dominant at all levels of the atmosphere and it is the growth and decay of this component that was the subject of the experimental work to be described in this thesis.

1.3 THE PRIMARY COSMIC RAY ENERGY SPECTRUM

Cosmic ray energy spectra are usually presented in one of two forms. The integral spectrum relates to energy, the number of cosmic rays above that energy and the differential spectrum involves the number per unit energy interval at the particular energy (both also per unit area, solid angle and time). If these spectra are

simple power laws in energy, one need only subtract one (1) from the integral exponent (index) to obtain the differential exponent. For this reason, no attempt will be made to use only one type of spectrum.

The integral energy spectrum of cosmic rays is shown in figure 1.1 for energies greater than 10^{10}eV. It can be seen that the spectrum is indeed approximately a power law with an exponent of -1.8. It is of interest to note that the integral rate at 10^{16}eV is about one per square metre per steradian per year. In figure 1.2, the flux has been multiplied by $E^{1.5}$ to flatten the spectrum and highlight the deviation from a simple power law. The main feature is a steepening at a few times 10^{15}eV, commonly known as the knee. Since, at these energies, the energy of the primary cosmic ray is inferred indirectly from air shower measurements, with subsequent disagreements between the results of different research groups and methods, the exact form of the knee is unknown. Another feature of the spectrum, an apparent flattening above 10^{19}eV, is called the ankle.

1.4 COMPOSITION AT LOW ENERGIES

This section deals mainly with the chemical composition of the primary cosmic rays and its variation with energy as a guide to what may be expected in the energy range 10^{15} to 10^{17}eV. For this purpose, the energy per nucleus will be used. By way of introduction, however,

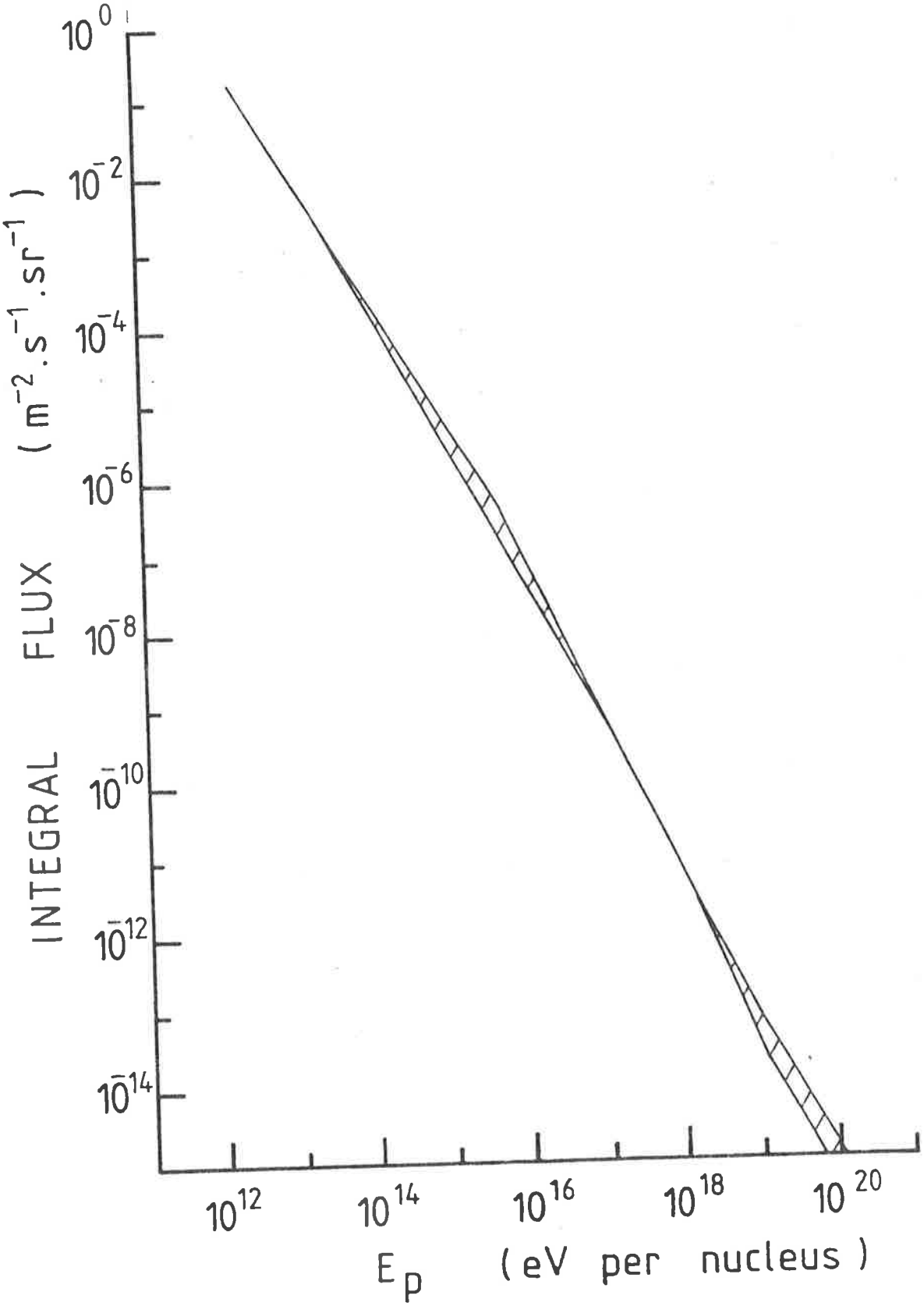

Fig 1.1 The integral flux of cosmic rays at the top of the atmosphere. The cross-hatched areas represent experimental uncertainties (after Gaisser and Yodh, 1980).

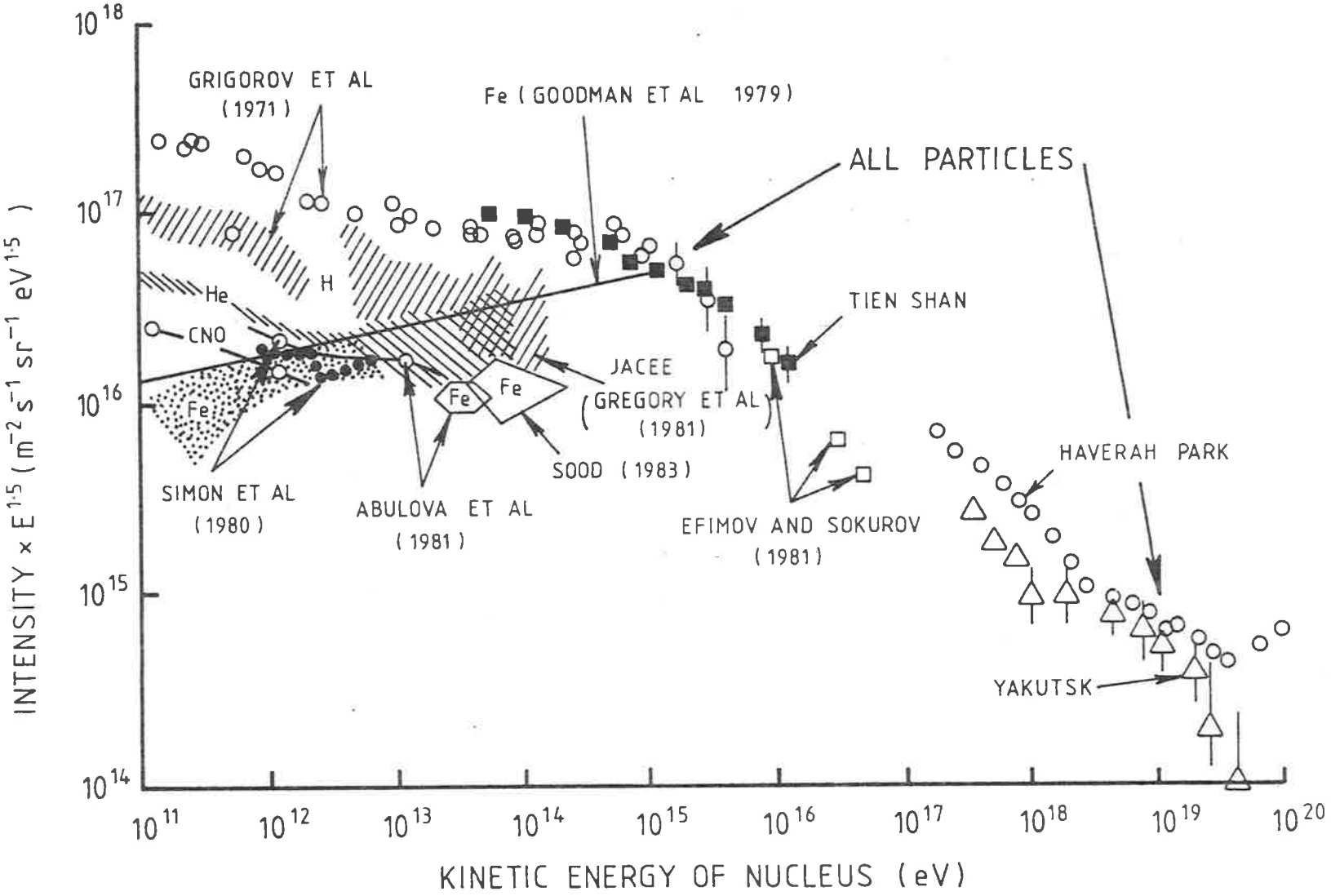

Fig 1.2 The energy spectrum of the primary cosmic rays showing the major components. The fluxes have been multiplied by $E^{1.5}$ to flatten the spectrum and accentuate changes in slope (essentially after Hillas 1981).

the chemical and isotopic composition at constant energy per nucleon will be briefly discussed as well as some of its implications concerning the nature of the source and the propagation of cosmic rays.

1.4.1 AT $\sim 10^{10}$ eV/NUCLEON

Table 1.1 lists the relative composition of various elements and charge groups, based on a compilation by Juliusson (1975) and the data of Simon et al (1980). The major difference between this composition and solar system abundances is that the light nuclei and very heavy nuclei are overabundant in the cosmic ray beam. The excess of these elements can be attributed to the spallation of heavier elements in the interstellar medium.

TABLE 1.1

THE RELATIVE COMPOSITION OF COSMIC RAYS AT 10^{10} eV/NUCLEON

Charge (Z)	Elements	%
1	Hydrogen	93.8
2	Helium	5.5
3-5	Light Nuclei(Li,B,Be)	0.08
6-8	Medium Nuclei(C,N,O)	0.4
10-16	Heavy Nuclei	0.14
17-25	Very Heavy Nuclei	0.014
26-28	Iron Group	0.02

The abundances of these spallation products (secondaries) enable one to calculate the amount of matter

traversed by the cosmic rays. The mean amount (λ_e) is energy dependent and is approximately given by:

$$\lambda_e = 6 g\ cm^{-2} (E/GeV)^{-0.5}$$

in the region 1 to 100 GeV/nucleon. For a review of the uncertainties in the derived values and the range over which this applies see Stephens (1981).

After corrections for spallation effects, the derived cosmic ray source (CRS) composition agrees well with solar system (SS) abundances, most differences showing a strong correlation to the first ionization potential of the atoms. In this respect, the source composition closely resembles that of solar energetic particles, with the major exception being that of carbon which is overabundant in the CRS by a factor of $\sim$two. The abundances of $Z>26$ elements also indicate a source composition consistent with SS values, although an enhancement of r-process material (i.e. supernova source) cannot be ruled out (Mewaldt 1981).

The existence of unstable isotopes amongst the secondary elements allows an estimation of the 'age' of cosmic rays. A value of 14(+13, -5) million years has recently been calculated from the $^{10}Be/^{9}Be$ ratio at 100 MeV/nucleon (Garcia-Munoz et al, 1981). This corresponds to a mean number density in the confinement region of $\sim$0.23 atom cm^{-3}, which is well below the accepted density of 1 atom cm^{-3} in the galactic disc. Other possible 'clocks' are ^{26}Al, ^{36}Cl and ^{54}Mn.

The relative isotopic abundances at the source have been calculated for several elements and, in general, the ratios are at variance with the SS values. The enhancement factor (CRS ratio divided by the SS ratio) is $\sim$3.5 for (^{22}Ne/^{20}Ne) and $\sim$1.6 for (^{25}Mg/^{24}Mg), (^{26}Mg/^{24}Mg), (^{29}Si/^{28}Si) and (^{30}Si/^{28}Si) (Wiedenbeck and Greiner 1981). It has been argued (Webber 1982) that ^{20}Ne is underabundant in the CRS by a factor of two, bringing the ^{22}Ne over-abundance in line with that of the other neutron rich isotopes. ^{14}N is also apparently underabundant at the source (Mewaldt et al 1981).

The chemical composition of cosmic rays suggests processes such as those occurring in stellar flares as the major source of cosmic ray material, while the isotopic evidence requires a different nucleosynthetic history to that of the sun. At the recent Paris Cosmic Ray Conference, Cassé (1981) provided a brief review of possible source models. The age and mean escape length derived from the secondary cosmic rays indicate that they spend a significant amount of time in low density regions such as the galactic halo or 'superbubbles' (see section 1.5).

1.4.2 FOR E$\leq 10^{14}$eV/NUCLEUS

Turning now to the composition at constant energy per nucleus, figure 1.2 also shows the integral fluxes of various components of the cosmic rays above the atmosphere.

The hydrogen and helium spectra can both be fitted by simple power laws with an index of -1.7 up to 10^{14}eV. (It has been assumed that the recent JACEE proton spectrum of Gregory et al 1981 is correct, rather than the Grigorov et al 1971 spectra which exhibited a steepening above 10^{12}eV which is now believed to be an instrumental effect.)

Between 10^{11} and 10^{13}eV the fraction of iron in the primary beam is clearly rising, while to a lesser extent this is also true of the CNO component. The spectrum of the spallation products Li, Be and B is much steeper than that of the other components, thus these elements are likely to be insignificant at higher energies. Above 10^{13}eV there are few measurements of the primary composition for elements heavier than helium. The point for iron at 2×10^{13}eV is from an emulsion experiment flown at an atmospheric depth of 12g cm^{-2} by Abulova et al (1981). An integral flux has been obtained for iron at 10^{14}eV by Sood (1983) using the Cerenkov light produced by the incident primary to increase the effective collecting area and to discriminate in favour of high Z particles. The composition in this region should be further elucidated as more results of the JACEE experiment become available.

The basic features of the spectra displayed in figure 1.2 can be explained by assuming the same source

spectral index for all components and allowing for the energy dependent escape length discussed in section 1.4.1. Thus at low energies iron is severly depleted due to spallation losses which decrease with increasing energy and decreasing escape length, finally becoming negligible at about 10^{11}eV/nucleon (i.e. $\sim 10^{13}$eV/nucleus for iron). The same will be true of the CNO component although the effects will be less.

In this view the composition at 10^{13}eV/nucleus, which is approximately H:He:CNO:Fe:(Z=10-16) in the ratio 4:2:2:2:1, is the same as the source composition and would remain unaltered until the cosmic rays begin to be lost from the galactic disc at a rigidity of about 10^{15}V/c.

Although a source producing a single index power law spectrum of cosmic rays over many decades of energy may be attractive because of its simplicity, a suitable acceleration mechanism is difficult to find. Therefore, it is probably unwise to extrapolate on the assumption of a constant source index, especially in view of the uncertainity in the highest energy data. As an example, Simon et al (1980) find that although their highest energy data for iron are consistent with a differential index of -2.7 near 5×10^{12}eV/nucleus, the statistics are not sufficient to rule out the iron spectrum of Goodman et al (1979a) which has an index of -2.4 from 5×10^{12} to

$\sim 10^{15}$eV. (This experiment and its interpretation will be discussed later, as will other air shower measurements that relate to the composition/interaction problem.)

1.5 ANISTROPIES

(This section is based largely on recent reviews by Watson 1981 and Hillas 1982b.)

Since cosmic rays are charged, their paths in the galactic magnetic field are not straight lines. The Larmor radius of a relativistic particle is given by:

$$r_L \sim E/ZB \text{ parsecs}$$

if E is in units of 10^{15}eV and B in microgauss. The magnetic field in the galactic disc is generally assumed to have mean values in the range 2-4 microgauss.

In current models, the galaxy has a 'halo' of hot, low density gas extending several kiloparsecs beyond the disc. The extent of the halo is uncertain, as is its associated magnetic field, although the synchrotron emissivity of the halo indicates a field $\sim 1\mu G$. Thus, even for protons, the paths of cosmic rays only approach straight lines on the galactic scale at energies $\sim 10^{20}$eV. At most energies the cosmic rays spiral around the magnetic field lines and are reflected or scattered by irregularities in the field, producing a highly isotropic flux at the earth.

The quantity measured to indicate the directional properties of the cosmic rays is the

anisotropy whose amplitude is:

$$\delta = (I_{max} - I_{min})/(I_{max} + I_{min})$$

where I_{max} and I_{min} are the maximum and minimum intensities respectively. The direction (or phase) of the anisotropy is mainly determined in right ascension because, firstly, only a limited declination band is accessible at the latitude of any particular detector and, secondly, the atmospheric collimation used in low energy experiments gives a result which is an average over that band. At energies where individual shower directions can be measured it is also possible (with some difficulty, see e.g. Clay and Gerhardy 1982b) to determine a declination dependence.

The variation of amplitude and phase of the anisotropy from 10^{11}-10^{20}eV is shown in figure 1.3. Below 10^{14}eV both the amplitude and phase are essentially constant at about .06% and 40°. Kiraly et al (1979) conclude that the constancy of the anisotropy from 10^{11}-10^{14}eV indicates that cosmic ray propagation and sources are not too different over the whole range and that the cosmic ray life-time is also nearly constant, unlike its energy dependence below 10^{11}eV.

Above 10^{14}eV the phase begins to change rapidly while the amplitude increases roughly as $E^{0.5}$ above $2x10^{14}$eV. These changes are consistent with the existence of irregularities in the local interstellar medium on a scale of a few parsecs and may be linked with the knee in the energy spectrum if this is associated with propagation effects.

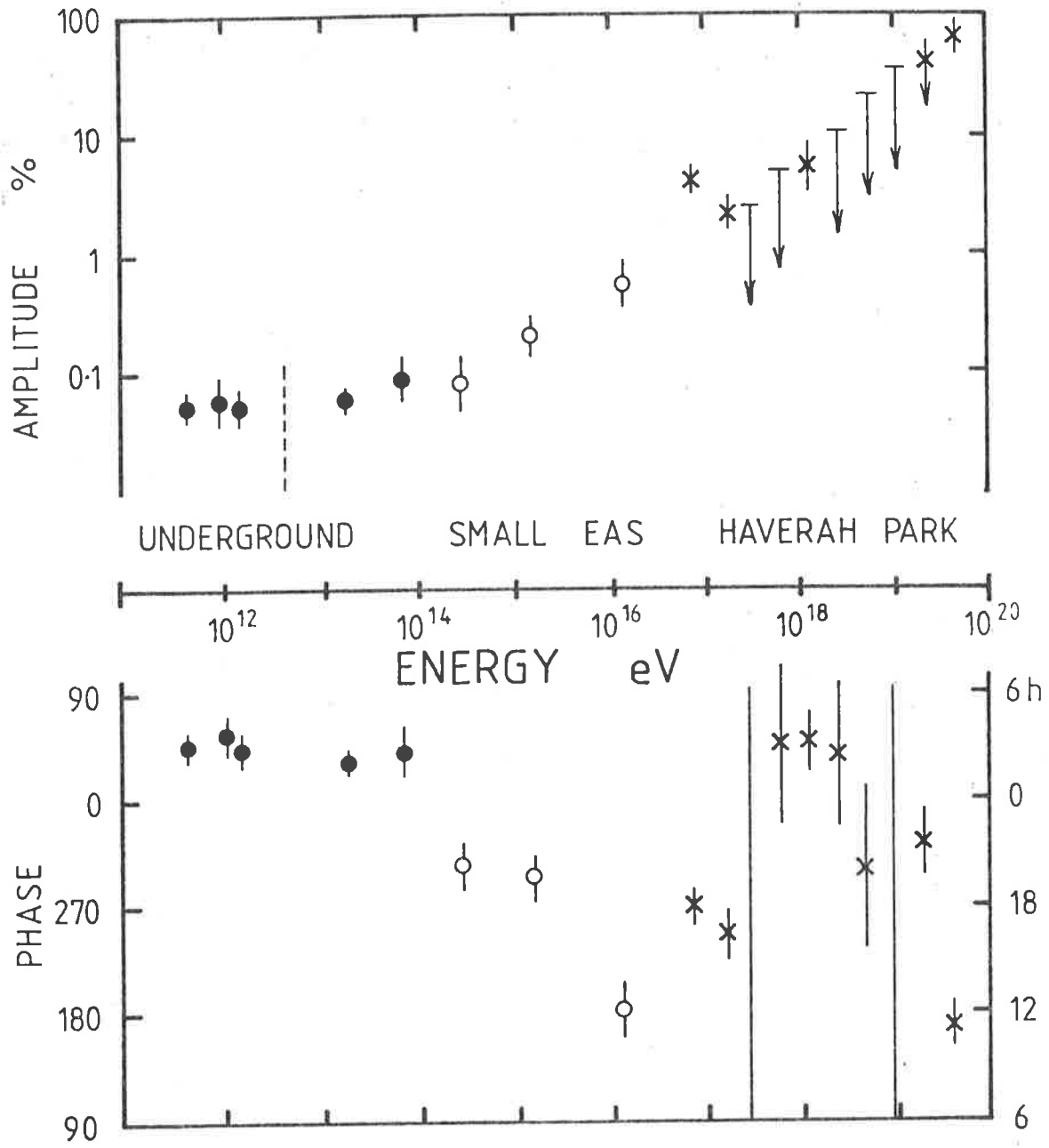

Fig 1.3 The amplitude and phase of the observed anisotropy of the primary cosmic rays (after Watson 1981).

Between 5×10^{17}eV and 10^{19}eV, analysis of the Haverah Park data in galactic latitude shows an excess of showers from the south (Astley et al 1981). There is a sharp reversal above 10^{19}eV with the cosmic rays arriving preferentially from high galactic latitudes (Cunningham et al 1980). If the cosmic rays at this energy are protons, the arrival directions require an extragalactic source.

1.6 ACCELERATION AND PROPAGATION

Various mechanisms have been suggested for the acceleration of cosmic rays. Many of these involve very energetic astrophysical phenomena such as supernovae explosions (e.g. Colgate and Johnson 1960) or pulsars (Ostriker and Gunn 1969). Other modes such as second order Fermi acceleration (Fermi 1949) derive their energy from small scale random motions of magnetized gas in interstellar space. The currently most popular model, shock acceleration (see e.g. Blandford and Ostriker 1978, Bell 1978) incorporates elements of both types. The shock itself may be associated with supernovae, novae, strong stellar winds, etc., while the acceleration occurs as a result of the cosmic ray being repeatedly scattered across the shock front, leading to first order Fermi acceleration (i.e. involving non-random motions in the medium). The same mechanism might accelerate the very highest energy cosmic rays in intergalactic space.

Shock acceleration requires particles to have an energy exceeding some minimum value ($\sim$10MeV, Cowsik 1980). Thus supernovae explosions, the second order Fermi mechanism etc., may still play a role by supplying the necessary 'seed' particles. It would seem, however, that pulsars are not relevant as it is now believed that they cannot accelerate ions (Arons 1980).

The main factor favouring shock acceleration (apart from meeting the obvious constraint that it is energetically feasible) is that this mechanism is capable of producing a power-law spectrum over a wide range of energies determined predominantly by the scale length of the shock region. A restriction is imposed on any acceleration mechanism by the observed secondary to primary (S/P) ratio which decreases with energy (as outlined in 1.4.1) indicating that there is no significant reacceleration of the secondaries. Thus, although Axford (1980) estimates that every point in the galaxy is passed by a supernova shockwave about ten times during the lifetime of a cosmic ray ($\sim 2 \times 10^7$ years) providing ample opportunity for acceleration in the inter-stellar medium, the S/P ratio requires that there be only one or two acceleration incidents. Cesarsky and Lagage (1981) calculate an upper limit of $\sim 10^{15}$eV for the contribution from supernovae shocks when reacceleration is limited in order to provide agreement with the observed S/P energy dependence. Their spectrum is extended another decade

when the contribution from stellar winds is included. The maximum energy is proportional to the charge of the particle which would lead to composition changes near the cutoff. It is of interest to note that the Cesarky and Lagage model mimics the knee in the energy spectrum.

A variation of the shock acceleration mechanism involves structures known as superbubbles. Heiles (1979) discovered neutral hydrogen 'supershells' with sizes of several hundred parsecs. These shells have been interpreted as the matter swept up by the stellar winds and supernovae of OB associations. These mechanisms create a low density cavity ($n \sim 10^{-2}$ atoms cm^{-3}). The whole structure is known as a superbubble and they are expected to have lives $\sim 10^{7}$ years before breaking up. Kafatos et al (1981) envisage cosmic rays being confined within the bubble while being accelerated by the shock mechanism at the shell as well as by new supernovae shocks within the bubble. Although this model produces reasonable values for the cosmic ray age and mean density traversed, it involves continuous acceleration and therefore cannot be readily reconciled with the observed S/P energy dependence. Streitmatter et al (1983) circumvent the problem by restricting the acceleration to the collisions of individual supernovae shells with the supershell, thereby limiting the acceleration in both time and space. They also place the solar system within a superbubble which ceases to confine the cosmic rays

effectively at high energies giving rise to the anisotropy and spectral features at $\sim 10^{15}$eV.

The observed S/P ratio also places limits on the time between injection and acceleration. Injection at energies below the spallation threshold does not avoid the problem since, in this case, inionization losses would severaly deplete the cosmic rays of high Z nuclei, contrary to observation (Eichler 1980).

Calculations of the source abundances of the elements from their observed abundances and those of the spallation products are usually performed using a propagation model of the 'nested leaky box' type (Cowsik and Wilson 1973). In such models the cosmic rays are initially confined near the source with a rigidity dependent leakage into a larger confinement region such as a spiral arm or the galaxy as a whole. The decreasing escape length discussed in 1.4.1 then represents escape from the source region, not the galaxy. Escape from the larger volume in which the solar system is situated is energy independent until the Lamor radii of the cosmic rays became comparable with the scale of the magnetic inhomogeneities. This occurs at a rigidity of $\sim 10^{15}$V/c and would be accompanied by changes in the observed spectrum and anisotropy. This model provides a relatively simple explanation for the knee in the spectrum and the increase in the magnitude of the anisotropy above 2×10^{14}eV.

It is worth noting that if the knee results from a cut-off due either to acceleration or confinement effects, it would generally occur at a particular value of rigidity. Thus one would expect the iron spectrum to steepen at an energy per nucleus 26 times that at which the proton spectrum changes. The nett result would then be that high Z nuclei would dominate the primary beam just above the knee.

At the very highest energies the blue shifted microwave background radiation limits the cosmic ray lifetime to 10^8 years. The major energy loss is by photo-pion production above a threshold of 5×10^{19}eV for protons. The fact that the spectrum becomes flatter in this region, assuming no significant upturn in the source spectrum, suggests that if cosmic rays at that energy are extragalactic, then the relatively local Virgo supercluster must be the dominant source.

1.7 PARTICLE INTERACTIONS AT AIR SHOWER ENERGIES

The purpose of this section is to indicate that at air shower energies particle interactions show significant variations from their behaviour at accelerator energies. The topic has been recently reviewed by Gaisser et al (1978) and Gaisser and Yodh (1980).

An important concept used in the extrapolation to higher energies of multiple particle producing interactions is that of scaling (Feynman 1969, also Benecke et

al 1969 in the form of limited fragmentation). In a scaling model the distribution of the secondary particles tends to an asymptotic limit as the total energy (E_o) tends to infinity if one uses an appropriately scaled variable. For example, if the secondaries have an energy distribution $f(E, E_o)$ this can be replaced by $f(E/E_o)$ which is independent of the total energy. Scaling leads to a logarithmic increase in the number (multiplicity) of the secondaries with energy. Other models (Fermi 1951, Landau 1953) predict a multiplicity increasing as $E^{\frac{1}{4}}$. There is currently insufficient data to determine the correct dependence (see Erlykin 1981).

Two empirical observations that led Feynman to believe that asymptopia was being approached were the constancy of the total cross-sections and of the mean traverse momentum of the secondaries at accelerator energies. However, the proton-proton cross-section appears to increase above 10^{11}eV (Yodh et al 1972, Amaldi et al 1977) although its behaviour above 5×10^{13}eV is still unknown. Similarly, accelerator experiments in the last decade have shown a slow increase in transverse momentum (see the review by McCubbin 1981) while air shower experiments indicate a more rapid increase above 2×10^{14}eV (McCusker et al 1969, Ashton et al 1977, Ashton and Nejabat 1981).

A good example of the unpredictability of particle interactions are the Centauro events (Lattes et

al 1973) which have been observed in air showers with primary energies near 10^{15}eV. In these events an anomalously small fraction of the energy is in the electromagnetic (π°) component as compared to the hadronic ($\pi^{\pm}$ and nucleon) component. The relevance of such uncertainties to the interpretation of air showers will become more obvious in the next chapter where the air shower will be considered in some detail.

CHAPTER TWO

CERENKOV RADIATION FROM EXTENSIVE AIR SHOWERS

2.1 EAS

As outlined in section 1.2, cosmic rays incident on the atmosphere produce cascades of energetic particles. In this section the basic processes involved in the development of EAS will be examined. Initially, the primary particle will be assumed to be a proton. The way in which the shower is likely to be modified in the case of a heavy primary will be discussed in 2.1.3.

2.1.1 BASIC PROCESSES

An air shower is initiated when a primary cosmic ray proton collides with a nucleus (typically nitrogen) in the atmosphere. The proton passes through the nucleus colliding with one or two nucleons in the process. These nucleons are ejected from the target nucleus which, as a whole, does not gain much energy from the collision. Only the most basic features of the individual nucleon-nucleon collisions that contribute to EAS will be discussed here. Detailed discussion of collision models and experimental data at EAS energies can be found in the review articles of Miesowicz (1971), Feinberg (1972), Gaisser et al (1978) and Gaisser and Yodh (1980).

The incident cosmic ray proton essentially passes through the target nucleon, losing about half of

its energy in the process. Particle production accompanying the collision is usually divided into two (momentum) regions. The fragmentation region contains the remnant of the primary and other leading particles (fragments) presumably produced by the subsequent decay of the excited primary. The fragmentation region accounts for the bulk of the energy. The other, so called pionization, region corresponds to small centre of mass momentum and is where most new particle production occurs.

Pionization itself can be viewed as particles evaporating from a hot fireball of hadronic matter produced by the collision. A simple explanation of the process can be given in terms of a model developed by Pomeranchuk (1951) and extended by Landau (1953). The fireball expands and cools, its constituents interacting until their separation exceeds the range of the strong force which is mediated by virtual pions with a range $\sim m_\pi^{-1}$ (in units with $\hbar=c=1$). As a result, the fireball cools to a temperature $T\sim m_\pi$ before the constituents can evaporate. As a result of the low temperature at which the fireball evaporates, most of the particles it produces are pions and they have a Bose thermal distribution in the frame of the fireball. Because of the thermal spectrum, the transverse momentum of the pions will be typically $\sim 3m_\pi$, i.e. $\langle p_T \rangle \sim 420$ MeV/c.

Although pions represent the bulk of the particles produced, there may also be heavier mesons, antinucleons

strange particles, etc. The multiplicity of produced particles carrying most of the energy is roughly $2(E/10^9 eV)^{\frac{1}{4}}$ for incident protons of energy greater than 10^9eV (Longair, 1981).

For sufficiently energetic primaries, pions of all charges are conventionally believed to be produced in approximately equal numbers. Neutral pions have a very short half-life (1.78×10^{-16}s) and, even at the relativistic energies at which they are produced in air showers, can be considered to decay immediately into two photons. The charged pions have longer half-lives (2.55×10^{-8}s) and may interact further or decay into a muon and muon neutrino. It is the pion decay products that give rise to the more extensive components of the EAS.

The gamma rays from the π^0 decays produce electron-positron pairs in the field of a nucleus. (The word electron will be used to refer to both electrons and positrons.) These in turn produce further gamma rays by bremsstrahlung emission. The nett result is known as an electromagnetic (e-m) cascade. The effects of Coulomb scattering result in the electrons of the e-m cascade reaching sea level in a disc with a typical lateral spread of about 100 metres and a thickness of a few metres.

Muons from the charged pion decays have half-lives of 2.2×10^{-6} s and those with Lorentz factors greater

than about 20 survive to sea level. Low energy muons may decay into electrons together with electron and muon neutrinos. Although the muons are not appreciably scattered and travel at small angles to the shower direction, they have a sea level lateral extent of the same order as the e-m cascade by virtue of their production heights (up to 20km).

The third component of an EAS is the hadronic core consisting of the primary particle remnant and other hadrons surviving from the fireballs. The core constituents will have further interactions with nuclei which will produce more pions and thereby add to the e-m and muon components of the shower. (The leading particle will, of course, dominate these processes.) The lateral extent of the core (for hadron energies $\gtrsim 10^{10}$eV) is only a few metres for low primary energies but this increases (approximately linearly with energy) above 10^{14}eV due to the increase in mean p_T discussed in section 1.7.

Figure 2.1 is a schematic representation of the basic processes contributing to the EAS.

2.1.2 THE ELECTROMAGNETIC (e-m) COMPONENT

Because of the cascading of the electrons and photons, the electromagnetic component is numerically dominant so long as the hadronic core has sufficient energy to generate new pions. After the core has lost its energy, the muon component persists longer than the

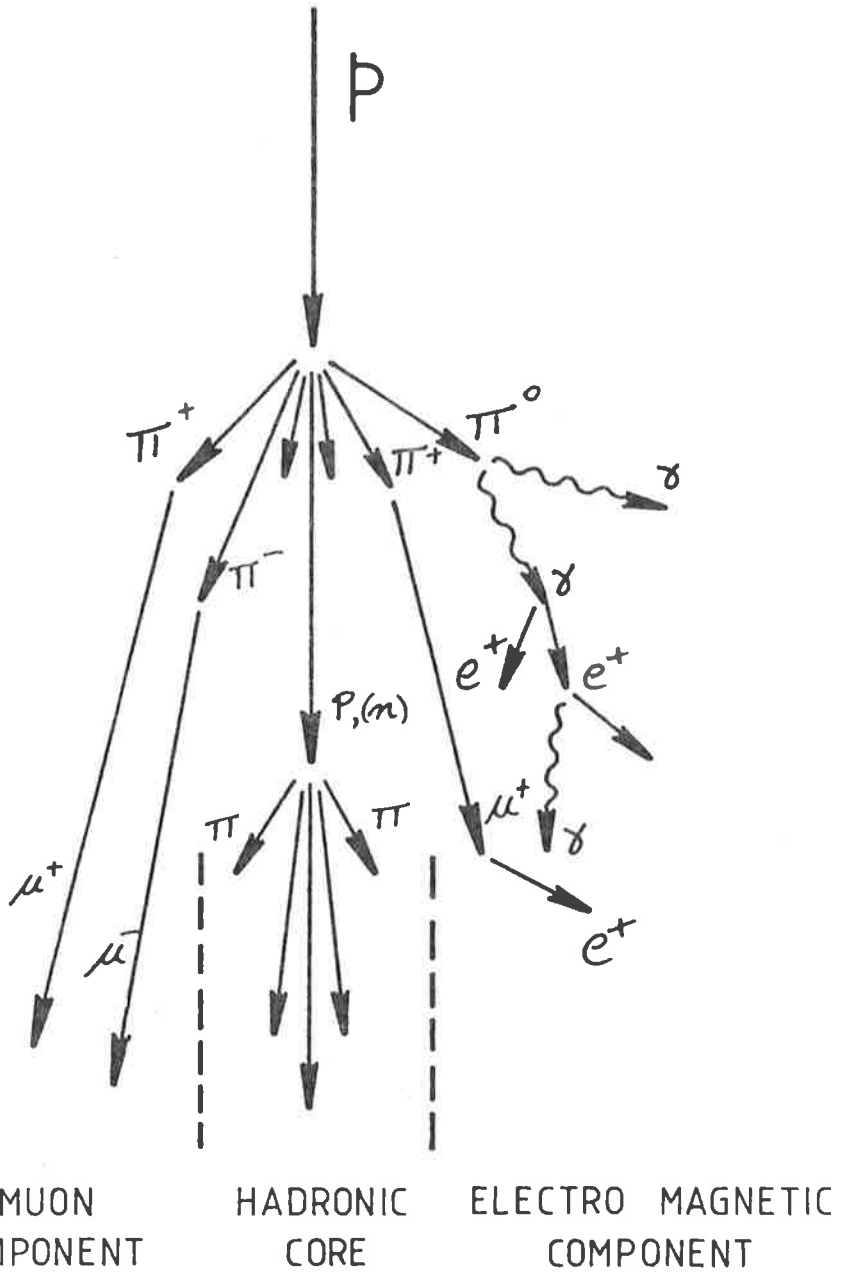

Figure 2.1 A schematic of an extensive air shower. The neutrinos accompanying the pion and muon decays have been omitted for clarity.

e-m cascades. For showers initiated by primaries of energy $\lesssim 10^{13}$eV only the muon component survives to sea level, but for primary energies $\gtrsim 10^{14}$ electrons are the main sea level component.

The behaviour of pure e-m cascades is well understood (Kamata and Nishimura 1958). Since the growth and decay of individual e-m cascades is much more rapid than that of the nucleonic component of an EAS, it is the latter which dominates the overall development of the shower's electron component. However, some properties of the EAS electrons can be well represented using results that only strictly apply to pure cascades.

For example, an e-m cascade can be characterized by an 'age' parameter, s, which increases with depth, being zero at the start of the cascade and one at the depth at which there are a maximum number of electrons. Such properties of the cascade as the electron energy distribution and lateral distribution are then functions of the age with the initial energy only contributing as a scale factor. For the e-m component of an EAS, because one has a superposition of many individual cascades of different ages, the age parameter is not well-defined but is nevertheless still used as a convenient measure of a shower's state of development. In particular, the lateral distribution is usually fitted to an NKG function (which is an approximation by Greisen 1956,

to the theoretical expression of Kamata and Nishimura 1958, for pure e-m cascades but which includes an empirically derived term to make it fit EAS data) to obtain a best fit age, although it is well known that for an individual EAS the apparent age depends on the distance from the core at which most measurements are made. (See e.g. Capdeveille and Gawin 1982 for a recent treatment of this problem.)

For current purposes it is sufficient to note some expressions which are good approximations to the shower characteristics. The energy dependences are based on e-m considerations while the density distributions are empirical.

The integral energy spectrum of the shower electrons near maximum is (Allan 1971)

$$N(>E) = N_e/(1+E/30) \qquad \text{Eq. 2.1}$$

where N_e is the total electron number and E is in MeV. Based on the calculations of Roberg and Nordheim (1949) one has for the rms scattering angle

$$\theta(E) \cong .7/(1+E/E_s) \text{ radians} \qquad \text{Eq. 2.2}$$

E_s (=21 MeV) is the characteristic Coulomb scattering energy in air. This scattering results in the electrons having a lateral and longitudinal spread. The lateral density distribution (the density ρ at a distance r from the shower axis) can be represented by the so-called 'Moscow approximation' (Greisen 1960)

$$\rho(N_e,r) = \frac{N_e}{2\pi r_0} \cdot \frac{e^{-r/r_0}}{r} \ m^{-2} \qquad \text{Eq. 2.3}$$

with $r_0 \cong 60$ metres. The longitudinal density distribution, as a function of time (t) in nanoseconds, can be described by (Woidneck and Bohm 1975)

$$d(t) = 0.39t^{0.9}e^{-0.6t} \qquad \text{Eq. 2.4}$$

Because of the energy dependence of the scattering, the most energetic electrons will be found near the front of the disc and close to the shower axis.

2.1.3 THE DEVELOPMENT OF EAS

The development of the e-m component, dominated as it is by the nuclear component, can provide information about the interactions of the primary cosmic ray particle. In particular, the initial growth of the electron numbers (N_e) and the atmospheric depth (x_m) at which the maximum number occurs, depend on the energy of the primary cosmic ray and the way it distributes that energy. This in turn provides clues to the nature of the primary and its interactions. On the other hand, the behaviour beyond shower maximum appears to be well established - an exponential decay with an attenuation length (λ_{att}) ~ 200g cm^{-2}.

There are two parameters which are particularly useful for characterizing the development: viz, the depth of the first interaction and the depth of maximum. It is the latter which is the subject of this thesis.

The shower size at maximum is reasonably model independent and is related to the primary energy (E_p) by

(Allan 1971)

$$N_e(x_m) = E_p/2\times10^9 eV \qquad \text{Eq. 2.5}$$

Less well established is the relationship between the sea level size and the primary energy. As a rough guide one can use (Allan 1971)

$$N_e(sl) = 10^6 (E_p/10^{16} eV)^{1.15} \qquad \text{Eq. 2.6}$$

but the exact form depends on the variation of x_m with E_p which in turn depends on the composition of the primary beam and on high energy interactions. This will be discussed in more detail in 2.1.4.

Assume for the moment that the depth of maximum increases by 100g cm^{-2} per decade of primary energy. Eq. 2.5 holds for heavy primaries as well as for protons but the depth of maximum will vary for different nuclear species with the same energy. The simplest way to treat heavy primaries is using the superposition model. In this a primary of atomic mass A and energy E_p is assumed to produce the same EAS as A showers each of energy E_p/A. On this basis, an iron induced shower (A = 56) would be expected to have its maximum about 175g cm^{-2} higher in the atmosphere than a shower induced by a proton of the same energy. The fact that the nucleons of a heavy nucleus are not totally independent will slightly increase the difference between the depths of maxima.

Since showers develop on an energy per nucleon basis, the energy spectra of the muon and hadron components

combined with a knowledge of the total energy should also be sensitive to primary composition.

Another difference between proton and heavy nucleus induced showers arises because of the different mean free paths of the primary particles. The proton mean free path in air is 80g cm^{-2} at low energies reducing to about 60g cm^{-2} at 10^{16}eV (Ellsworth and Yodh 1981). For iron nuclei the mean free path is only 14g cm^{-2} (Daniel and Dugaprasad 1962). Thus for proton initiated showers the first interaction will occur deeper in the atmosphere on average and will have larger fluctuations between showers. Because about half of the available energy is dumped in the first interaction, fluctuations in its depth will produce comparable effects on the depth of maximum. Fluctuations in later development will also be less for a heavy primary induced shower because, being the sum of A smaller showers, it will deviate less from the 'average' shower than might a shower produced by a single nucleon.

2.1.4 THE ELONGATION RATE

The way the shower depth of maximum changes with energy has been called the elongation rate. The concept of an elongation rate (ER) which could be related to the nuclear physics of the shower was introduced by Linsley (1977) and subsequently generalized and refined (Linsley 1979, Gaisser et al 1979).

In its simplest form, Linsley's ER theorem can be explained as follows. If the primary cosmic ray has energy E and the secondary multiplicity varies as E^B then the average γ-ray energy from the π° decays will go as E^{1-B}. Since the depth of maximum for an e-m cascade increases by one radiation length (X_o = 38g cm^{-2}, is the interaction length for pair-production and bremsstrahlung) for an e-fold increase in energy, the ER for an EAS will be

$$D_e = \frac{dx_m}{d\ln E} = (1-B)X_o \qquad \text{Eq. 2.7}$$

Thus the change of depth of maximum per decade of energy (D_{10}) has a maximum value of 87g cm^{-2} for a constant composition. Changes in composition can be dealt with using the superposition model so that the effective primary energy is E/A. One therefore obtains

$$D_e = (1-B)X_o\left(1-\frac{\overline{d\ln A}}{d\ln E}\right) \qquad \text{Eq. 2.8}$$

where $\overline{\ln A}$ is the logarithmic mean primary mass number. The quantity B would also include terms resulting from the energy dependence of the cross sections for inelastic hadron-air nucleus interactions.

While the ER theorem provides a useful tool for interpreting shower depth of maximum, the simplified model for shower development on which it is based means that it cannot be applied rigorously. Monte Carlo simulations of showers have been performed to determine the elongation rate for various interaction models.

McComb and Turver (1981a) find that for scaling models (multiplicity $\sim$lnE giving a small effective B) D_{10} varies between 90 and 100g cm^{-2} depending on the energy dependence adopted for the cross sections. Ellsworth and Yodh (1981) obtain D_{10} values in the same range but tending towards 87g cm^{-2} as they follow secondary particles to a lower threshold energy.

It would appear that for a constant primary composition the maximum value for D_{10} is 100g cm^{-2}, assuming no drastic changes in the particle physics.

The elongation rate is also implicit in any relationship between primary energy and the shower size at a fixed depth (such as in Eq. 2.6). Since the size attenuates past maximum ($\lambda_{att} \sim 200$g cm^{-2}) the size at the observing level (e.g. sea level) will be

$$N_e(sl) = \alpha N_e(x_m) \exp[-(x_{sl}-x_m)/\lambda_{att}]$$

so that

$$N_e(sl) \propto N_e(x_m) \exp [x_m/\lambda_{att}] \qquad \text{Eq. 2.9}$$

From Eq. 2.5 one has

$$N_e(x_m) \propto E_p$$

and from Eq. 2.7

$$x_m = D_e \ln E_p + \text{constant}$$

Thus Eq. 2.9 becomes

$$N_e(sl) \propto E_p^{\,1+D_e/\lambda_{att}} \qquad \text{Eq. 2.10}$$

So, even if the relationship between $N_e(sl)$ and E_p can be established at one size, it cannot be extrapolated without a knowledge of the elongation rate. To determine

the primary energy for an individual, rather than an 'average', shower from the sea level size the depth of maximum is required, although fluctuations in the development beyond maximum may still complicate matters.

2.2 CERENKOV RADIATION

Cerenkov radiation is produced when a charged particle travels through a dielectric medium with a velocity greater than the speed of light in the medium. It is analagous to shock wave effects in acoustics and mechanics. The radiation was first studied experimentally by Cerenkov (1934, 1937) and theoretically explained by Frank and Tamm (1937).

Blackett (1948) suggested that Cerenkov radiation produced by cosmic rays made a small contribution to the total integrated night sky flux and subsequently Galbraith and Jelley (1953) detected intense light pulses associated with air showers. Cerenkov radiation has an $\nu d\nu$ frequency distribution, so the emission peaks towards the ultraviolet. Because the atmosphere is transparent to the visible and near ultraviolet, and because this is also the region of maximum sensitivity of most photomultipliers, Cerenkov light is a convenient tool with which to probe shower development. The early work on Cerenkov radiation from air showers has been reviewed by Boley (1964) and Jelley (1967).

2.2.1 CERENKOV LIGHT FROM EAS

In a medium of refractive index n, a charged particle will have a threshold velocity v_{th} for Cerenkov production given by

$$v_{th} = c/n$$

If one uses $n = 1+\eta$, the threshold energy, E_{th}, for a particle of rest mass m is

$$E_{th} = mc^2(1/\sqrt{2\eta} - 1)$$

In air at STP where $\eta = 2.9\times10^{-4}$ this approximates to

$$E_{th} = mc^2/\sqrt{2\eta} \qquad \text{Eq. 2.11}$$

which is 21 MeV for an electron, 4.4 GeV for a muon and 39 GeV for a proton. It can be seen from the shower electron energy distribution of Eq. 2.1 that even at higher altitudes where η is less than its sea level value, about a half of the electrons will be above the Cerenkov threshold.

Cerenkov light is emitted in a cone about the direction of the particle motion. The angle of emission is

$$\theta = \arccos(c/nv)$$
$$\approx [2\eta(1-E_{th}^2/E^2)]^{\frac{1}{2}} \text{ radians for } \eta<<1. \qquad \text{Eq. 2.12}$$

For an electron at sea level, the maximum value of this angle is 1.3°. Comparing this with Eq. 2.2 for Coulomb scattering ($\sim$10° at 100 MeV) it is obvious that the angular distribution of the Cerenkov light from an air shower will be dominated by the Coulomb scattering of the electrons.

The number of photons emitted is given by

$$\frac{dN}{dl} = 4\pi\alpha \ (1-E_{th}^2/E^2) \int \eta \frac{d\lambda}{\lambda^2} \text{ photons/m} \quad \text{Eq.2.13}$$

At shower maximum, for an electron with $E>>E_{th}$, this results in $\sim$200 photons/g cm^{-2} in the 350-450nm wavelength range. Allowing for the electron energy distribution and atmospheric transmission, one may expect $\sim 10^5$ photons per shower electron at sea level.

2.2.2 LATERAL DISTRIBUTION

Because the angular distribution of the Cerenkov light from an EAS is largely determined by the electron distribution, the light has a strong forward collimation. Thus light emitted from low in the shower does not contribute as much to the flux at large core distances as does light from higher altitudes. As a result, the higher in the atmosphere that the shower maximum occurs, the more light there will be at larger core distances and the flatter the lateral distribution of the Cerenkov light will be. Therefore, the Cerenkov lateral distribution can be related to the shower development. Also, the total integrated Cerenkov flux provides a measure of the primary energy which is relatively insensitive to fluctuations in the shower development (c.f. the sea level size).

Calculations of the expected lateral distribution progressed from those using simplistic models (e.g. Jelley and Galbraith 1955), through the more realistic calculations of Zatsepin and Chudakov (1962) and

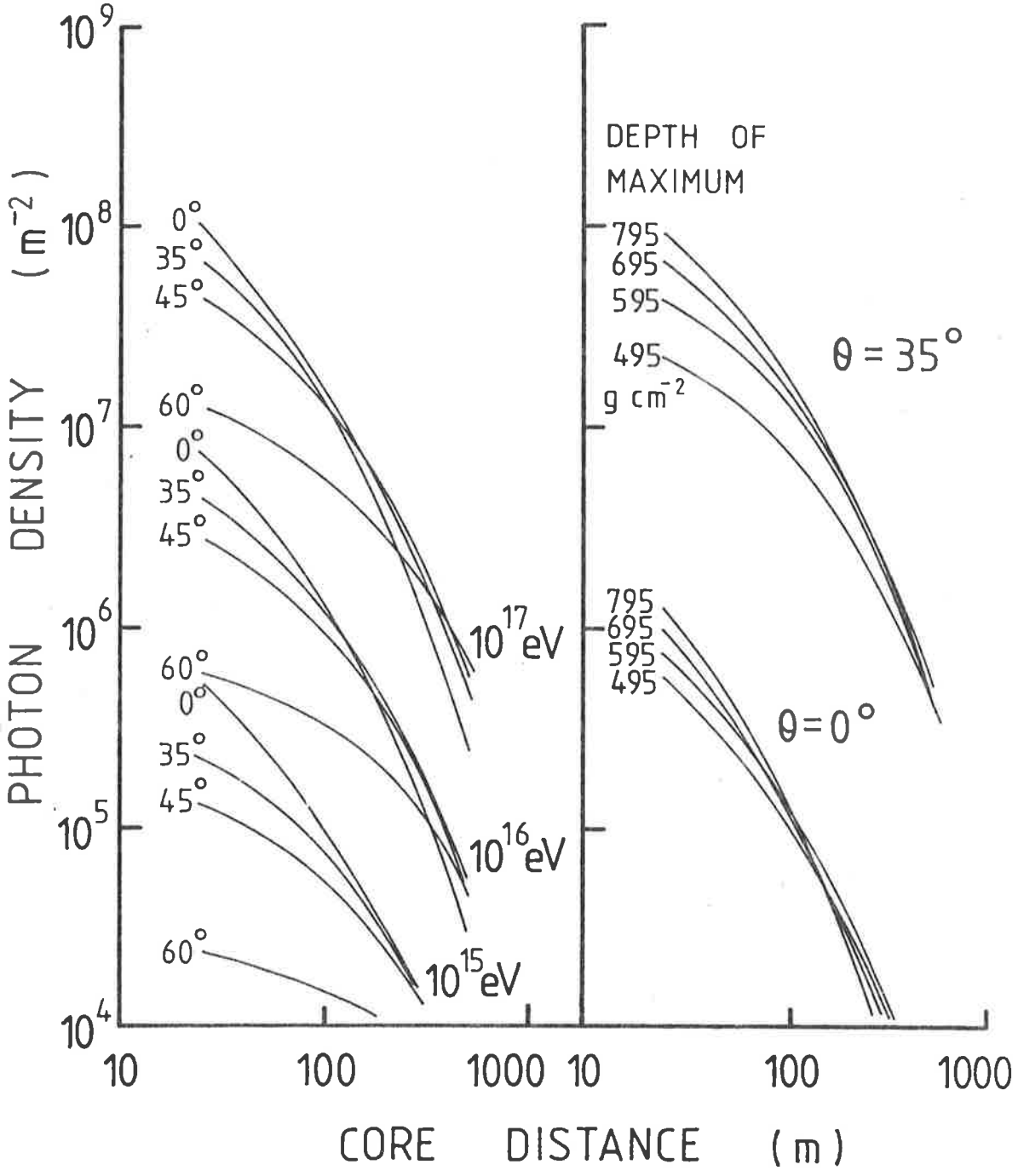

Figure 2.2 Cerenkov light lateral distributions as calculated by McComb and Turver 1981.

Sitte (1962) to sophisticated calculations using Monte Carlo techniques to simulate both the nuclear and electromagnetic components of EAS.

The calculations have produced several results which are particularly relevant to the experimental work of this thesis. Firstly, there is a core distance at which the flux is approximately proportional to the primary energy and nearly independent of the shower development. For showers with primary energies of 10^{15} to 10^{17}eV this distance is about 200 metres (see e.g. the results of McComb and Turver 1981b reproduced in figure 2.2). Secondly, even at 300 metres from the core, the photon flux is $\sim E_p/(10^{11}\text{eV})\ m^{-2}$ (figure 2.2).

The calculations have also enabled the depth of maximum of showers to be determined from experimental measurements of the lateral distribution. The results of such experiments will be discussed in chapter six.

2.2.3 TIME STRUCTURE

The Cerenkov light pulse will have a time structure determined by refractive index effects, geometrical path differences, and the size of the emitting region. To examine the first two effects, consider the arrival times of light originating from various heights along the shower axis and detected at a core distance, r (figure 2.3). The emitting point is assumed to be moving at the speed of light in vacuum. The arrival time of light from h relative to the arrival

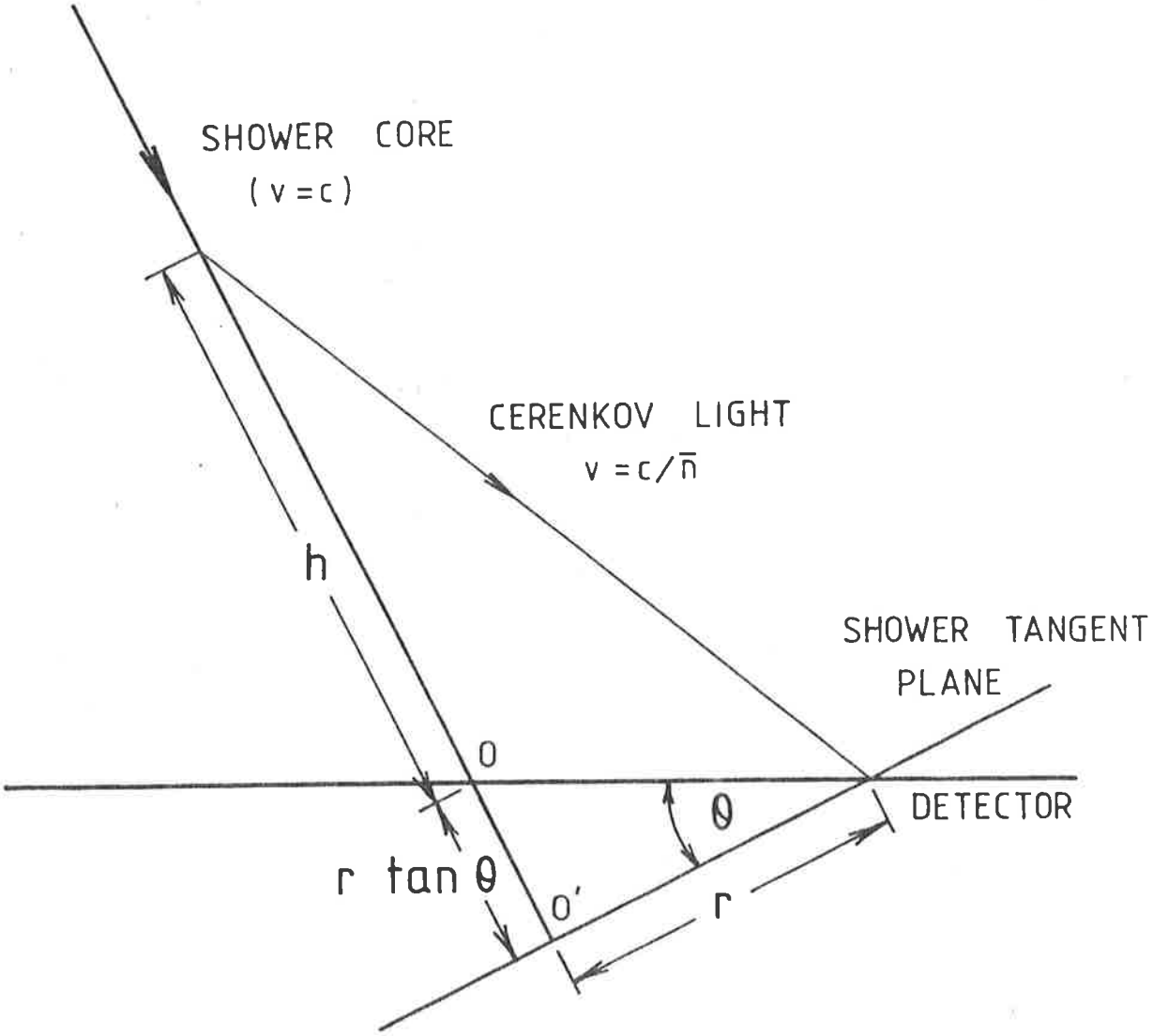

Figure 2.3 The basic shower geometry. The arrival time of the Cerenkov light is taken with reference to the arrival of the shower tangent plane. In principle, if r and θ are known, the arrival time can be converted to a height of origin. In practice, uncertainties in zenith angle, and hence the distance 00^1, make this straight forward technique unworkable. Using time differences (e.g. the FWHM) eliminates the need for a reference time. In the text the simple case of a vertical shower is considered.

of the shower at 0' is

$$t = (\bar{n}(h^2+r^2)^{\frac{1}{2}} - h)/c \qquad \text{Eq. 2.14}$$

Since Cerenkov light is preferentially emitted at small angles, one may assume $r<<h$ and Eq. 2.14 can be approximated to

$$t = (\bar{\eta}h+r^2/2h)/c \qquad \text{Eq. 2.15}$$

$\bar{n}$ and $\bar{\eta}$ represent the appropriate averages from ground level to the height h. It can be seen from Eq. 2.15 that for small core distances the first term dominates and light from low in the shower arrives first. For larger values of r the refractive index effects become less important and the second term representing geometric path differences is the major factor. The time sequence is now reversed, light from high in the shower arriving first. Because of these two opposing effects there only exists a one to one relationship between height and time of arrival for $r \cong 0$m and $r \gtrsim 150$m.

It was recognized early in the study of the Cerenkov light from EAS that the pulse shape contained information about the development of the electron component (Jelley 1958). The first measurements of the pulse shape were made by Boley et al (1961, 1962) using a highly collimated photomultiplier (.03sr) looking at vertical showers with $E_p \sim 10^{15}$eV and core locations within $\sim$5 metres of the detector. Under these conditions the size of the emitting region was expected to dominate the pulse width and the results were interpreted as a

measure of the electron disc thickness. Other experiments and calculations were also performed with narrow angle detectors. The calculations of Castagnoli et al (1967a) established the dependence of pulse shape on development while those of Sitte (1970) and Bosia et al (1972a) showed a dependence on shower age parameter. Measurements of the pulse width were made by Castagnoli et al (1967b) and Bosia et al (1970a,b, 1972b) but no variation with shower parameters that would indicate a dependence on shower development was demonstrated.

Experiments by Bosia et al (1973) showed that the detector geometry determined the observed pulse shape and the calculations of Böhm et al (1975) provided the explanation. If the shower axis was not parallel to the detector axis, the Cerenkov pulse represented an oblique cross section of the shower and was thus a measure of the electron lateral distribution. This explained the structure observed in some pulses in terms of allowable fluctations in the shower's lateral electron structure (Bosia et al 1975).

One other aspect of calculations for narrow angle detectors is the work of Rieke (1969) and Grindlay (1971) aimed at differentiating between gamma ray and cosmic ray initiated showers in an effort to reduce the cosmic ray (nuclei) background in searches for high energy gamma ray sources.

The current technique of determining shower development from the Cerenkov pulse shape follows the suggestion of Fomin and Khristiansen (1972) that, at large core distances, not only did the pulse shape depend on the development but that it could also be used to determine the actual cascade curve.

The way in which the shower development maps onto the pulse shape at large r can be best illustrated by ignoring the refractive index effects. The Cerenkov flux as a function of time can be written as

$$\emptyset(t)dt = N_e(h)A(r,h)\ dh/h^2 \qquad \text{Eq. 2.16}$$

$N_e(h)$ is the electron number at the height corresponding to the time according to Eq. 2.14. $A(r,h)$ is the Cerenkov flux in the direction of the receiver and depends on the electron energy and angular distributions and the local refractive index, all of which can be considered 'knowns'. The solid angle subtended by unit area at the ground is $1/h^2$ and dh is the height interval contributing to the unit time interval dt.

Differentiating Eq. 2.15 (ignoring the η term and the sign) and rearranging one obtains

$$dh = 2h^2c\ dt/r^2 \qquad \text{Eq. 2.17}$$

Substituting this into Eq. 2 yields

$$\emptyset(t) = N_e(h)\ A(r,h)\ 2c/r^2 \qquad \text{Eq. 2.18}$$

Thus, in principle, the shower development curve $N_e(h)$ can be readily obtained from the Cerenkov pulse shape at

large core distances. In practice, the major problem is to determine the arrival time of the light at the detector relative to the arrival of the shower plane at the same point as this requires an accurate determination of the shower direction.

Orford and Turver (1976) circumvented this problem by using a large number of detectors and assuming that any particular point on the pulses (e.g. 10% of full height) corresponded to a single point on the shower. This enabled the locus of the point to be determined geometrically. In this manner they could build up a shower (Cerenkov) profile as well as trace the shower axis. The assumption was based on unpublished shower simulations (but see Protheroe and Turver, 1977) and was shown by Ivanenko and Makarov (1977) to be equivalent to assuming that the function A(r,h) in Eq. 2.18 is sufficiently slowly varying to be considered constant over the core distance range of the measurements. The technique has been used to determine Cerenkov development features (Hammond et al 1977) and, in conjunction with simulations, to determine the depth of the shower electron maximum (Andam et al 1981).

Another method of reconstructing the cascade curve was investigated by Grigor'ev et al (1979). They first used the pulse width to determine the height of maximum (based on simulations) and then, by identifying that position with a point on the pulse, were able to

establish the zero of their time scale and relate time to height by use of Eq. 2.14.

A more widely used technique has been to relate the Cerenkov pulse full width at half maximum (FWHM) to the height of shower maximum and hence determine its depth without attempting a detailed reconstruction.

A guide to the sensitivity of the FWHM to the height of maximum can be obtained by differentiating Eq. 2.15 to obtain

$$dt = (\eta - r^2/2h^2)/c.dh \qquad \text{Eq. 2.19}$$

Assuming that the atmospheric depth (x) is related to height by

$$x = x_0 e^{-h/h_0}$$

where x_0 is the total atmospheric depth and h_0 the pressure scale height, leads to

$$dt = -(\eta - r^2/2h^2)e^{h/h_0}(h_0/cx_0)dx \qquad \text{Eq. 2.20}$$

The refractivity η will vary with height as

$$\eta = \eta_0 e^{-h/h_1}$$

where h_1 is the density scale height ($h_1 \cong 1.2h_0$). If the points on the shower corresponding to the half height points on the Cerenkov pulse are separated by a fixed grammage, the pulse FWHM, τ, will vary as (approximating $h_1 = h_0$)

$$\tau = \left| -a + br^2 e^{h/h_0}/h^2 \right| \qquad \text{Eq. 2.21}$$

It is obvious that the FWHM depends strongly on both core distance and height of maximum ($h<h_0$ in general). Because of the angular distribution of the Cerenkov

light from the shower, the height from which the maximum light is received will in fact be above the shower electron maximum. This angular effect also means that at larger core distances the height of Cerenkov maximum will move up in the atmosphere so that an exact r^2 dependence would not be expected.

Despite the many assumptions and approximations made in deriving the above relationship, it is in good agreement with the results of calculations and experiments. The simulations and measurements of the Durham group are in agreement with an r^2 dependence (Hammond et al 1978, Protheroe and Turver 1979, McComb and Turver 1982b), while the Moscow group obtain a value of 1.7 from experiment (Kalmykov et al 1977) and values between 1.7 and 2.4 from simulations (Kalmykov et al 1979). The simulations also enable them to derive a relationship between the height of maximum (h_m) and the pulse width at 300 metres from the core (τ_{300}). It is

$$h_m = 17.05 - 9.17 \log_{10}(\tau_{300}) \qquad \text{Eq. 2.22}$$

where τ_{300} is in nanoseconds and h_m in kilometres. This has been plotted in figure 2.4 along with the result of using Eq. 2.20 with $dx = 300g\ cm^{-2}$ and $h = h_m + 1km$ to allow for the difference between the particle and Cerenkov maxima. The main point of comparison is the slope which is unaffected by the arbitary choice of values. The deviations can be understood in terms of a decrease in dx due to the angular distribution of the light for

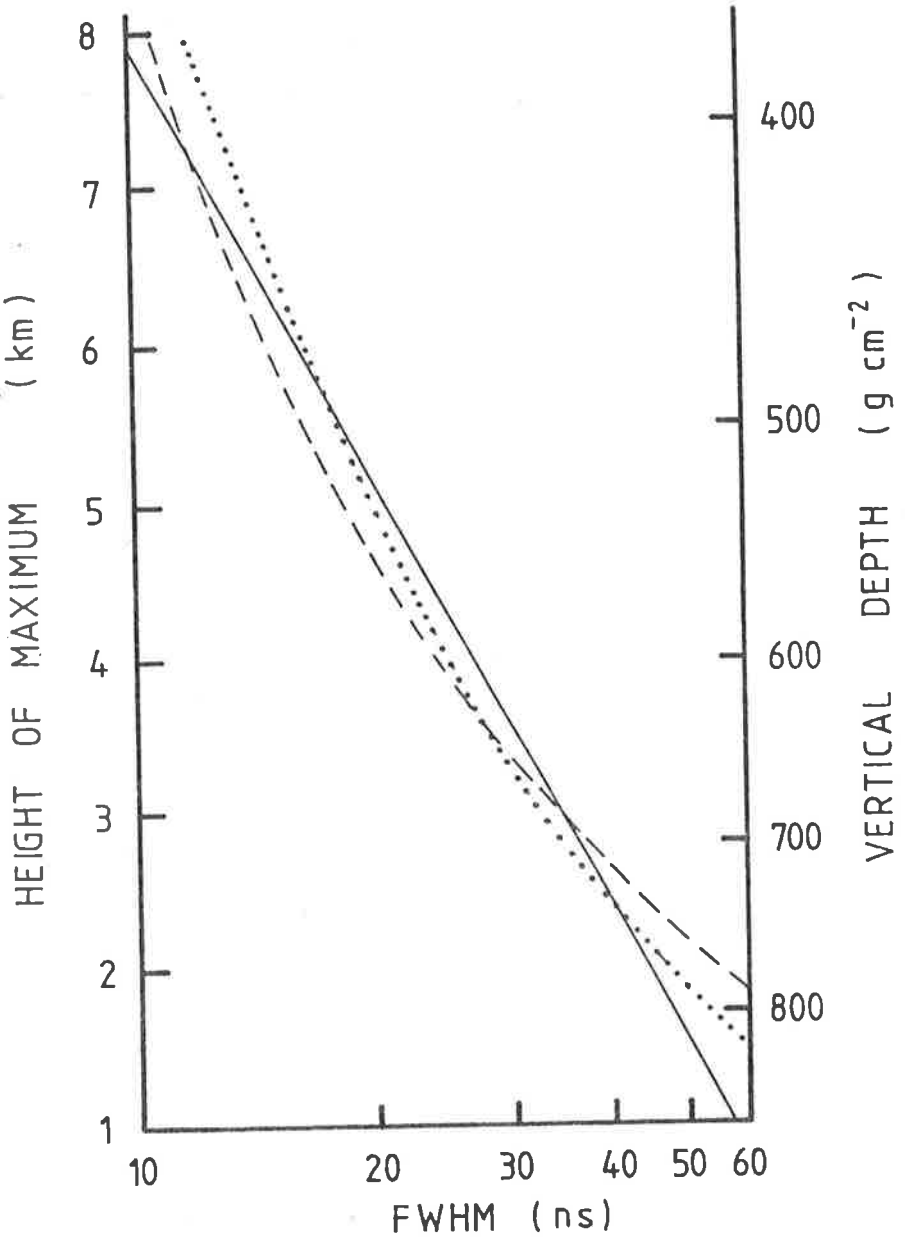

Fig 2.4 The relationship between the FWHM at 300m and the height of maximum. Solid line-Kalmykov et al 1979; dotted line-Patterson and Hillas 1983; broken line- the results of the simple consideration outlined in the text.

small heights and the increasing Cerenkov threshold at high altitudes. The results of recent calculations (Patterson and Hillas 1983) agree with Eq. 2.22 and furthermore indicate that it is valid over a wide range of zenith angles.

Thus the way in which the Cerenkov pulse FWHM varies with core distance and height of maximum has a simple physical interpretation at large core distances. The FWHM should, therefore, provide an unambiguous measure of the shower depth of maximum if the core distance and zenith angle are known.

The following chapters describe an experiment (and its results) to measure the Cerenkov pulse FWHM and hence determine the depth of maximum for showers with primary energies $\sim 10^{16}$eV.

CHAPTER THREE

EXPERIMENTAL DETAILS

3.1 INTRODUCTION

In chapter two it was shown that the Cerenkov pulse full width at half maximum (FWHM) at large core distances depends strongly on both the shower height of maximum and the core distance. The purpose of the work described in this thesis was to measure the FWHM of the Cerenkov pulse from extensive air showers and, in conjunction with independent measurements of other shower parameters, determine the depth of maximum of those showers. In this chapter the basic data acquisition and its preliminary treatment will be examined.

3.2 THE PARTICLE ARRAY

The experiment was conducted at the University of Adelaide's Buckland Park field station which is situated about 40 kilometres north of Adelaide on a coastal plain a few metres above sea level. On this site the Adelaide Cosmic Ray Group operates an extensive air shower detector array which routinely measures particle densities and arrival times in showers. These data enable the calculation of shower size, core location and arrival direction. The array also provides a prompt trigger which can be used to activate other

recording devices. The array and its performance are described in detail elsewhere (Crouch et al 1981) and only the features relevant to the Cerenkov pulse width experiment will be mentioned here.

3.2.1 PHYSICAL DESCRIPTION

For most of the duration of the experiment the array consisted of eleven one square metre plastic scintillators arranged and designated as in figure 3.1. All sites provided particle density measurements while the five central sites (A, B, C, D and E) gave timing information for the determination of shower direction. Particle densities were not available from B, C and E before February 1978 and sites I, J and K were not operational until the end of May 1978. The recording systems for the particle array and the Cerenkov experiment were housed near the centre of the array (initially in c1 and c2 and later in c3). The eleven scintillator pulse heights and four pulse times (relative to C) were digitized and recorded on magnetic tape for later analysis on the University's CDC Cyber 173 computer.

3.2.2 ARRAY PERFORMANCE

The triggering conditions for the array were that greater than 6 particles (equivalent vertical muons) be detected at A and greater than 8 at D, while all the fast timing sites must have detected at least 2 particles. These conditions ensured that almost all

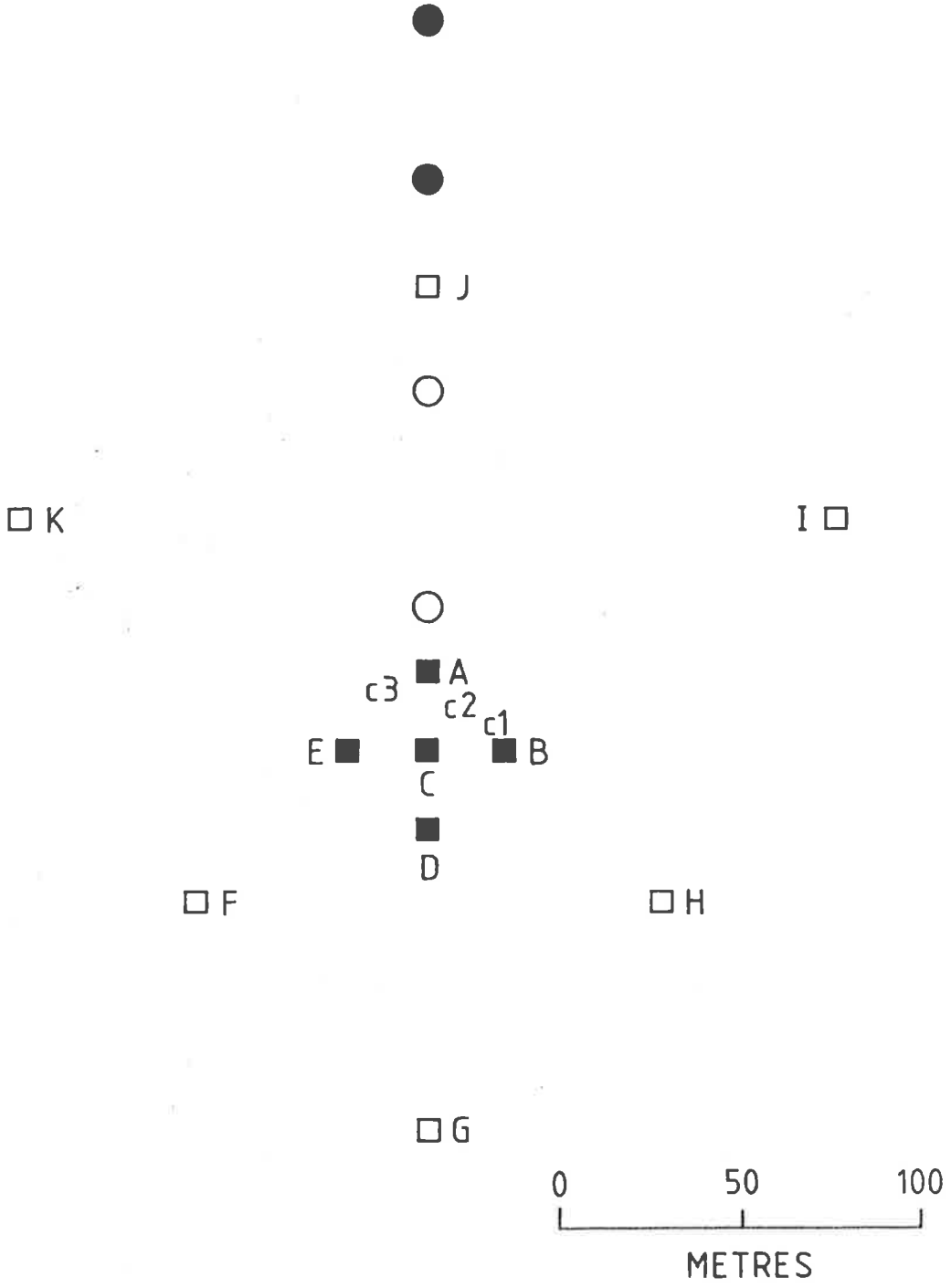

Fig 3.1 The Buckland Park array at the time of the experiment. The squares represent scintillator sites: empty squares-particle densities only; solid squares-times and densities. The photomultiplier for the Cerenkov experiment was variously placed at the sites indicated by the circles. Most data was collected with the PM at the two northern-most sites (solid circles).

triggering showers could be well analysed. As a result, showers of a given size have a well defined triggering area, roughly centred on C. For example, a $4x10^5$ electrons shower has greater than 90% triggering probability within about 30 metres of C, but this decreases to less than 10% outside 60 metres. With increasing shower size the array collecting area approaches the physical size of the array ($3x10^4 m^2$).

Shower sizes can be determined with a typical error of 10%, the core location to within 10 metres and the arrival direction to about 4°. These accuracies only apply to showers whose cores are located inside the area defined by FGHIJK. If the shower core lies outside this area, the resultant analysis is generally poor, if not impossible. In the determination of the shower direction the shower front is assumed to be planar.

The temporary lack of particle densities from B, C and E is insignificant both in terms of time ($\sim$5% of the experiment) and in its effect on core locations. (B, C and E help define the east-west location of the shower, but uncertainities in that direction have little effect on the core distance from the Cerenkov detector which was well to the north.) While a larger amount of data was obtained before the advent of I, J and K, these sites are only important for the analysis of showers whose cores fall in a region of

little interest to the Cerenkov experiment, i.e. r<150 metres. Thus, as far as it concerns the Cerenkov pulse width experiment, the array performance can be considered essentially unchanged throughout the experiment.

3.3 THE CERENKOV EXPERIMENT

The Cerenkov pulse width experiment used a photomultiplier viewing the night sky. The output was taken via a length of coaxial cable to a transient recorder which displayed the pulse on a TV monitor from which it was photographed. In this section the individual elements of the system will be examined in detail.

3.3.1 THE PHOTOMULTIPLIER

The photomultiplier tube was a Philips XP2040. This is a fast tube (anode pulse FWHM ≈4ns at 1500V) with a useful photocathode diameter of 110mm. The photocathode is of the S11 (u.v. extended) type with a peak quantum efficiency (∿21%) at just below 400nm. The tube was used with a plano-concave adaptor which cuts off transmission below about 300nm. The resultant spectral response is shown in figure 3.2. The base used with the photomultiplier is shown in figure 3.3.

To reduce noise from the Adelaide lights and from those parts of the sky from which few showers were recorded, the photomultiplier was collimated by a shield (rubbish bin/trash can) of about 0.5 metres diameter. The tube was positioned so that the cut off was centred

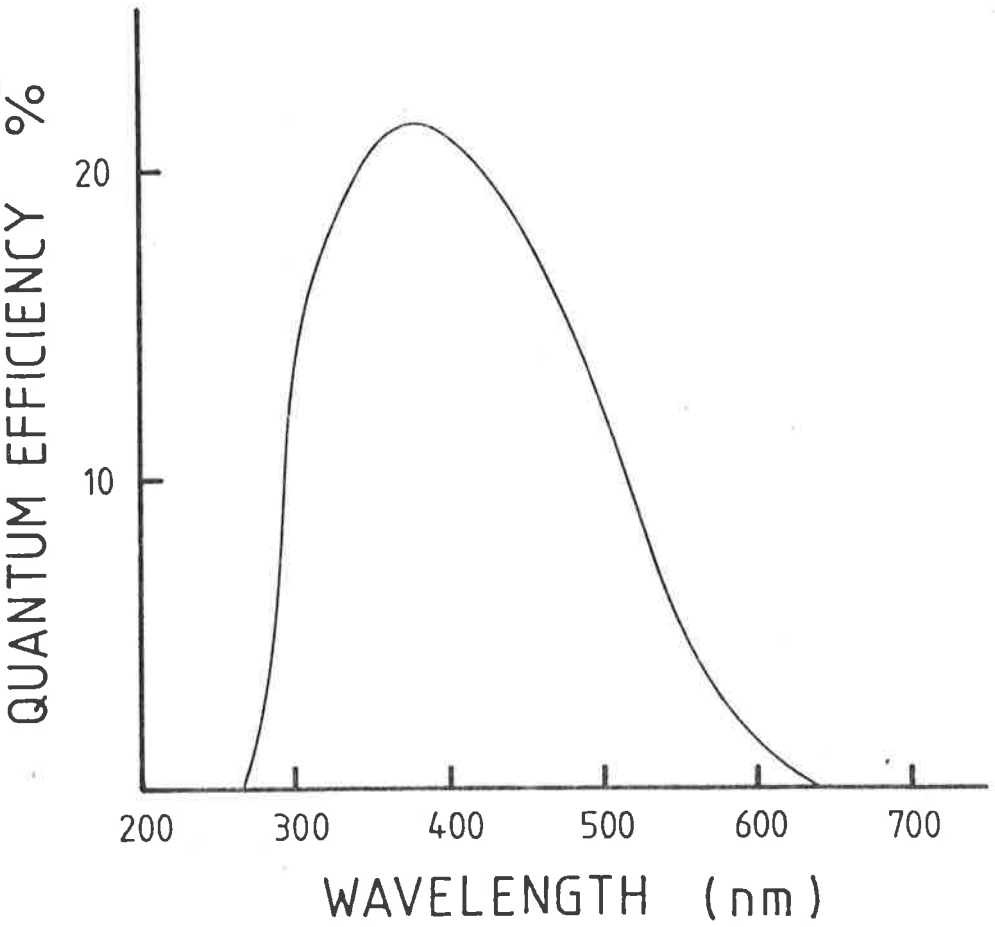

Fig 3.2 The spectral response of the XP2040 photomultiplier with faceplate.

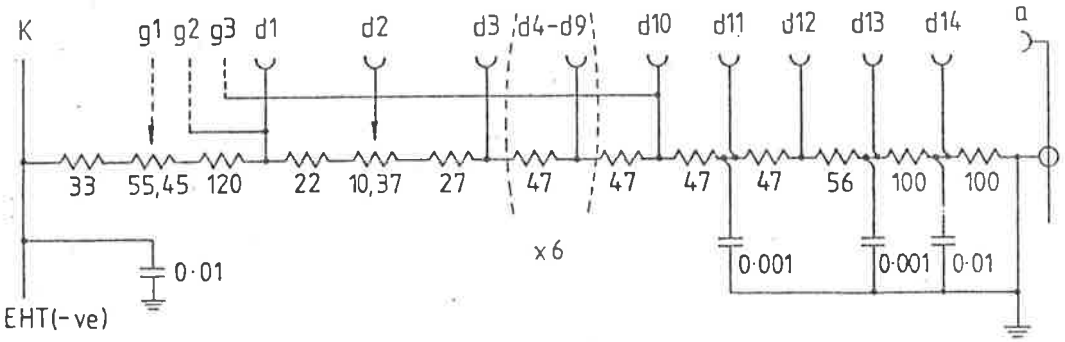

Fig 3.3 The resistance chain for the photomultiplier base. The resistances are in kilohms and the capacitances in microfarads.

on 45° with the collimation having some effect ∿6° either side of this. Since only ∿1% of the detected showers had angles of incidence greater than 40° where edge effects due the collimation may distort pulse shapes, the collimation should not complicate the interpretation of the results.

3.3.2 CABLE

To obtain good sensitivity to the shower depth of maximum the Cerenkov pulse needs to be measured at least 150 metres from the shower axis. However, for logistic reasons the recording equipment was housed near the centre of the array, an area where most of the detected showers' cores are located. These circumstances made it necessary to locate the photomultiplier at a large distance from the transient recorder. The two were connected by 200 metres of RG 8A/U 50 ohm coaxial cable. To compensate for the relatively poor bandwidth of this length of cable (see figure 3.5b) a short piece of cable (27cm) terminated by a small resistance (∿10Ω) was added to the end of the main cable in parallel with the input to the transient recorder. At low frequencies the reflection from this extra cable is out of phase with the incoming signal, while at a frequency corresponding to four times the cable length (∿160 MHz) the reflection is in phase. The overall effect is to flatten the frequency response by preferentially attenuating the low

frequencies. The terminating resistance was adjusted to give optimal compensation without producing pulse overshoot.

3.3.3 THE TRANSIENT RECORDER

The pulses were recorded using a Tektronix 7912 Transient Digitizer whose output was displayed on a TV monitor and photographed. The input signal was initially amplified by a Tektronix 7A19 wide-band amplifier plug-in which, used in conjunction with the 7912, has a bandwidth of 500 MHz. The horizontal sweep was provided by a Tektronix 7B92 time-base.

The 7912 utilizes a scan converter tube in which the signal, written by the writing beam onto a target, is temporarily stored and subsequently read off by a separate reading beam. A dot array, similar to the graticule on an ordinary oscilliscope, is internally generated and also written onto the target on a time shared basis with the input signal. In the experiment the 7912 was used in the NON-STORE mode in which the read gun scans the target in a television raster format. The output was then displayed on a TV monitor. Using a signal generator with a digital frequency read-out, the graticule was found to be accurate to within the available resolution.

The system is summarized in figure 3.4.

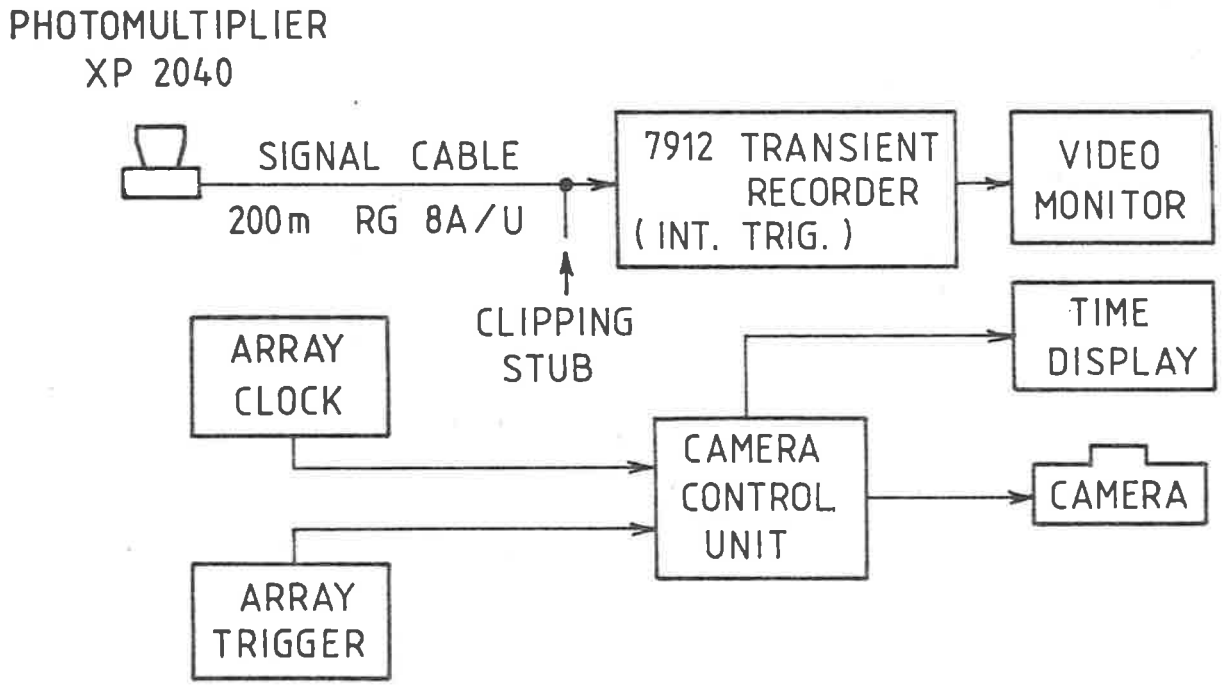

Fig 3.4 A block diagram of the Cerenkov system.

3.3.4 THE SYSTEM RESPONSE

The frequency response of the total Cerenkov system was determined by the observation of noise pulses. One source of such pulses was the Cerenkov light emitted by the passage of high energy, cosmic ray produced, muons through the photomultiplier window. The pulses produced in this way are extremely short (less than 10^{-10} seconds) but do not uniformly illuminate the whole photocathode. These pulses were observed with the photomultiplier covered to exclude other light sources and with the voltage at 1600V to give a suitable gain. A second source of narrow light pulses that was utilized was the night sky. These pulses were presumed to be the Cerenkov light from low energy, high developing showers. In this case, the pulses were observed under the same conditions of photomultiplier voltage and background light as pertained to the actual observations. Pulses of the latter type were recorded regularly to monitor the night to night performance of the system.

A pulse FWHM of 5.3ns was chosen to characterize the system response as this was typical of the muon induced pulses and just less than the shortest pulse width from the night sky. A typical instrumental response pulse is shown in figure 3.5a and the corresponding frequency response of the system in figure 3.5b.

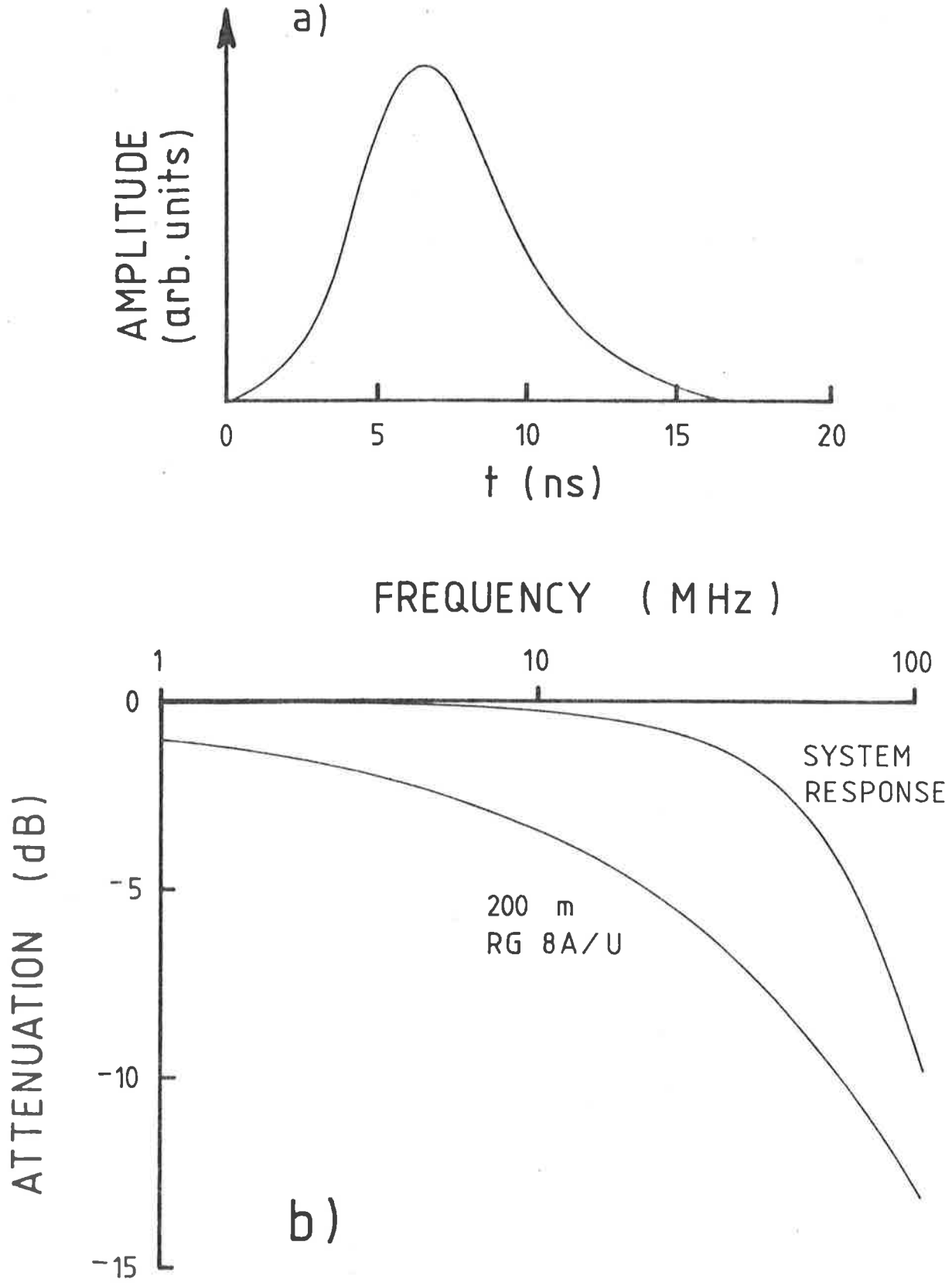

Fig 3.5 (a) An impulse response pulse.
(b) The frequency response of the signal cable and of the total system(normalised to 0dB at DC).

3.4 OPERATING CONDITIONS

The data were collected during the two years 1978 and 1979. The experiment was run on clear, moonless nights. Sky clarity was determined, in the first instance, by direct visual inspection. A further check was provided by a camera automatically taking 30 minute exposures of the sky. Clouds could be detected by dimming or breaks in the star trails.

The photomultiplier was used at a voltage in the range 1500-1550 volts so as to maximize the gain while at the same time maintaining the continuous anode current well below the maximum rating of 200μA. The transient digitizer was operated on a time base of 5ns/division, giving a total sweep of 40ns. Because the Cerenkov pulse arrival time at the photomultiplier may differ from the core impact time by up to 500ns, depending on the shower angle of incidence and the core location, the use of an array trigger would have resulted in an unacceptably large jitter. For this reason, the transient digitizer was triggered internally at a mean rate $\sim$0.1Hz. The output display was photographed on the arrival of a trigger from the particle array. The intensity of the photographed trace, the exposure time of the camera (1/8 second) and the triggering rate combine to produce a less than 1% chance of misidentification of a pulse. (In fact, only one pulse that was accepted for analysis proved to be

clearly anomalous when the particle data for the event was examined.)

The detector was initially placed at various distances from the centre of the array so that the dependence of the FWHM on core distance (r) could be determined from small r up to the limiting distance at which pulses could be efficiently detected. Most of the data were obtained with the photomultiplier either 160m or 205m north of C site. At these positions usable Cerenkov pulses were recorded for about one third of all particle array triggers.

3.5 PULSE INTEGRITY

Due to photoelectron statistics the recorded pulse will not necessarily be an accurate reproduction of the 'real' pulse. A guide to the expected magnitude of the statistical effects can be obtained by using the value of $E_p/10^{11}$eV photons m^{-2} at 300 metres quoted in 2.2.2. Since typical values for the experiment are $E_p \sim 10^{16}$eV and $r \cong 200$ metres, showers will be recorded at typical photon densities in excess of 10^5 photons m^{-2}. The collecting area of the photomultiplier is $10^{-2}m^2$ leading to $\sim 10^3$ photons or $\sim 10^2$ photoelectrons. These numbers indicate that statistical effects may not be insignificant.

In conjunction with a colleague (D.F. Liebing), two photomultipliers were operated at the same site for

a brief period. The two systems were not identical and the pulses cannot be compared directly, but the high correlation between the pulse widths from the two systems indicated minimal statistical effects. Indeed, a comparison of those few pulses with unusual structure showed that the structure was reproduced to a high degree in both systems, eliminating a statistical interpretation of this phenomenon (Thornton et al 1979).

3.6 ALLOWANCE FOR THE SYSTEM RESPONSE

The major difference between the true Cerenkov pulse and the recorded pulse arises because of the limited bandwidth of the system. To recover the true Cerenkov pulse a deconvolution of the instrumental response from the observed pulse is required. The recovery of the FWHM is no less complicated, although it does lend itself to some simplifying approximations.

The convolution theorem states that if σ_o^2, σ_s^2 and σ_c^2 are the variances of the observed system and Cerenkov pulses respectively, then

$$\sigma_o^2 = \sigma_s^2 + \sigma_c^2 \qquad \text{Eq. 3.1}$$

This can be written as

$$a\tau_o^2 = b\tau_s^2 + d\tau_c^2$$

or $$\tau_c^2 = (a\tau_o^2 - b\tau_s^2)/d \qquad \text{Eq. 3.2}$$

where τ is used as an abbreviation for the FWHM and the subscripts have the same meaning as for σ^2. The variables a, b and d, relating τ^2 to σ^2, depend only on the shape of the pulse.

Thus the true FWHM can be determined if a, b and d are known. b is a constant which can be found by measuring the FWHM and variance of an instrumental response pulse ($b \cong 0.5^2$). On the other hand, a and d will vary from pulse to pulse. Measuring the variance of each observed pulse as well as its FWHM, would enable a to be calculated. This requires a large number of measurements per pulse which not only detracts from the simplicity of the FWHM method of determining the height of maximum, but would also have been prohibitively time consuming, a suitable pulse reader/digitizer not being available at the time. Without a full deconvolution to find the shape of the real Cerenkov pulse, d remains unknown.

However, the problem can be simplified by considering two limiting cases. Firstly, when $\tau_c >> \tau_s$ the observed pulse shape will be determined by the real Cerenkov pulse shape and so $a \cong d$ and $\tau_o >> \tau_s$. In this trivial case Eq. 3.2 reduces to

$$\tau_c^2 \cong \tau_o^2 \qquad \text{Eq. 3.3}$$

The second extreme is when $\tau_c << \tau_s$ and the observed pulse shape is dominated by the system response. In this case $a \cong b$ and Eq. 3.2 becomes

$$\tau_c^2 \cong (\tau_o^2 - \tau_s^2)b/d. \qquad \text{Eq. 3.4}$$

If one chooses $f = b/d \to 1$ as $\tau_o^2 \to \tau^2 >> \tau_s^2$ then Eq. 3.4 for small pulse widths also satisfies the conditions for large pulse widths. Hence, if the ratio b/d as well as

the rate at which it tends to unity can be determined, Eq. 3.4 can be used to derive a measure of the true FWHM from the observed value.

It should be stressed that this technique is only useful so long as one is considering averages and cannot be applied to individual pulses whose shape factors will show some variation at a fixed FWHM. Thus a major assumption in this method is that the pulse shape is either well correlated with the pulse FWHM or shows little variation for different core distances or depths of maximum. The former is probably the case. Reference to Eq. 2.21 indicates that for pulses with the same FWHM the ratio r/h is approximately constant, indicating that shower maximum is being viewed at about the same angle. Since it is the angular distribution of the Cerenkov light from an EAS that largely determines the falling edge of the pulse, pulses with the same FWHM should have similar falling edges and, hence, similar overall shapes.

The optimal value of f for small pulse widths can be estimated from trial deconvolutions. Figure 3.6 shows a typical pulse with FWHM≈10ns and the result after deconvolution. The deconvolution was performed using fast fourier transforms with a bandwidth of 200MHz applied to eliminate the inevitable high frequency noise. Some final subjective smoothing was applied and the resultant pulse convolved with the

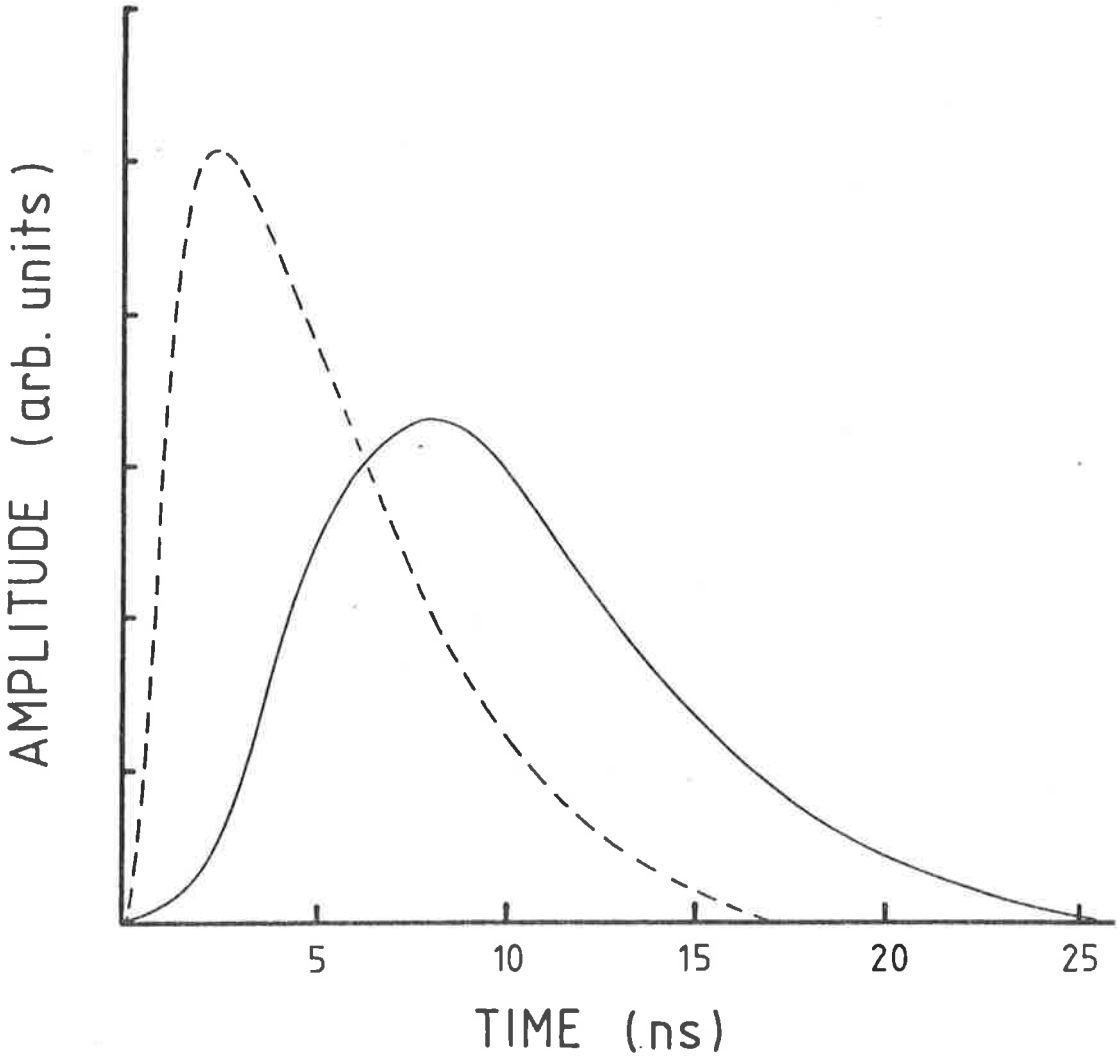

Fig 3.6 A typical atmospheric Cerenkov light pulse (solid line) and the result after deconvolving the system response(broken line).

instrumental response to ensure that it still corresponded to the original observed pulse. In this case f ≅ 0.6. For pulses with observed widths less than 10ns, the deconvolution rapdily becomes more difficult and it is doubtful whether sufficient information has been retained for the true pulse to be extracted with any degree of integrity. For these narrow pulses a value of f = 0.5 was adopted for convenience but it must be recognized that the resultant reduced pulse width will be an overestimate of the (unknowable) true width.

Deconvolutions using larger width observed pulses indicated that f can be considered to have attained a value of unity by the time the observed pulse width was ∿16ns. As a result f was chosen such that

$$f^{-1} = \begin{cases} 2 & \text{if } \tau_o < 9\text{ns} \\ 1 + \exp\left[-[(\tau_o - 9)/4]^2\right] & \text{if } \tau_o \geq 9\text{ns} \end{cases}$$

Eq. 3.5

CHAPTER FOUR

THE DEPENDENCE OF THE FWHM ON EAS PARAMETERS

4.1 INTRODUCTION

In this chapter the dependence of the Cerenkov light pulse FWHM on other shower parameters will be examined and some functional forms of the relationship discussed. The parameters used are:

(i) FWHM or τ: the full width at half maximum of the Cerenkov pulse after correction for instrumental limitations, as discussed in section 3.6.

(ii) $N_e(sl)$: the shower size (electron number) at the observation level as determined by the analysis of the particle array data;
or N_e: the shower size at an atmospheric depth of 1030g cm^{-2} (equivalent to vertical sea-level) inferred from $N_e(sl)$ and the shower incidence angle assuming an attenuation length of 185g cm^{-2}.

(iii) $\cos\theta$: the cosine of the shower zenith angle, also determined from the particle data.

(iv) r: the distance of the Cerenkov detector from the shower core, measured in the plane normal to the incidence direction.

The dependence of the FWHM on the other three parameters will be compared with the results of other Cerenkov pulse width experiments and also used to derive an estimate of the elongation rate for showers with sea-level sizes $\sim 10^6$. The radial dependence will be particularly relevant to the analysis in chapter five. Since there are no strong physical arguments to suggest the exact form the dependences may take, the choice of functional forms considered here will be based on the ease of comparison with other results.

Although the main results will be obtained by regression analysis, most of the data will also be presented graphically as this enables one to gain an appreciation of the dependences, and of the suitability of the functional forms, that cannot readily be obtained from the regression coefficients alone. The actual fit is done by reducing the chosen functional form to a linear form and then performing a multi-parameter linear regression to determine the coefficients of best fit. (The programs used were based on those of Bevington 1969.) All the variation is assumed to be in the dependent variable (the FWHM). This is not an unreasonable approximation since for a fixed value of N_e, $\cos\theta$ and r, the spread found in the FWHM exceeds the combined uncertainties in the determination of the other three parameters. Typical uncertainties in these parameters, based on a mean core distance of

200 metres, a mean angle of 20° and the array performance as described in 3.1.2 are:

$$\frac{\Delta N_e}{N_e} \sim 10\%, \quad \frac{\Delta \cos\theta}{\cos\theta} \sim 3\% \text{ and } \frac{\Delta r}{r} \sim 5\%.$$

On the other hand, the spread in the FWHM is ∿40%. No weighting is applied, so the results are the best fit to the linear form of the function.

4.2 THE DEPENDENCES

Figure 4.1 is a graph of the dependence of the FWHM on r for showers with a mean size near 10^6. (Some additional information may be found in Appendix 1.) An interesting feature is the apparent minimum pulse width at ∿80 metres. The increase towards the shower core should be treated cautiously since the result of the pulse width reduction formula is not particularly meaningful when applied to such narrow pulses (observed FWHM ∿5.5-6.5ns, but only measured to the nearest half nanosecond.) Nevertheless, the effect seems to be real, at least in a qualitative sense. A minimum pulse width at just below 100 metres is predicted by such simple considerations as were used to derive Eq. 2.21, due to the opposing effects on the arrival times of the refractive index and geometric path differences. It is also reproduced in calculations that examine such small core distances (e.g. McComb and Turver 1981b; Patterson and Hillas 1983). This feature was not examined further.

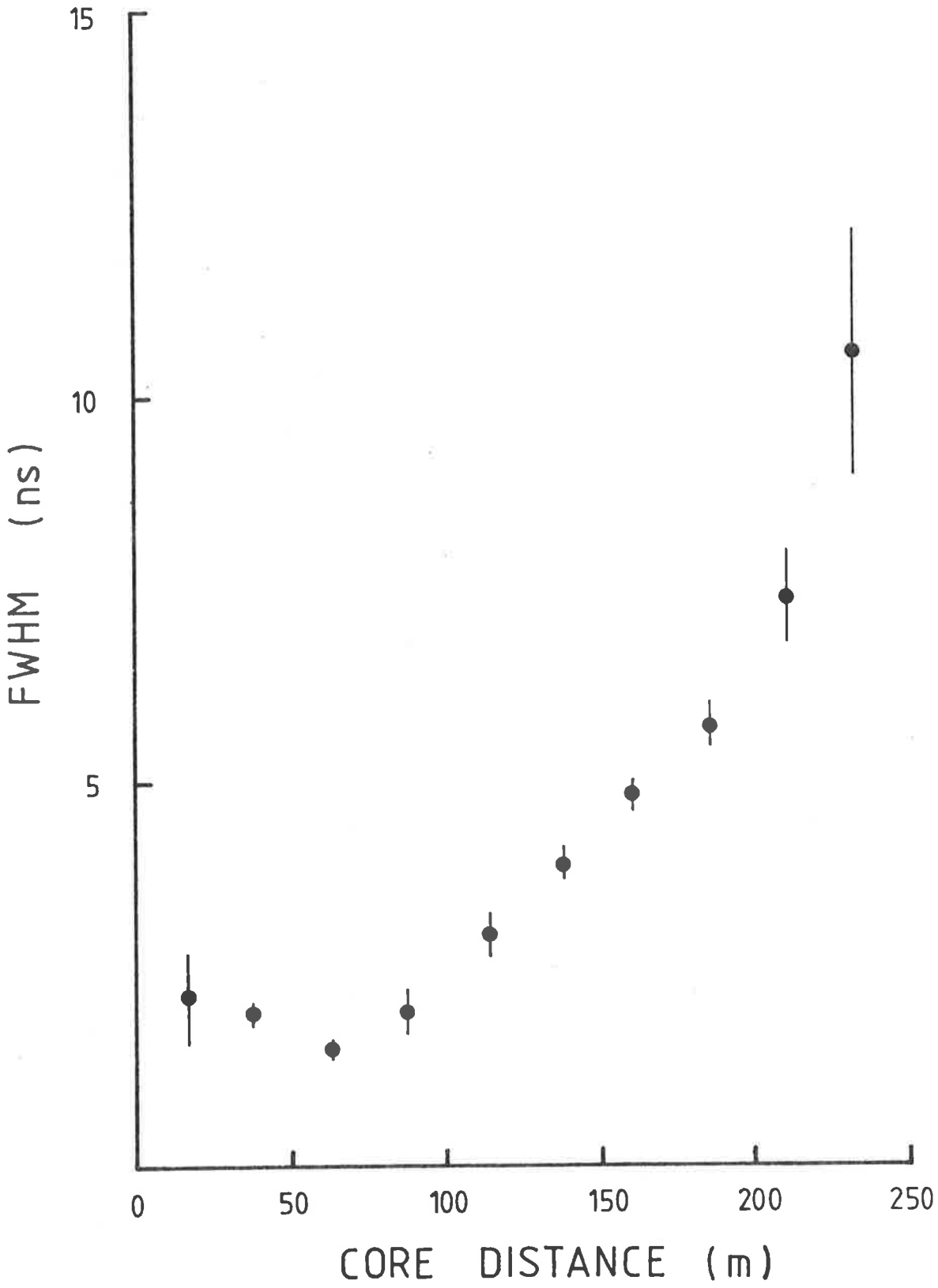

Fig 4.1 The FWHM as a function of core distance for showers with $N_e \sim 10^6$. The errors do not include the contribution from the rounding off of the original pulse widths to the nearest half-nanosecond.

The same effects that lead to the minimum FWHM occurring as r∿80m also result in such "minimum" pulses containing no information about the shower development. Good sensitivity to the shower depth of maximum can only be obtained from pulses whose FWHM are dominated by geometric path differences. Therefore, all subsequent analysis was restricted to events whose core location was at least 150 metres from the photo-multiplier. (Hillas 1982a has suggested that a safer limit would be in the range 170-200 metres.)

Two forms of the radial dependence will be considered:

(i) The Durham group (Hammond et al 1978) have suggested that the radial dependence should be of the form

$$FWHM = a + br^2.$$

In figure 4.2 the FWHM is plotted as a function of r^2 for the same data sample used in figure 4.1. It can be seen that such a relationship will fit the data well.

(ii) The second alternative is a power law. This form has been used to fit the results from Yakutsk (Kalmykov et al 1977, Grigor'ev et al 1978). The suitability of a power law to describe the data can be judged from figure 4.3a

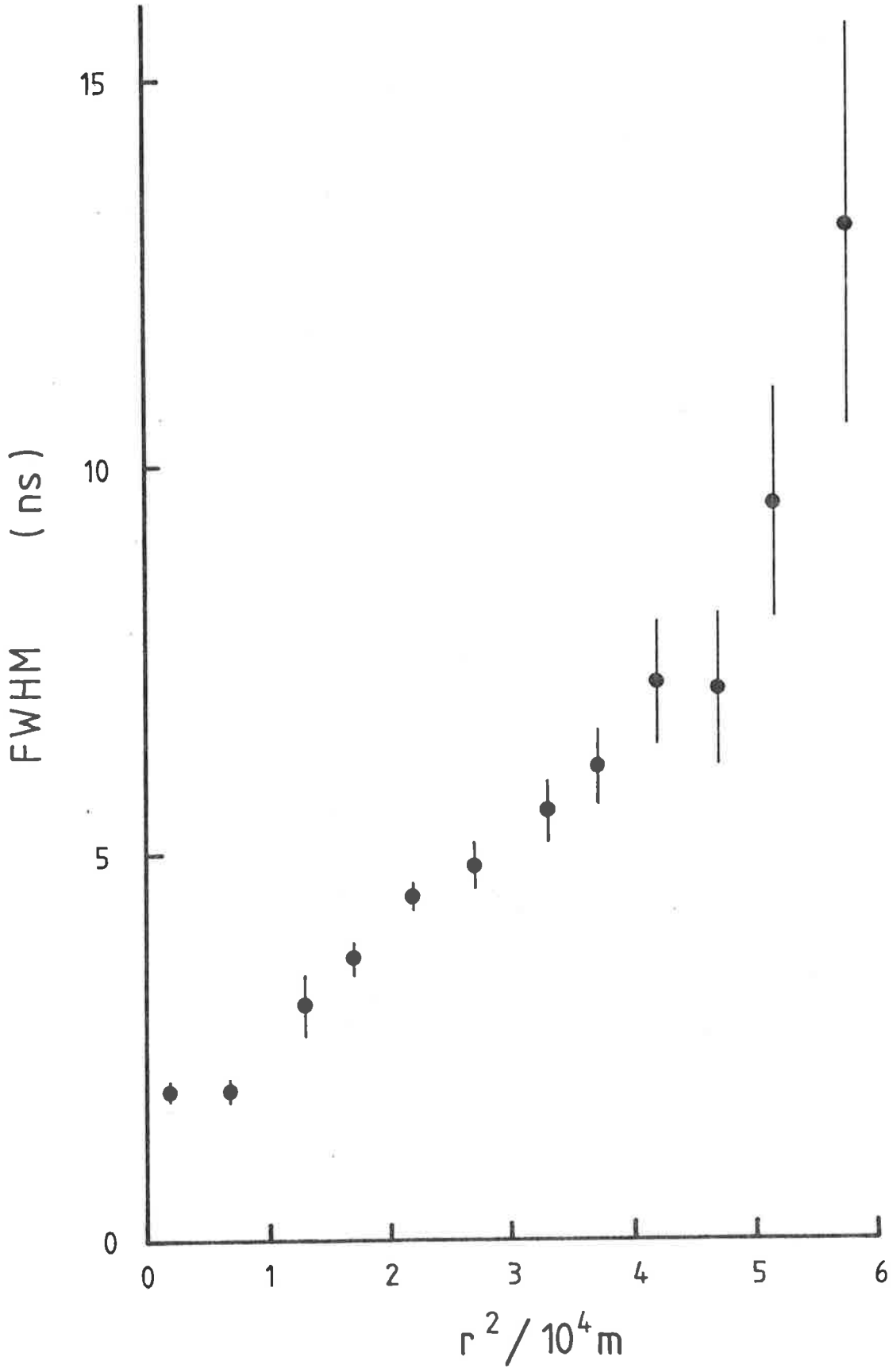

Fig 4.2 The FWHM as a function of the square of the core distance for $N_e \sim 10^6$.

where log (FWHM) is plotted against log(r) for three size bins. It is clear that a power law can be used to fit the data.

It is the latter alternative that will be used for most of the analysis in this chapter. The quadratic form will be considered in section 4.4. The question of the "correct" radial dependence will be discussed in more detail in section 5.1.

There are two sizes in terms of which the data may be analysed. The directly measured shower size, $N_e(sl)$ is the most obvious, but the extrapolated size at a fixed depth, N_e, has the advantage that it should correspond, on average, to constant primary energy, Ep, regardless of the angle of incidence. The main analysis will be performed using N_e but the results obtained using $N_e(sl)$ will also be presented and discussed.

The task then is to incorporate the size dependence into a relationship of the form

$$FWHM = ar^n.$$

The two most simple ways are to make either a or n a function of N_e. From figure 4.3a it is not obvious which is the better choice. A variable exponent has been used to analyse an earlier subset of the current data (Thornton and Clay 1978b), while Kalmykov et al (1979) and Patterson and Hillas (1983) have presented

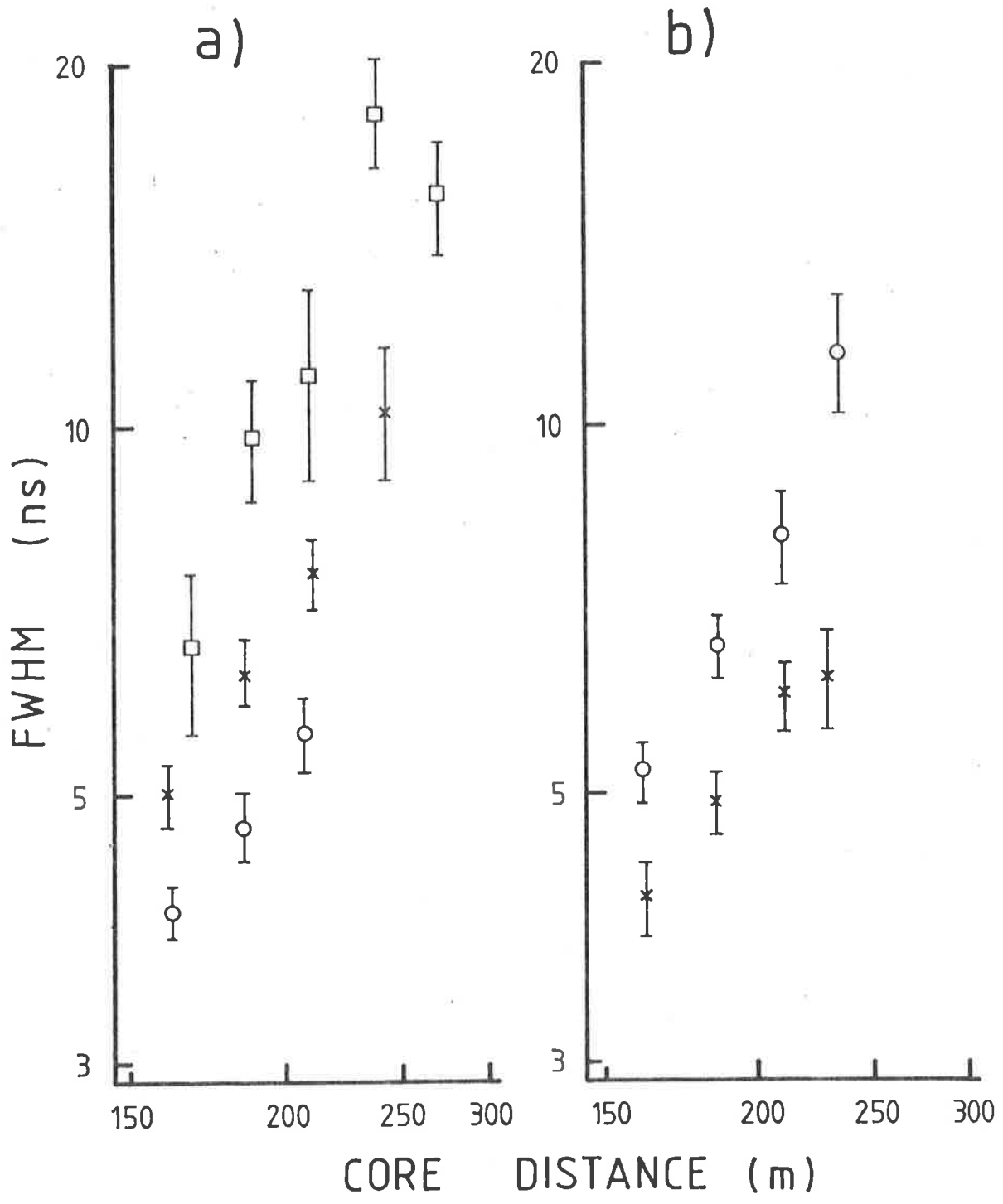

Fig 4.3 Log-log plots of the FWHM as a function of r.
(a) For different size bins: circles-$N_e \sim 4\times10^5$; crosses-$N_e \sim 1{:}4\times10^6$; squares-$N_e \sim 5\times10^6$.
(b) For two angle bins: circles - $\overline{\sec}\ \theta=1.03$; crosses - $\overline{\sec}\ \theta= 1.14$.

the results of calculations which indicate that the exponent depends on the shower height of maximum and hence N_e. On the other hand, Kalmykov et al (1977) also fit their data to a form

$$FWHM = aN_e^{\beta} r^n .$$

This has the advantage that it is separable, which is a useful property in further analysis. This is the form preferred here. The variable exponent case will be examined in section 4.4.

The nature of the angular dependence can be judged from figure 4.3b. There is nothing to suggest that the data should not be fitted by a pair of parallel lines. Hence the angle can be included as a multiplicative factor in the same manner as the size.

4.3 THE FIT

As a result of the previous considerations, the data was fitted to a relationship of the form

$$FWHM = a(\cos\theta)^{\alpha}(N_e/10^5)^{\beta} r^n$$

by means of a multi-parameter linear regression on the logarithms of the parameters. Because no weighting was applied to the data points, the result is the best fit to log (FWHM). The resulting values are

$$\log(a) = -2.84 \pm 0.34 \quad \text{(for r in m and FWHM in ns)}$$

$$\alpha = 3.34 \pm 0.33$$

$$\beta = 0.26 \pm 0.02$$

$$n = 1.51 \pm 0.15$$

The crosscorrelation coefficients are given in table 4.1.

The total correlation coefficient between log (FWHM) and the other parameters is 0.78.

Table 4.1

	log(cosθ)	log(N_e)	log(r)
log (FWHM)	0.24	0.58	0.62
log (cosθ)		-0.25	0.00
log (N_e)			0.44

With over 310 events in the sample the probability of obtaining a correlation coefficient $\gtrsim 0.24$ from an uncorrelated sample is $\lesssim 0.1\%$. Hence, even the apparently low correlation between log (FWHM) and log (cosθ) is significant. The significance of the overall fit can be assessed by testing the hypothesis that the coefficients (α, β and n) are zero. This is done by applying an F-test to compare the variance in the data that is accounted for by the regression with that which is not. The value obtained (F = 164) greatly exceeds the 1% level of $F_{3,310} \cong 4$.

The fit derived in this section can be conveniently written as

$$\text{FWHM} = 1.5\ (\cos\theta)^{3.3} (N_e/10^5)^{0.26} (r/100\text{m})^{1.5}\ \text{ns}.$$

If $N_e(\text{sl})$ is used instead of N_e, then the value of α is 1.7, while the other exponents and the coefficient remain unchanged.

4.4 OTHER FITS

As was previously noted there is not a unique form that can be fitted to the data. In this section

some other possibilities will be examined briefly.

The most important alternative is that preferred by the Durham group for the radial dependence, viz.

$$FWHM = a + br^2.$$

This does not include any terms for the angular and primary energy dependence which are specified separately at a fixed value of r. The same general approach was used to analyse this data. To find the radial dpendence, the FWHM was first reduced to fixed N_e and θ using the dependences from section 4.3. The dependence thus obtained was then used to normalize the FWHM to a fixed r so that the $\cos\theta$ and $\log N_e$ dependence could be obtained.

The results were:

$$FWHM = 1.9 + 1.6(r/100)^2 \text{ ns}$$

for vertical showers and $N_e = 10^6$, while at 200 metres.

$$FWHM = -9.3 + 12.9 \cos\theta + 4.5 \log(N_e/10^5).$$

Another possibility, mentioned in section 4.3, is that of having a size dependent radial exponent. There are two ways this can be expressed which highlight different aspects of the data. They are:

$$FWHM \sim (r/r_o)^{n+b\log N_e}$$

and $$FWHM \sim N_e^{\beta} r^{n+b\log N_e}.$$

It can be easily shown that $\beta = -b\log r_o$. In the first case it is obvious that the FWHM has no size dependence at $r = r_o$. Simple theoretical considerations (see e.g. section 2.2.3) predict that $r_o \sim 80$m. Although

this is outside the range being analysed, it is of interest to see if r_o is of this order. On the other hand, a very small r_o would imply a radial exponent that is essentially constant with size, as assumed in section 4.3. The second expression allows a direct comparison of the amount of the size dependence in the radial exponent to that in the coefficient.

The result of the linear regression was:

$\beta = 0.20 \pm 0.56$

$b = 0.03 \pm 0.25$

$n = 1.45 \pm 0.31$.

The uncertainties in β and b make an estimate of r_o impossible. The large uncertainties arise because only two independent variables have been used to produce three values. As a result these numbers can only be suggestive rather than significant. Also, in view of the deconvolution difficulties, any size dependence in the radial exponent may be masked.

4.5 COMPARISON OF DEPENDENCES

The dependence of the FWHM on other shower parameters which has been derived here cannot be directly compared to the results from Yakutsk and Haverah Park, since those results apply to generally larger showers observed at larger core distances. Nevertheless such a comparison is not without merit and will be useful when the interpretation of the dependences is discussed later.

The Russians (Kalmykov et al 1977, Girgor'ev et al 1978) find for their data

$$\alpha = 2.5 \pm 0.4,\ \beta = 0.06 \pm 0.04 \text{ and } n = 1.7$$

for $10^7 < N_e < 5.10^8$ and $250 < r < 970$ metres.

The α value corresponds to $N_e(sl)$. Using the relationship derived in Appendix 2 a value of $\alpha = 2.9 \pm 0.4$ can be derived for the case of shower size at a fixed depth.

As has been mentioned before, the Durham group assume an $a+br^2$ dependence. They also do not attempt to remove their instrumental response (FWHM = 19ns) from the observed pulses, and they use the Cerenkov density at 500 metres ($\rho(500)VE$) as a measure of the primary energy.

Their results obtained at Haverah Park are

$$FWHM(r) = 2.17 + 2.97(r/100)^2 \text{ ns}$$

for vertical showers with 2×10^{17}eV primary energy and

$$FWHM = -45.14 + 120.3 \cos\theta + 9.92 \log\rho(500)VE$$

at 400 metres (Hammond et al 1978).

The easiest way to compare these results with the others is to derive an equivalent α and β from them. The $FWHM(\cos\theta)^{\alpha} N_e^{\beta}$ form leads to

$$\alpha = \frac{\cos\theta}{FWHM} \frac{\partial FWHM}{\partial \cos\theta}$$

and

$$\beta = \frac{N_e}{FWHM} \frac{\partial FWHM}{\partial N_e}$$

Applying these to the Durham relationship for r = 400 metres (FWHM=69 ns) and making the assumption that the energy

parameter $\rho(500)VE$ is proportional to $N_e^{0.9}$ (see section 2.1.3) one obtains α = 1.7 and β=0.06. (After removal of the instrumental response the values would be slightly larger with α = 2.3 and β=0.08 being likely upper bounds.)

Recent results from the Dugway experiment (Chantler et al 1982) of the Durham group give a value of $\alpha \simeq 2.5$ for $Ep \sim 10^{17}$-10^{18}eV and r = 200-250 metres at a vertical atmospheric depth of 835g cm^{-2}. These results are summarized in table 4.2.

Table 4.2

	r(m)	N_e or E_p	α	β	n
Present work	150-300	$\sim 10^6$	3.3	.26	1.5
Yakutsk	250-970	$\sim 5 \times 10^7$	2.9	.06	1.7
Haverah Park	400	$\sim 2 \times 10^{17}$eV	1.7	.06	2
Dugway	200-250	10^{17}-10^{18}eV	2.5		2

The major differerence between the results of the present work and the results at higher energies is in the size dependence. The value of β obtained here suggests a much larger elongation rate at $\sim 10^{16}$eV than for $E_p > 10^{17}$eV. The general agreement between the results for α and n is expected as these parameters depend largely on geometric factors rather than on shower development. A more formal examination of these parameters will be undertaken in the next section.

4.6 INTERPRETATION: α, β AND THE ELONGATION RATE

Since the thickness of atmosphere traversed by the shower can be calculated from its zenith angle, the parameter α can be used to estimate the dependence of the FWHM on the height of shower maximum. With this information the size dependence parameter β can then be interpreted in terms of the rate of change of depth of maximum with size and hence E_p. Some relationships are derived in appendix 2. The results are

$$x_n = \frac{\partial x_m}{\partial \ln N_e} = x_n [\ln \frac{x_o}{x_m \cos\theta} + 1] \beta/\alpha \qquad \text{Eq. 4.1}$$

and

$$D_{10} = \frac{\partial x_m}{\partial \log E_p} = 2.3/(1/x_n - 1/\lambda) \qquad \text{Eq. 4.2}$$

where x_m is the shower depth of maximum, x_o the vertical thickness of the atmosphere, λ the shower attenuation length, x_n the increase in depth of maximum for an e-fold increase in shower size and D_{10} the rate of change of depth of maximum per decade of primary energy.

An evaluation of Eq. 4.1 requires a knowledge of the depth of maximum. A value of 500g cm^{-2} was chosen as appropriate for $N_e \sim 10^6$ based on a formula given by Allan (1971). The results of this experiment and other experiments confirm that this is indeed a suitable choice of x_m. The various values adopted in

the evaluation of D_{10} are

$$\alpha = 3.3 \pm 0.3 \qquad \beta = 0.26 \pm .02$$

$$x_m = 500 \pm 100 \text{g cm}^{-2} \qquad x_o = 1030 \text{g cm}^{-2}$$

$$\lambda = 185 \pm 20 \text{g cm}^{-2} \qquad \cos\theta = 0.93$$

The elongation rate thus derived is

$$D_{10} = 260 \pm 50 \text{g cm}^{-2}/\text{decade } E_p.$$

Although this result is based on simple considerations the value is so much larger than the accepted "normal" value of $D_{10} \lesssim 100 \text{g cm}^{-2}$ that it must be considered as strong evidence for an unusually large elongation rate for showers with sea-level sizes $\sim 10^6$.

It should be noted that the derivations are independent of the radial behaviour of the FWHM. It would also appear that the result does not depend on the manner in which allowance is made for the system response. Performing the regression on the unreduced pulse widths leads to

$$\alpha = 1.7, \quad \beta = 0.14 \quad \text{and} \quad n = 0.9$$

but the ratio β/α is ~ 0.08. This is close to the value obtained using reduced pulse widths.

As a further check on the validity of the result the same technique was used to determine the elongation rate for the Yakutsk and Haverah Park data, assuming $x_m \sim 700 \text{g cm}^{-2}$ for their showers. The value derived for Yakutsk is $x_n \cong 20 \text{ g cm}^{-2}$ which is in excellent agreement with the value of $x_n = 22 \pm 13 \text{g cm}^{-2}$ derived by Kalmykov et al (1977) by comparing their

FWHM to results of simulations. The value for the Haverah Park data is $D_{10} \cong 100 g\ cm^{-2}$ which agrees with the value of $D_{10} \cong 80 g\ cm^{-2}$ obtained in Hammond et al (1978) on the basis of simulations. Therefore, there can be little doubt about the validity of applying Eq. 4.1 to the derived size and zenith angle dependences to obtain an elongation rate.

In the following chapter results of simulations will be used to determine the actual depths of maximum.

CHAPTER FIVE

THE DEPTH OF MAXIMUM

In the previous chapter the Cerenkov pulse FWHM was examined in terms of its statistical relationship to other shower parameters. The elongation rate deduced from the size and angular dependences of the FWHM was larger than that expected from the elongation rate theorem without invoking a rapid change in one of the contributing factors. In this chapter published relationships will be used to determine depths of maximum for individual showers and thus establish the depth of maximum as a function of primary energy.

5.1 RADIAL EXTRAPOLATION

Kalmykov et al (1979) published the first useful relationship between the FWHM and the shower height of maximum based on shower simulations. The relationship gives the height of maximum as a function of the true FWHM at 300 metres from the shower core. The current data sample has previously been analysed using the "Kalmykov equation" by extrapolating the reduced FWHM to the value it would have at 300 metres, assuming the radial dependence determined by a multivariable regression applied to all the data outside 150 metres, as in section 4.3 (Thornton and Clay 1979b, included in this thesis in appendix 3). The value of the radial exponent

used in this extrapolation has been criticized by Orford and Turver (1980) who believe that the appropriate dependence is of the form $a+br^2$ (see also 2.2.3). These criticisms (and others) have been discussed in another publication (Thornton and Clay 1981, appendix 4) and the matter of radial extrapolation will not be dealt with in great detail here.

The radial behaviour of the calculated FWHM, as well as the results of a convolution with a system response followed by a simple reduction similar to that described in section 3.6 is shown in figure 5.1 (reproduced from Patterson and Hillas 1983). It is clear that in the range 150-300 metres the true FWHM is not well represented by a simple power law, although it might be approximated to one of slope $\sim$3.6. On the other hand, the "deconvolved" FWHM masks some features of the true behaviour in such a way as to be nearly linear over the core distance range of interest with a slope $\sim$1.7 for the example given. Furthermore, extrapolation to 300 metres produces a pulse width in good agreement with the true value at that distance. Thus, for pulses observed at small core distances, the extrapolation to 300 metres, where the observed pulse width is not much different from the real width, fortuitously serves to minimize any errors that may be introduced by the lack of a full deconvolution.

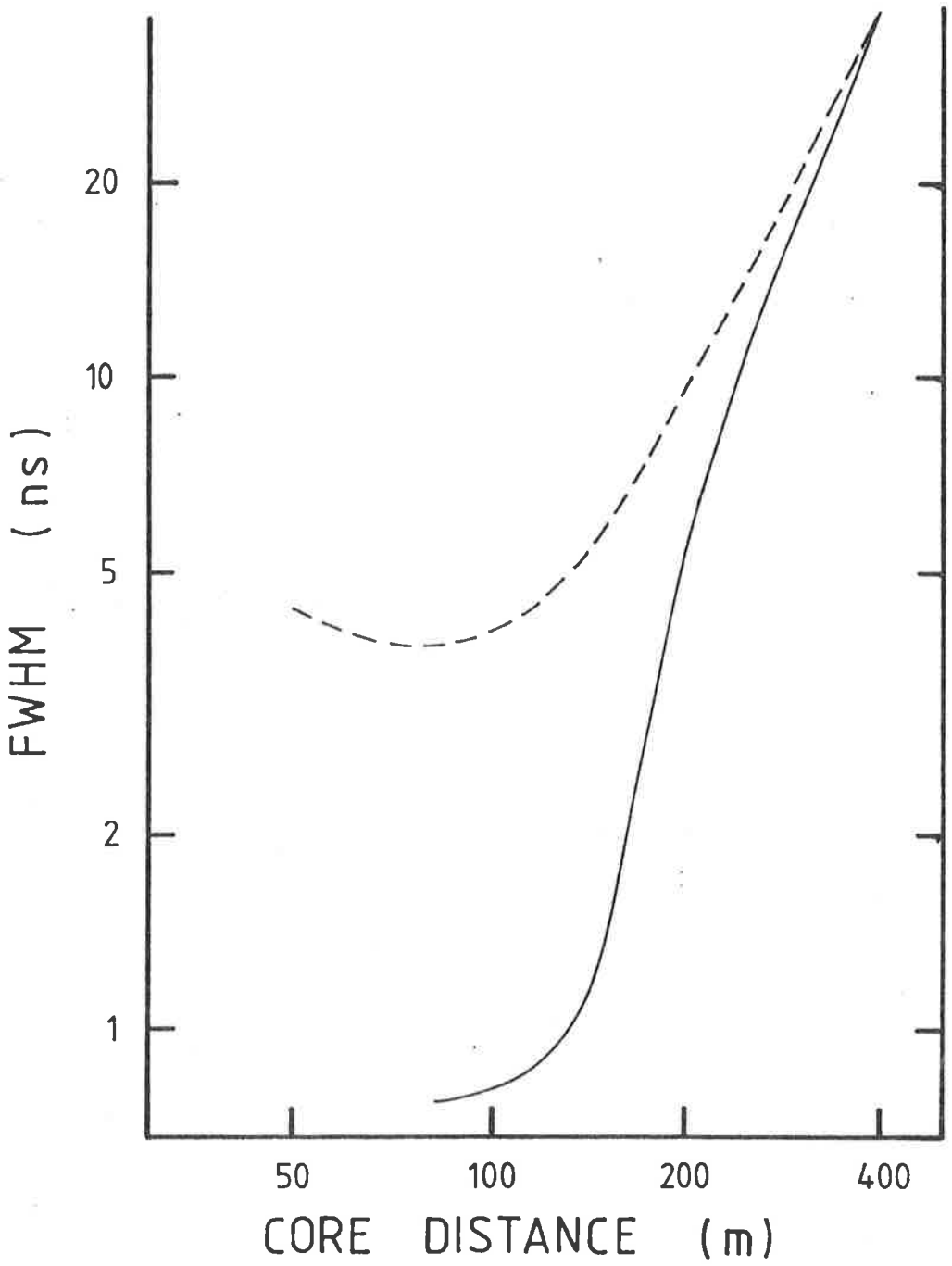

Fig 5.1 The radial dependence of the FWHM calculated by Patterson and Hillas 1983 for a 10^{16}eV proton initiated shower: solid line-the true pulse width; broken line-the result after a convolution with an instrumental response (FWHM= 5ns) followed by removal of the instrumental response by subtracting the FWHM in quadrature.

5.2 THE SIZE DEPENDENCE OF THE DEPTH OF MAXIMUM

The relationship determined by Kalmykov et al (1979) is:

$$h_m = 17.05 - 9.17 \log\tau_{300} \qquad \text{Eq. 5.1}$$

where h_m is the height of maximum in kilometres and τ_{300} is the FWHM at 300 metres in nanoseconds. More recently the simulations of Patterson and Hillas (1983) have produced:

$$h_m = 33.25 - 32.14 \log\tau_{300} + 8.01 (\log\tau_{300})^2 \qquad \text{Eq. 5.2}$$

These results are averages over several zenith angles although Eq. 5.2 appears to be weighted towards large angles (30° and 40°) for h_m>6km, while the sample used to derive Eq. 5.1 does not appear to contain any showers with h_m>6km.

Figure 5.2 shows the depth of maximum as a function of the shower size at a depth of 1030g cm^{-2} (equivalent to vertical sea level). A shower size attenuation length of 185g cm^{-2} (Clay and Gerhardy, 1982a) was assumed. A pressure scale height of 8.0km was used, this value being consistent with both local measurements (S. Young, private communication) and the U.S. Standard Atmosphere. The depths have been calculated in three ways: (i) extrapolating to 300 metres using the radial exponent of 1.5 obtained in section 4.3 and then applying Eq. 5.1; (ii) extrapolating using the $a+br^2$ fit from section 4.4 and Eq. 5.1; and (iii) using a radial exponent of 1.5 and Eq. 5.2. For the sake of

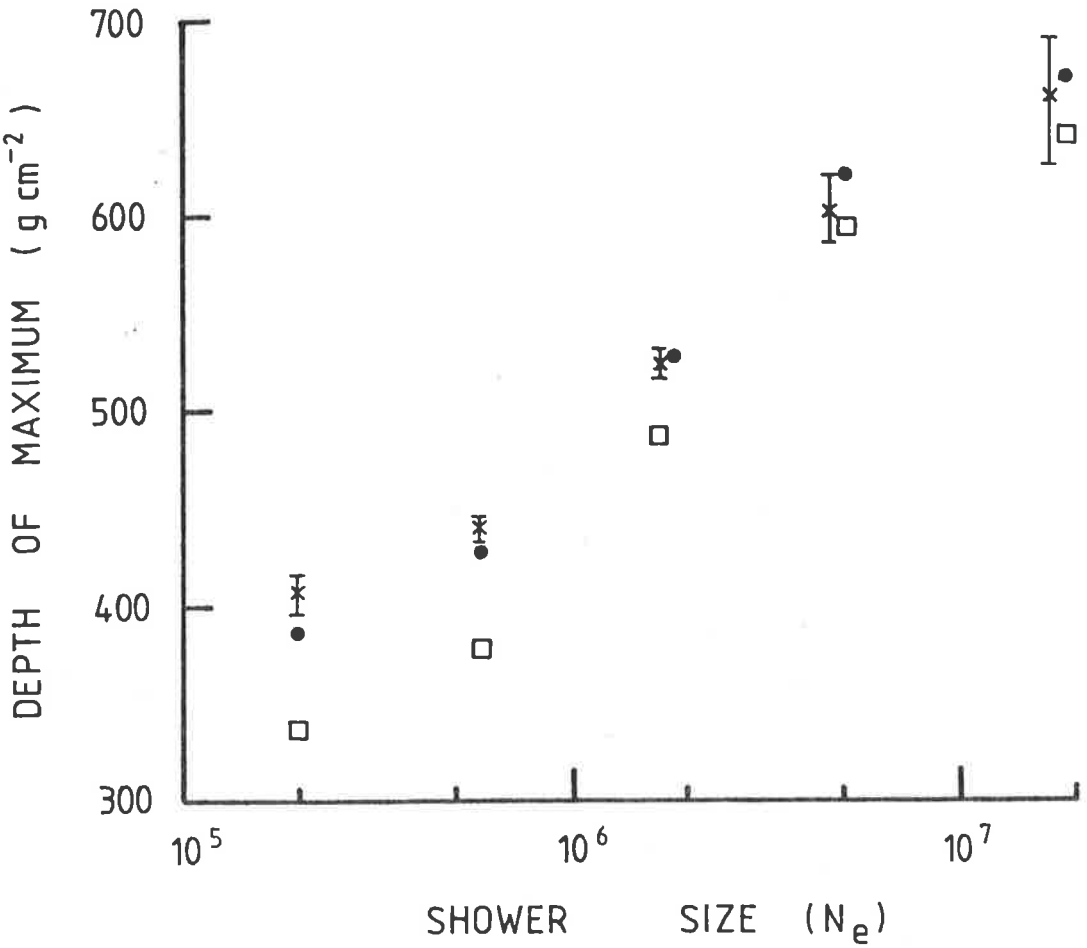

Fig 5.2 The depth of maximum as a function of shower size: crosses-using Eq.5.1 and an $r^{1.5}$ radial extrapolation; squares-Eq 5.2 and $r^{1.5}$; solid points-Eq5.1 and $a+br^2$. In each bin the uncertainties are similar in all three cases. The crosses are at the true bin mean, the others being displaced for clarity.

clarity, error bars are not put on individual points. The single error given for each size bin corresponds to (i) above, but is not much different from that for (ii) or (iii). Uncertainties in core distance, shower zenith angle and the radial exponent (assuming it is a random rather than systematic error) lead to an additional error of about ±50g cm^{-2} in individual depths of maximum but this would only increase the error on the bin mean depth of maximum by ∿10%. (The points are tabulated in appendix 1.)

The general agreement between the results of (i) and (ii) indicate that the radial behaviour assumed in the extrapolation to 300 metres is not critical, although there is a small systematic trend toward a larger elongation rate in the latter case, i.e. using the $\tau = a+br^2$ dependence.

The disagreement between (i) and (iii) becomes significant for showers with x_m<500g cm^{-2}, which is equivalent to h_m>6km for vertical showers. This discrepancy reflects the inability of the equations to represent high developing showers. Almost all the simulated showers on which Eq. 5.1 and Eq. 5.2 are based have depths of maximum greater than 500g cm^{-2}. Although Patterson and Hillas extend the heights of maximum covered to above 6km by using non-vertical showers, it is not clear that the apparent angular independence they find below 6km holds at these greater heights. For such high developing showers, with narrow

observed pulse widths, additional uncertainties are introduced by the pulse reduction and extrapolation which may lead to systematic shifts in the calculated depths of maximum. Thus, where the depth of maximum is less than $\sim$500g cm^{-2} the numbers should be treated cautiously.

For the remainder of this chapter the depth of maximum obtained using the Kalmykov equation (Eq. 5.1) will be used. This leads to the most conservative estimate of the elongation rate.

From figure 5.2 it can be seen that the depth of maximum varies by between 130 and 190g cm^{-2} per decade size, depending on how strongly the result is weighted toward the centre of the data sample. From Eq. 2.10 the above values lead to an elongation rate between 185 and 350g cm^{-2} per decade primary energy. This range agrees well with the value obtained in section 4.6 ($D_{10} = 260$g cm^{-2}) and confirms that the elongation rate for showers with sea level sizes $\sim 10^6$ electrons indicates a rapid change in the primary composition or in the interaction processes. Possible interpretations will be discussed in chapter six. Before proceeding to that, however, the data will be examined in more detail for signs of selection effects that may have biased the result, and the conversion from size to primary energy will be considered.

5.3 SELECTION EFFECTS

Since both a particle and Cerenkov trigger were required in the experiment there will be two possible sources of bias in the data. For example, for shower sizes below $\sim 5 \times 10^5$ the particle array shows a selection bias towards young (i.e. late developing) showers (Clay et al 1981). The Cerenkov system introduces biases because of the limited dynamic range. Pulses are only usefully recorded if they produce a pulse height above the triggering level (5-10mV) and less than the limit of the display (80mV). The pulse height is a function of the primary energy, the depth of maximum and the core distance at which the shower is observed. Complex biases may result if the core distance at which showers of a particular energy produce suitable Cerenkov pulse heights corresponds to regions of poor detection probability by the particle array.

Such biases should manifest themselves as inconsistencies in the dependence of the depth of maximum at a fixed size on other parameters. In particular, effects due to array biases at small sizes should be detectable in the zenith angle dependence since this will involve showers with different sea level sizes but having the same size at equivalent vertical sea level and the same mean primary energy if the sample is unbiased. Because of the steepness of the Cerenkov light pulse height radial distribution ($\sim r^{-3}$, see section 5.4),

selection biases due to the limited dynamic range should be most obvious in the radial dependence of the derived depth of maximum. Unfortunately, subdividing the data to look for such dependences results in a loss of statistics for individual points and this makes a detailed assessment of any biases difficult. The approach adopted here is to divide the data into only two subgroups in such a way that each group contains about a half of the total events. Even this minimal subdivision means that only poor statistics are available in the extreme size bins where biases might be expected to be most obvious. (The data are tabulated in appendix 1.)

In figure 5.3a the data have been divided into two zenith angle ranges with mean slant atmospheric depths of 1060 and 1160g cm^{-2}. (The bracketed point corresponds to only three events.) The trend below 10^6 is in the direction expected if the array preferentially detects young showers at small sizes. The larger zenith angle showers (smaller observed sizes)are fluctuated downwards relative to their near vertical equivalents, although the extent of the difference is not great. The difference at large sizes is unlikely to be related to the array performance but rather to the limited dynamic range. Nevertheless, the overall agreement is good. In figure 5.3b, where the data are divided into core distance ranges, an additional set of data has been included. (The bracketed points at $2x10^5$ and $1.6x10^7$

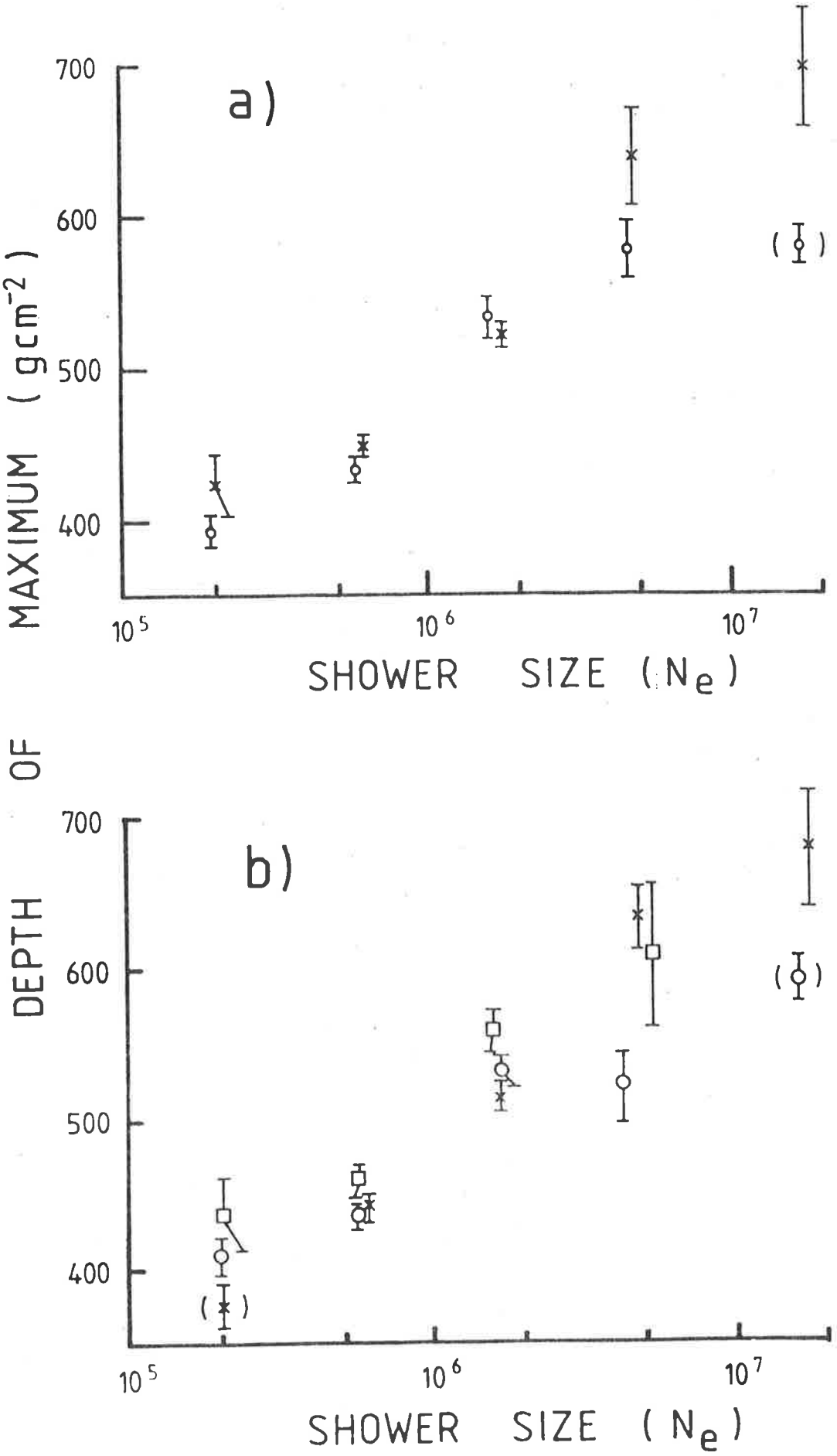

Fig 5.3 The depth of maximum for different angle and core distance bins.
(a) Circles - $\overline{\sec}\ \theta$=1.03; crosses - $\overline{\sec}\ \theta$=1.13.
(b) Squares - $\bar{r}$ = 137m; circles - $\bar{r}$ = 167m; crosses - $\bar{r}$ = 212m.

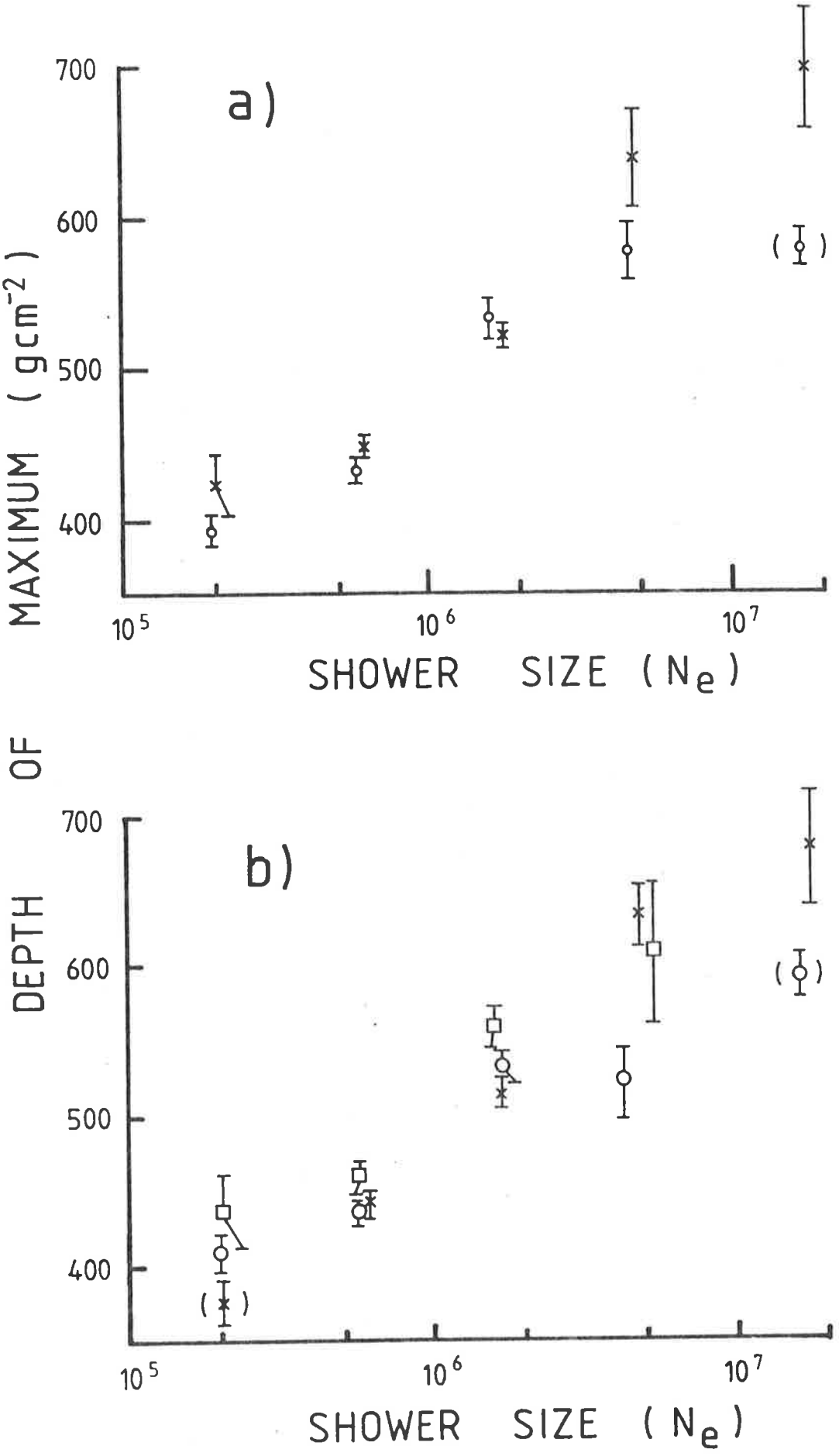

Fig 5.3 The depth of maximum for different angle and core distance bins.
(a) Circles - $\overline{\sec}\ \theta$=1.03; crosses - $\overline{\sec}\ \theta$=1.13.
(b) Squares - $\bar{r}$ = 137m; circles - $\bar{r}$ = 167m; crosses - $\bar{r}$ = 212m.

are based on four and two showers respectively.) The results obtained using showers in the core distance range $120 \leq r < 150$ metres are in surprisingly good agreement with the results for larger core distances. The shift to greater depths of maximum (by ~ 30g cm^{-2}) probably occurs because the radial exponent used to extrapolate to 300 metres is not appropriate for core distances less than 150 metres (see e.g. figure 5.1). It would seem that even at core distances less than 150 metres the Cerenkov pulse FWHM retains a useful sensitivity to the shower development. Once again the overall agreement between the different ranges is good. In view of the points for the other two bins at 5×10^6, the point for $150 \leq r < 185$ metres does not seem to represent a significant trend.

Although there is some suggestion of biases in the extreme size bins, the general impression is that the data is a representative size sample, particularly near 10^6 particles where there is the most data and the apparent elongation rate is greatest. Figure 5.4 shows the depth of maximum as a function of the shower size at equivalent vertical sea level, incorporating the uncertainities discussed in this section. Included in the figure are the results of Kuhlmann (Kuhlmann and Clay 1981) and Liebing (1983). The former, being the result of a Cerenkov lateral distribution experiment which uses a large number of detectors, should be relatively unbiased since in almost every event a lateral

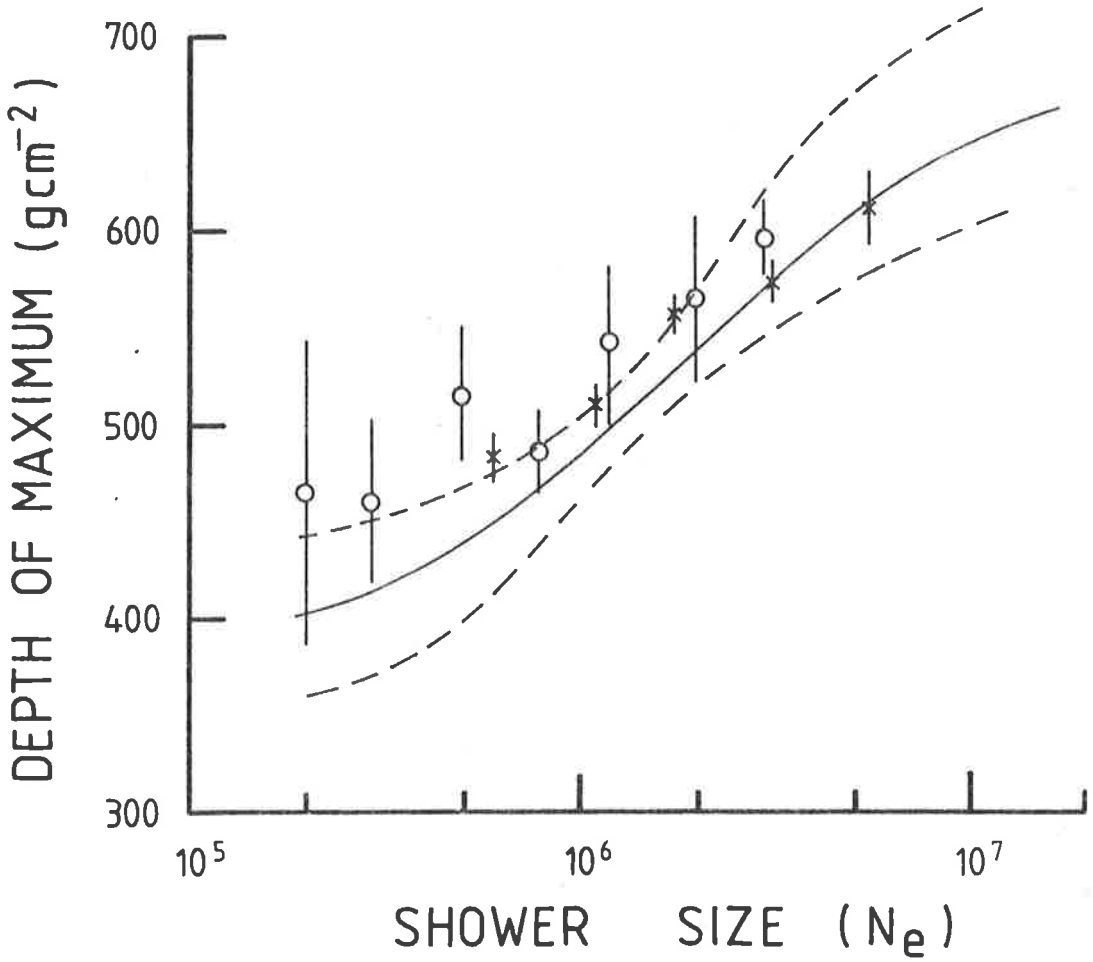

Fig 5.4 The depth of maximum as a function of shower size: circles- Kuhlmann and Clay 1981; crosses- Liebing 1983; the solid line represents the results of figure 5.2 while the broken lines indicate the uncertainties suggested by figure 5.3

distribution would be obtained. The Liebing results are based on Cerenkov FWHM measurements using several separated detectors which will minimize the effects of the limited dynamic range of the individual systems. For shower sizes greater than 2×10^6 the results of all three experiments are in good agreement. Below that size the data of Kuhlmann and Liebing favour a larger depth of maximum than indicated by the current experiment, although their results are not inconsistent given the uncertainity range that has been estimated here. A way in which an unbiased sample might be obtained from the data will be discussed in the next section.

5.4 THE ENERGY DEPENDENCE OF THE DEPTH OF MAXIMUM

The primary energy is a more useful (and more usual) parameter than the shower size in EAS studies. In 2.1.4 it was shown that a relationship between shower size and primary energy can be deduced from a calibration point and a knowledge of the size dependence of the depth of maximum. In this section the latter information will be used initially to establish a parameter proportional to primary energy. Later, the actual conversion to E_p will be considered.

The two characteristics of EAS that are used to establish an energy parameter are the proportionality of E_p and the size at maximum (Eq. 2.5) and the almost constant attenuation past maximum. The shower size at a fixed depth past maximum will be proportional to

$N_e(x_m)$ and hence to E_p. To minimize the amount of extrapolation involved, the depth for which this new size was calculated was chosen as (x_m+550)g cm^{-2}. This corresponds to vertical sea level (1030g cm^{-2}) for a shower size of about 10^6.

The conversion from N_e to $N_e(x_m+550)$ can be performed in two ways. The first is to convert the points from figure 5.2 directly, i.e. to convert the average N_e to an average $N_e(x_m+550)$. Each point moves towards $N_e=10^6$ by an amount proportional to (x_m-480)g cm^{-2} and the nett result is a non-linear contraction of the horizontal scale of figure 5.2. The points obtained in this way are the crosses in figure 5.5. The alternative is to determine $N_e(x_m+550)$ for individual showers and then find the appropriate means for the rebinned data. This technique results in the squares in figure 5.5. The only agreement between the results of the two methods is that at 10^6 the depth of maximum is about 480g cm^{-2}. (This is NOT because 10^6,480 was chosen as a standard point.)

If one accepts the conclusion to section 5.3 that the size sample is not particularly biased and that the depth of maximum at any size is, therefore, that appropriate to the average energy producing that size, the two results can only be reconciled if the energy sample is strongly biased (to beyond the extremes indicated in figure 5.4). Figures 5.6a,b show the

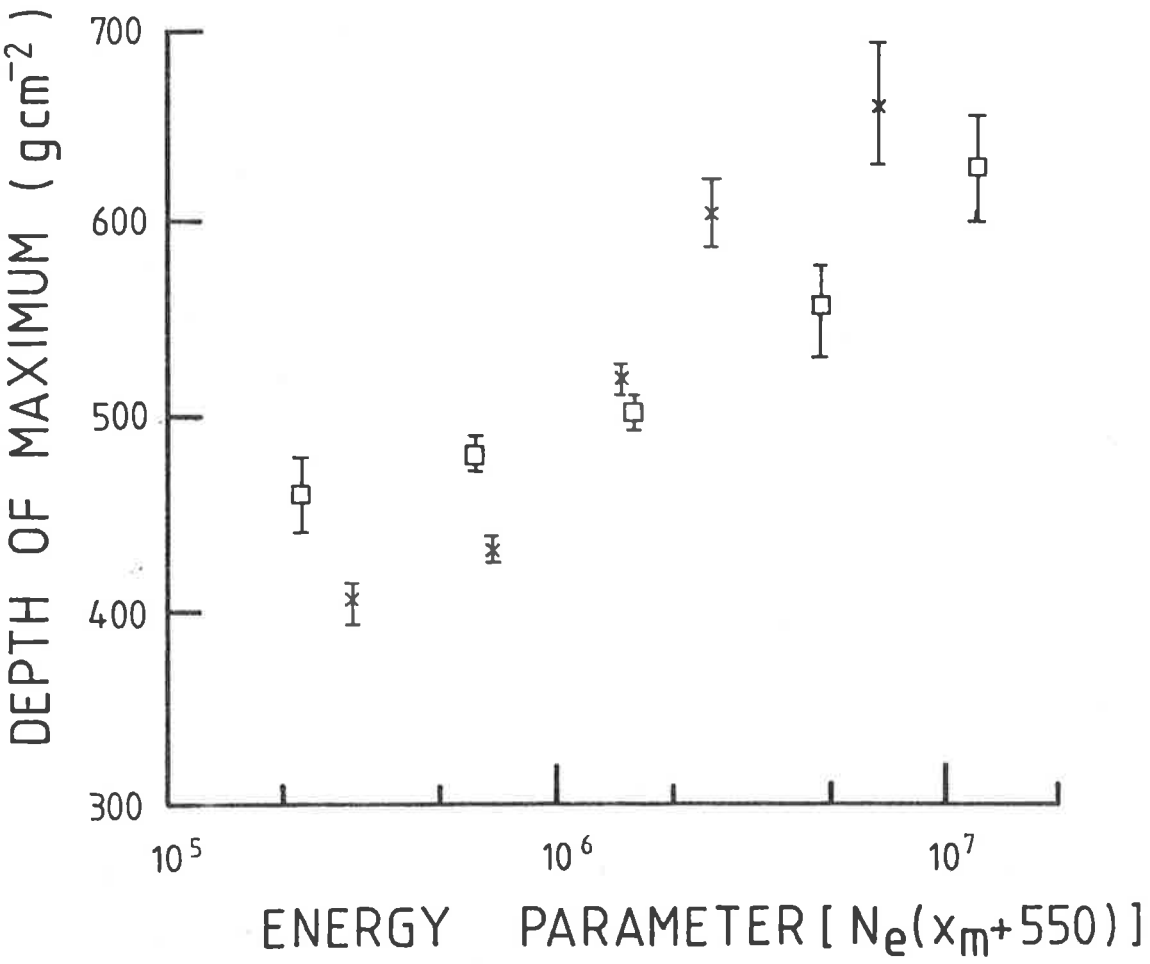

Fig 5.5 The depth of maximum as a function of the energy parameter, i.e. the size at 550g cm^{-2} past maximum: crosses- direct conversion from the crosses of figure 5.2: squares- the results obtained by calculating N_e (x_m + 550) for individual showers and rebinning.

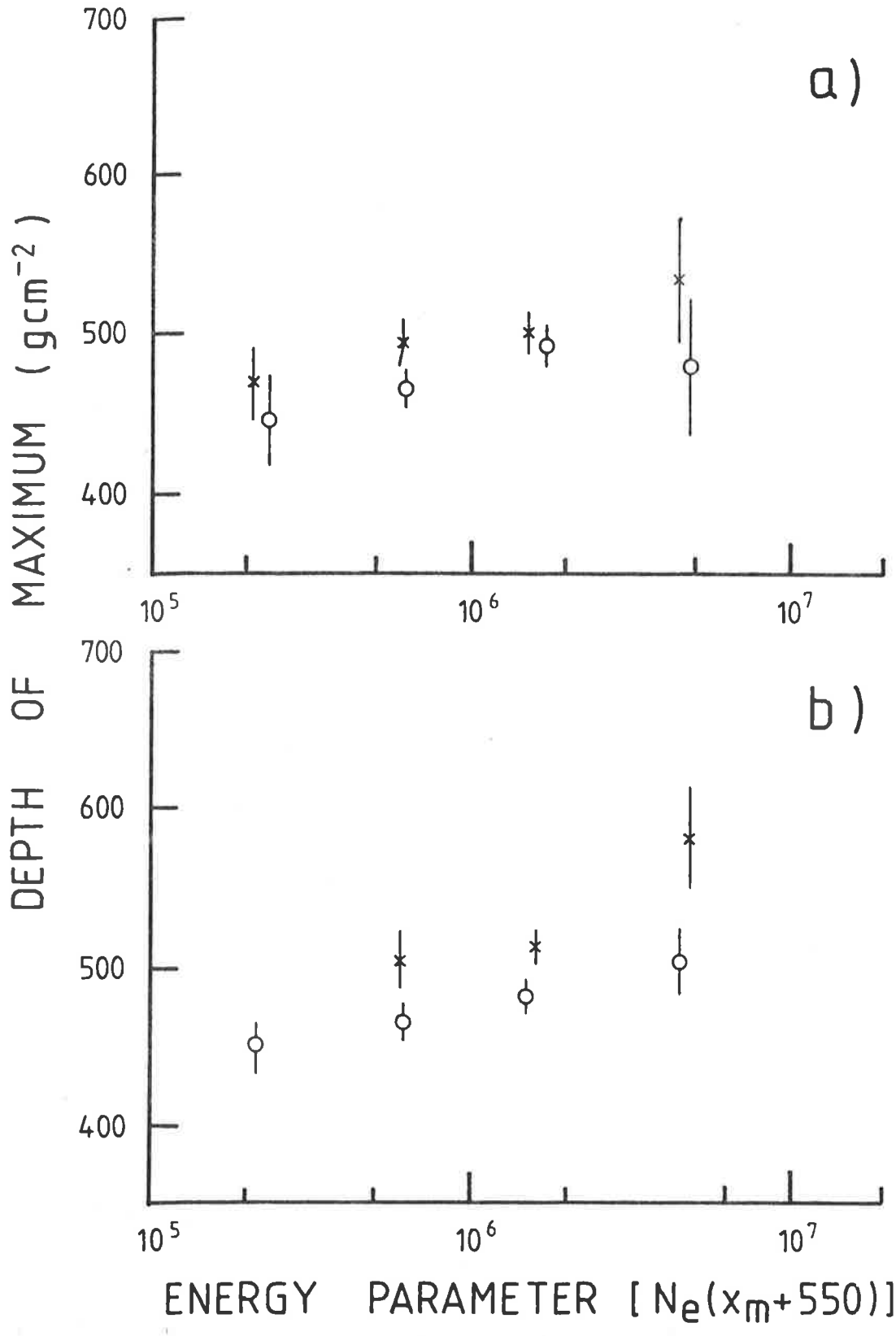

Fig 5.6 The depth of maximum for different angle and core distance bins.
(a) Circles - $\overline{\sec}\ \theta=1.03$; crosses- $\overline{\sec}\ \theta= 1.12$
(b) Circles - $\bar{r}$ = 167m; crosses - $\bar{r}$ = 212m

data subdivided in zenith angle and core distance ranges as were used in figures 5.3a,b. In figure 5.6a it can be seen that there is a consistent ($\sim$30g cm^{-2}) difference between the zenith angle bins. The radial dependence in figure 5.6b is even more extreme. These plots confirm that the biases are mainly in the energy sample. The same sources of bias as were discussed in section 5.3 will apply here. These biases will now be considered quantitatively so that a less biased sample can be selected.

In figure 5.7 $N_e(x_m+550)$ is plotted as a function of the core distance for individual showers ($r \geq 120$m). Some trends are evident. The bulk of the data is bounded on the lower right by a line running from the point in the top right hand corner to the point $(170, 10^5)$. There appears to be a similar, but less well defined, boundary on the upper left. There is also a paucity of points for sizes below 3×10^5.

The lower side features can be related to the particle array performance. The spectrum of detected shower sizes peaks at 3×10^5. Below this the effective area rapidly decreases to zero just below 10^5. This explains the shortage in the sample of showers with $N_e(x_m+550) < 3\times10^5$ and also means that showers in this region which fluctuate downward in the atmosphere, producing larger sea level sizes, will have much greater detection probabilities than upward fluctuating showers

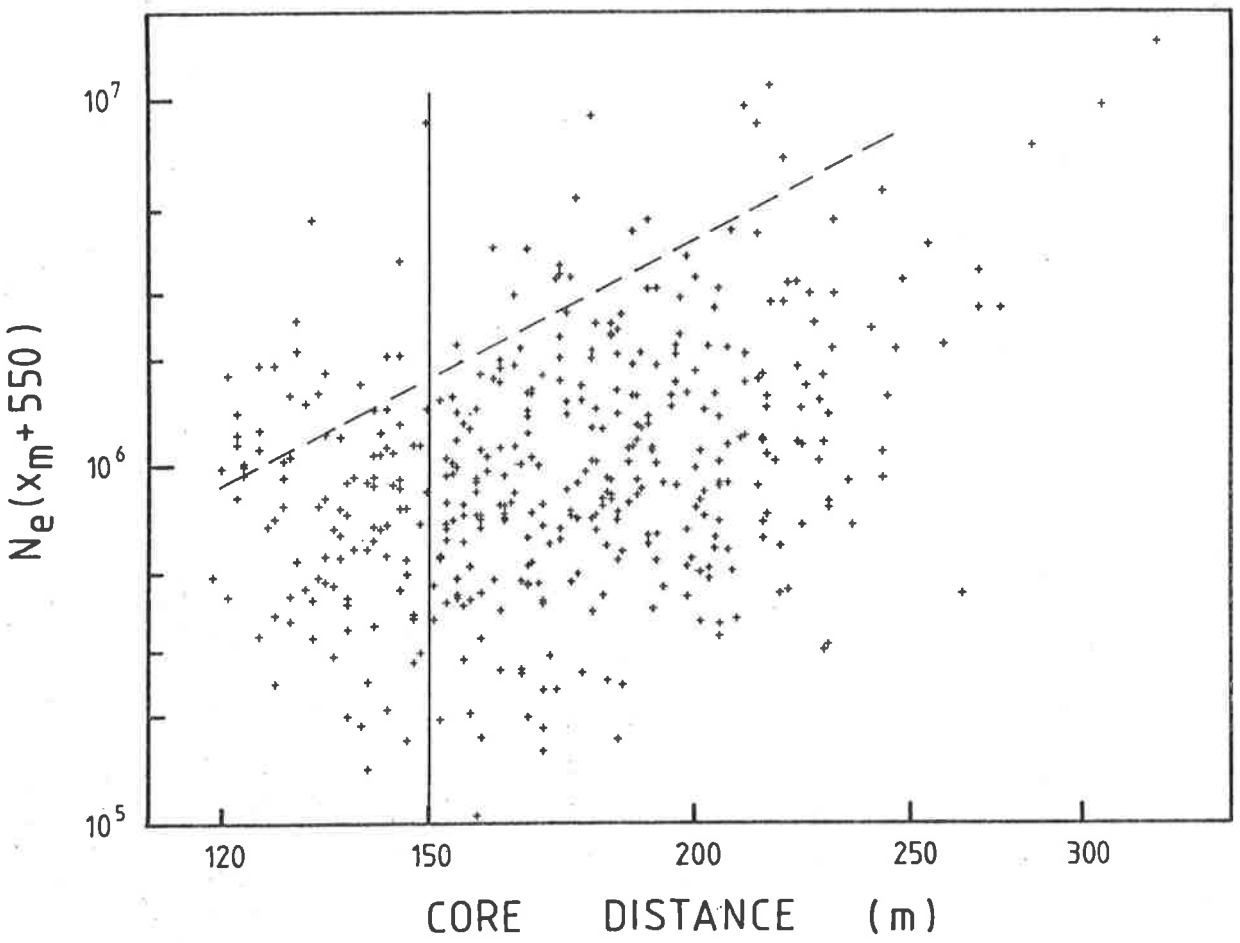

Fig 5.7 A scatter plot illustrating the distribution of observed showers with respect to core distance and energy parameter. The broken line indicates the slope expected for a cut-off due to dynamic range limitations for a fixed depth of maximum.

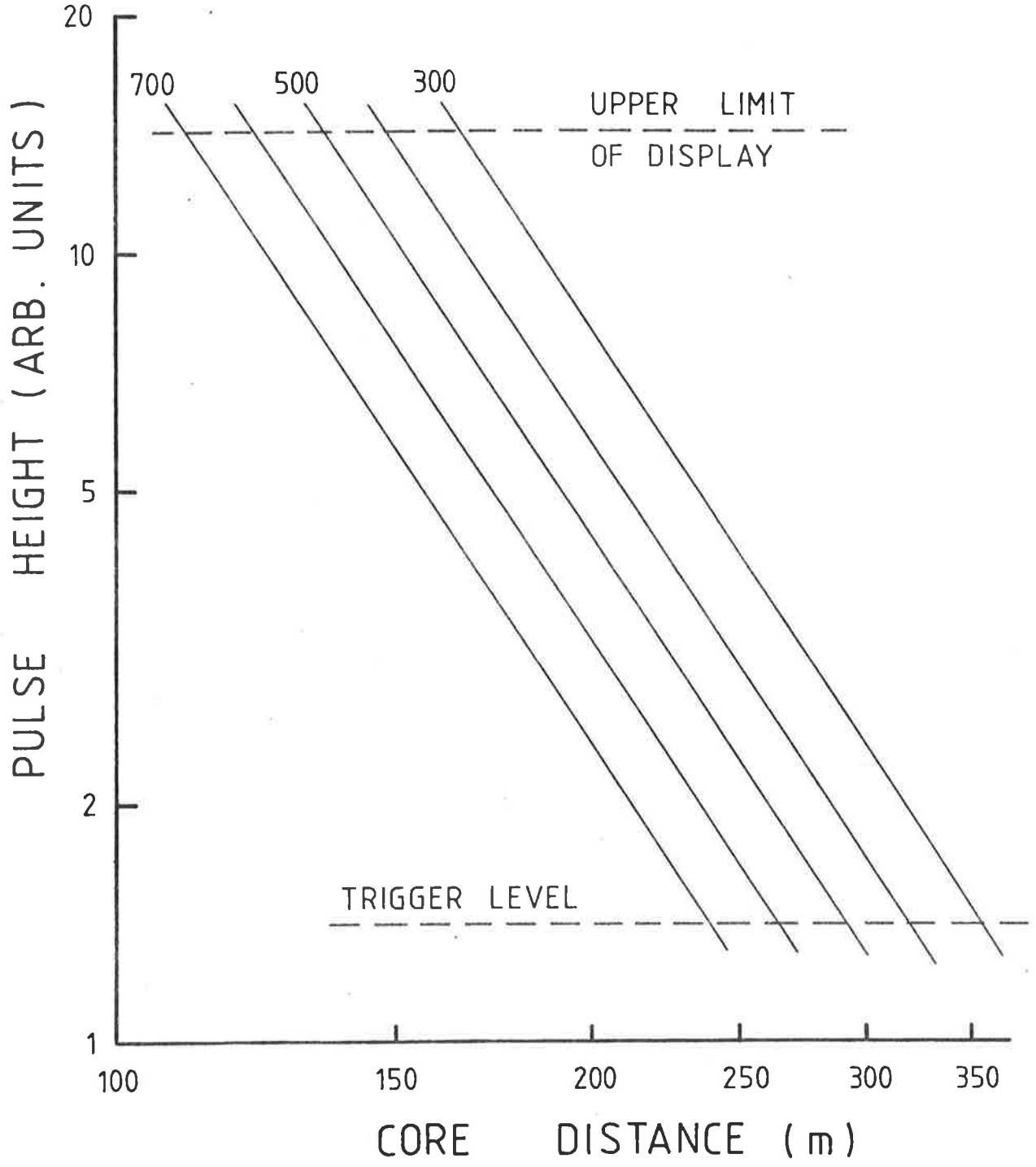

Fig 5.8 Approximate pulse height distributions for showers of an arbitary energy and depths of maximum varying between 300 and 700g cm^{-2}. It is clear that only over a restricted distance range will pulses be recorded independently of the depth of maximum.

of the same energy. Above $3x10^5$ the collecting area varies much more slowly with size and above 10^6 there is unlikely to be any significant array bias in general, although some bias may exist near the edge of the detecting area which is presumably marked by the lower right boundary in figure 5.7.

The upper left bound can be interpreted as a limit imposed by the dynamic range of the Cerenkov system. How the effects of a limited dynamic range can be counteracted can be considered with the aid of figure 5.8 in which approximate Cerenkov pulse height distributions are given for an arbitrary primary energy and various depths of maximum. The distributions are based on simulations which indicate that the Cerenkov flux lateral distribution has an approximately r^{-2} dependence between 150 and 300 metres (see e.g. McComb and Turver 1981b; figure 2.2 in this thesis; Hillas 1982a). The total flux has been divided by the FWHM which is based on the Kalmykov relationship, Eq. 3.5 and the approximation that the observed FWHM $\propto r$ (see section 4.6). Two horizontal lines representing the upper and lower limits of the dynamic range are included in the diagram.

For the example given in figure 5.8 there is only a narrow range ($170 \leq r \leq 220$m) in which all showers (of the particular E_p) are observed irrespective of flunctuations in their depth of maximum between 300 and 700g cm^{-2}. Dynamic range induced biases can be

eliminated by only considering events whose core distance lies within the "safe" range for the particular energy. A correspondence between figure 5.8 and the experimental situation can be established by reference to figure 5.7 where the broken line is an estimate of the upper dynamic range limit for most of the showers. This is assumed to correspond showers with $x_m \lesssim 600$g cm^{-2} at 10^6 based on the observed distribution of x_m (figure 5.9). This provides a calibration point which is approximately 10^6, 125 metres and 600g cm^{-2}. The lower limit of the dynamic range has been chosen as a tenth of the upper limit. Because the Cerenkov flux at a given distance is proportional to E_p and the pulse height distributions $\sim r^{-3}$ the radial limits vary as $N_e(x_m+550)^{1/3}$ for a fixed x_m.

Array based biases were reduced by eliminating those events whose observed size would have been below 3×10^5 if $x_m<350$g cm^{-2}. This removes all events with $N_e(x_m+550)<6\times10^5$ and many of those above that size, depending on their zenith angle. The radial limits imposed to minimize dynamic range bias are such that they also eliminate most showers whose cores fall near the array detection limit.

The foregoing considerations are not intended to provide a rigorous set of restrictions that will lead to an unbiased sample, but rather should be viewed as an attempt to identify the relevant selection effects and the areas in which they will be most pronounced, so

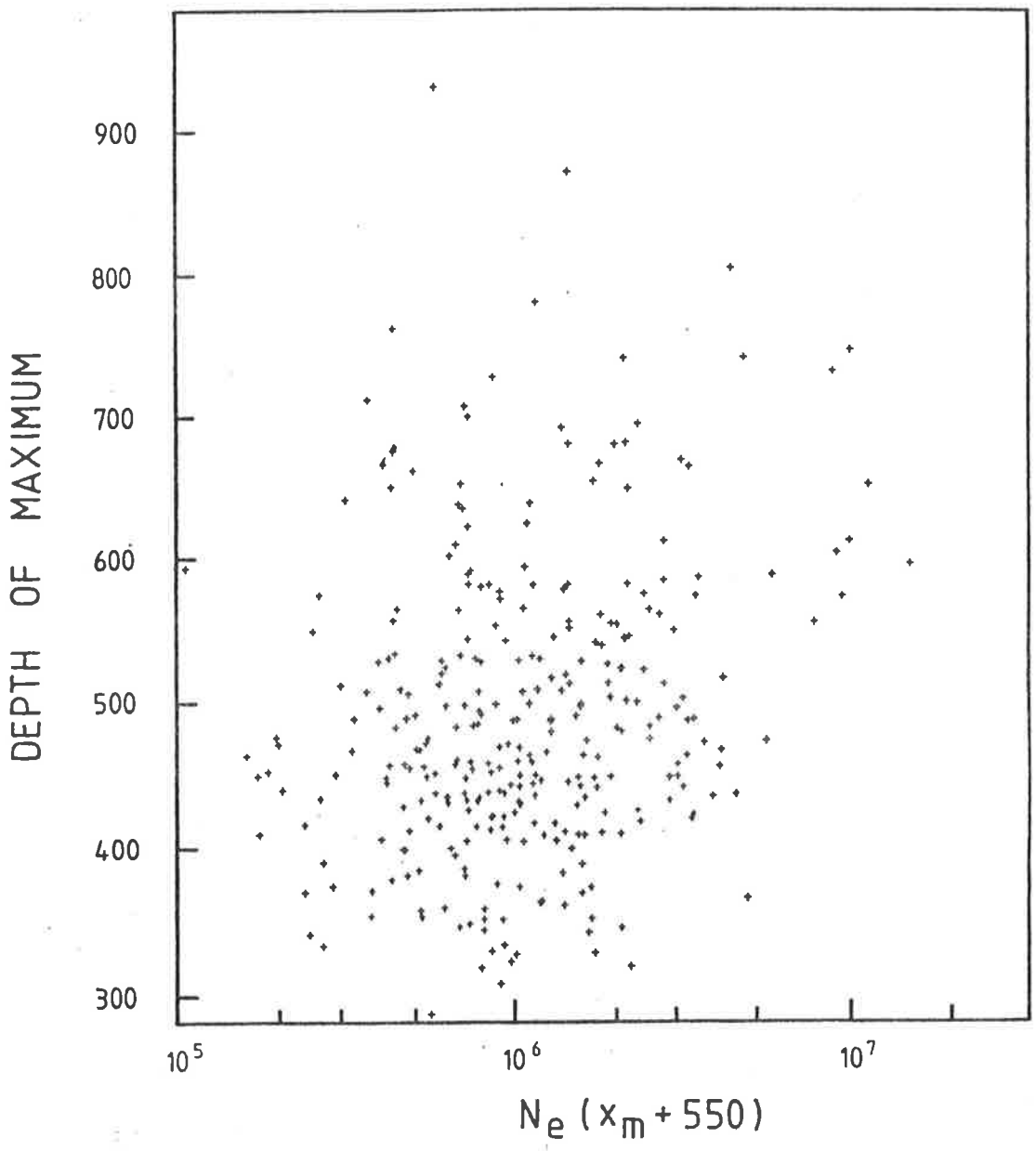

Fig 5.9 The depth of maximum distribution of the observed showers.

that a less biased sample may be extracted from the total data set. In essence, the restrictions imposed amount to little more than eliminating those showers that lie near the edges of the data sample in figure 5.7.

The data were initially analysed with the following constraints:

$$N_e(x_m+550) > 6\times10^5 \exp([\sec\theta-1]1030/185) \qquad \text{Eq. 5.3}$$

and $$10^6(r/220)^3 < N_e(x_m+550) < 10^6(r/170)^3 \qquad \text{Eq. 5.4}$$

The results are shown in figure 5.10 (the crosses). The data between $10^{6.0}$ and $10^{6.5}$ have been rebinned into quarter decade bins to give a better spread of points. The solid line is a smooth curve drawn through the crosses from figure 5.5 and corresponds to the direct conversion of the N_e bins to $N_e(x_m+550)$. In this case the conversion of individual showers agrees well with the bin mean conversion, unlike the case in figure 5.5. A second, less stringent, radial limitation was also used to select a data subset. It was based on the assumption that the lower limit for x_m could be raised from 300g cm^{-2} at 10^6 to 500g cm^{-2} at 10^7. Reference to figure 5.9 indicates that this is not an unreasonable assumption. In this case the upper size limit in Eq. 5.4 becomes $10^6(r/170)^{4.2}$ for r>170 metres. The resulting points are the circles in figure 5.10. The two lowest size points are not shown as they are almost exactly the same as the crosses. (As usual, the points are tabulated in appendix 1.) Once again a large elongation rate ($\sim$200g cm^{-2}/decade) is apparent.

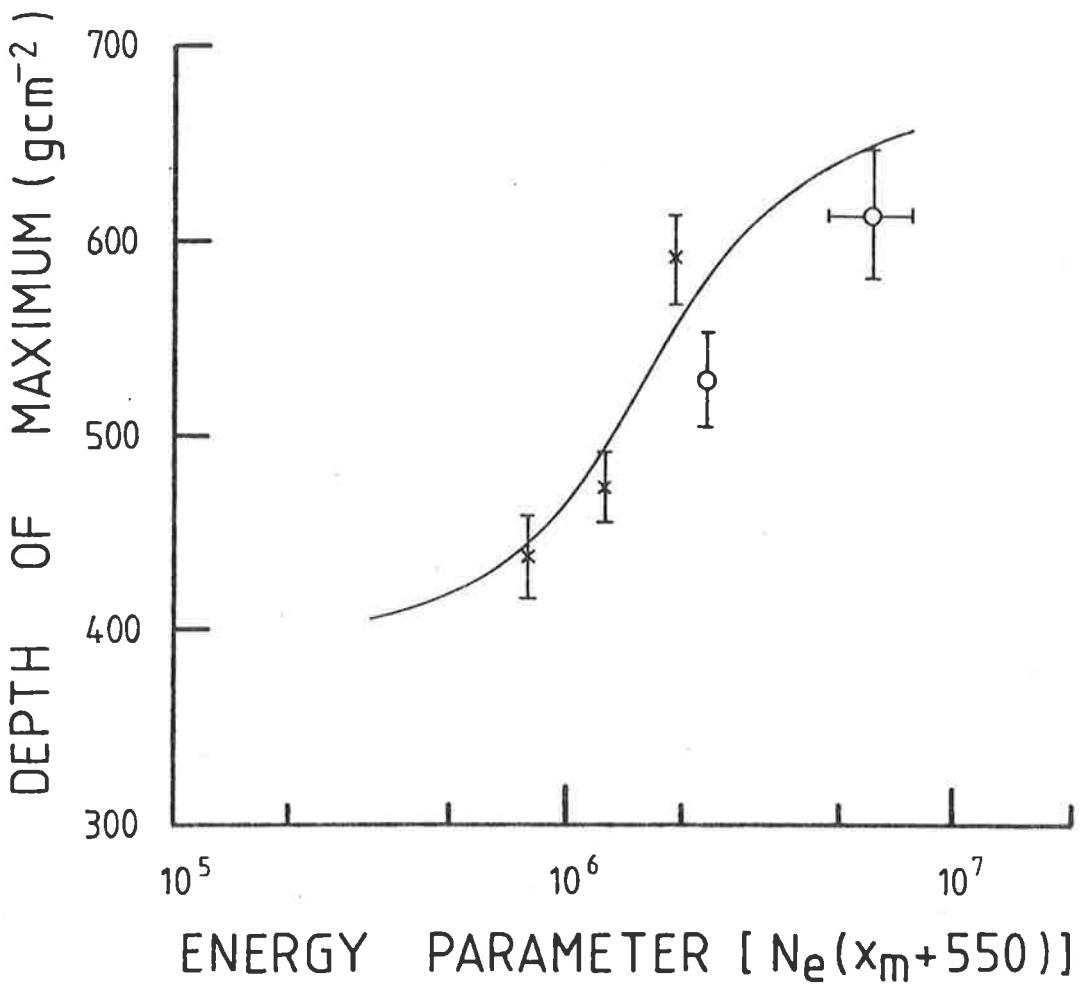

Fig 5.10 The dependence of the depth of maximum on the energy parameter for a restricted sample of showers: crosses-showers chosen using Eq 5.3 and Eq 5.4; circles-using a modified version of Eq 5.4; the line is a smooth curve drawn through the crosses of figure 5.5.

The results displayed in figure 5.10 confirm the basic validity, for this experiment, of obtaining the energy dependence of the depth of maximum by a direct conversion of the size binned data. Nevertheless, it is clear that this will not be true in general but will depend on the nature of the selection effects specific to a particular experiment.

Having established the dependence of the depth of maximum on the energy parameter $N_e(x_m+550)$ it is now useful to convert that parameter to the primary energy, E_p. The later part of the shower development has been measured by the method of equi-intensity cuts and for $E_p > 10^{16}$eV the shape of the development curve from 550g cm^{-2} to $\sim$1400g cm^{-2} is well established, although some doubts still exist about some absolute size assignments. (For some more recent results see Danilova et al 1977, Aguirre et al 1979, Clay and Gerhardy 1981 and Hara et al 1981). The corresponding primary energy can be calculated from the integral track length with only minor corrections required for non-ionization energy losses. The result is fairly model independent although simulations are needed to estimate the shape of the curve above 550g cm^{-2}. Hillas (1975, 1979) has performed the necessary calculations and on the basis of his results the conversion adopted here is:

$$E_p = 10^{10} N_e(x_m+550) \qquad \text{Eq. 5.5}$$

Unless the early part of the shower development is

radically different from what is generally accepted, the uncertainty in the conversion factor is probably about 30%.

The energy dependence of the depth of maximum that has been determined here is shown in figure 5.11 as a shaded region rather than a set of data points because the uncertainties discussed in sections 5.3 and 5.4 can be neither totally eliminated nor readily quantified. The crosses in the figure are points obtained at Akeno (Inoue et al 1981) using the Cerenkov FWHM and the Kalmykov relationship, while the circles and squares are the results obtained by the Durham group's Dugway Cerenkov lateral distribution and pulse shape experiments respectively (Andam et al 1982, Chantler et al 1983). The agreement between the three sets of results are excellent above 3×10^{16}eV while at lower energies the Akeno results give a greater depth of maximum than do the other two experiments.

5.5 SUMMARY

In this chapter the size dependence of the depth of maximum was obtained from the FWHM of the Cerenkov light pulse. Different methods of extrapolating the FWHM to 300 metres were shown to yield essentially the same result. The conversion from the FWHM to a depth of maximum was performed using published results based on shower simulations. The relationships are generally in good agreement but there is some uncertainty

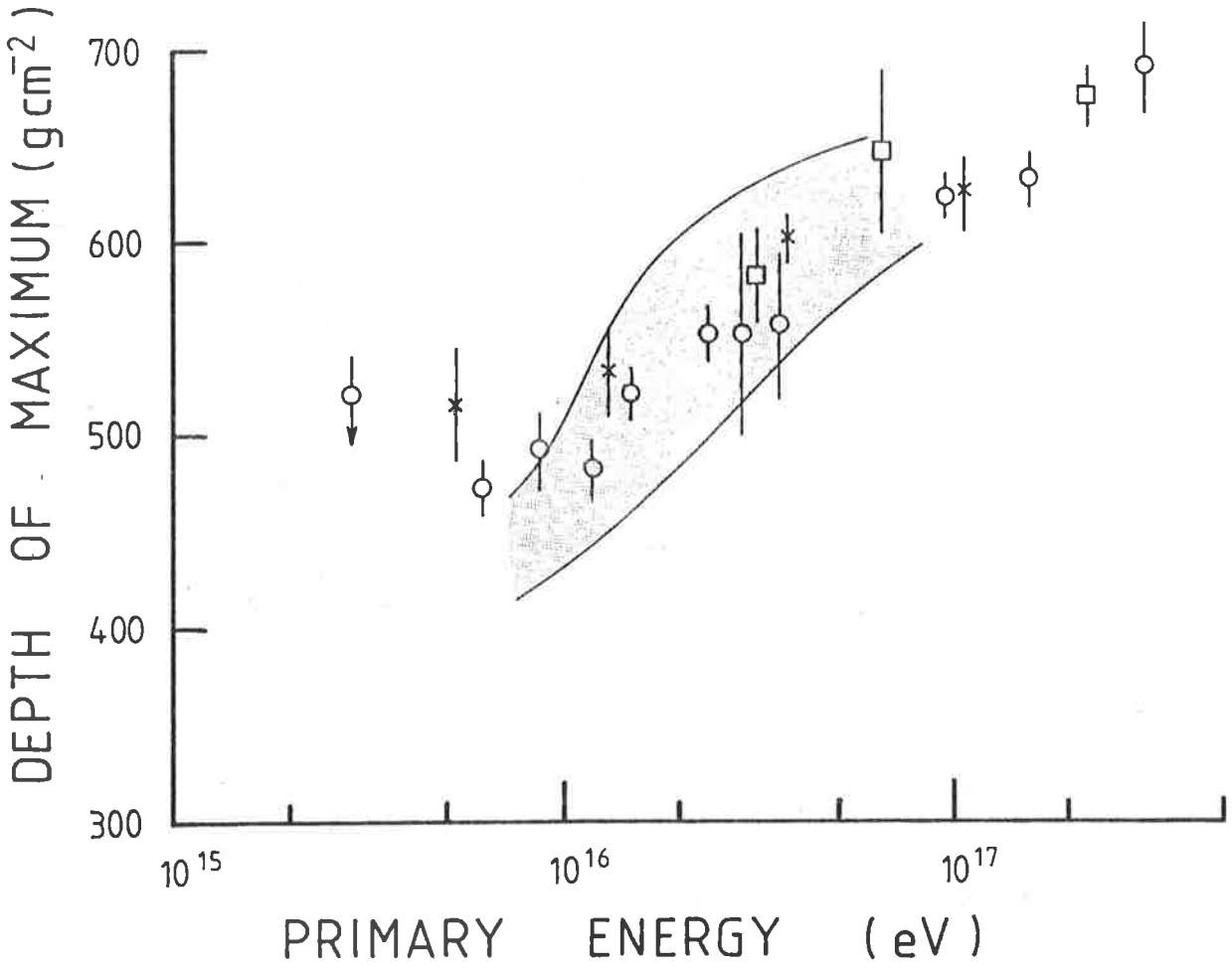

Fig 5.11 The energy dependence of the depth of maximum near 10^{16} eV: crosses - Inoue et al 1981; circles and squares - Andam et al 1982, Chantler et al 1983; shaded region - this thesis.

for showers with $x_m < 500$g cm^{-2}. An examination of the data indicated that there was no significant bias within the size sample. An elongation rate of $\sim$200g cm^{-2}/decade of energy was derived, in agreement with the value derived in chapter four on the basis of simple considerations.

The knowledge of the depth of maximum enabled a conversion between size and primary energy to be established. The different result obtained when the conversion was applied to individual showers rather than to mean values highlighted some sources of bias in the energy sample, in particular the limited dynamic range of the Cerenkov system and the fact that the particle array is sensitive to shower size rather than to primary energy. Although it was not clear how the combination of those two factors would affect the results, it was possible to identify and eliminate from the analysis those showers most likely to be affected. The final result was an energy depenedence of the depth of maximum similar to that obtained more directly from the size dependence.

In the next chapter possible interpretations of the large elongation rate for showers with $E_p \sim 10^{16}$eV will be considered.

5.6 POSTSCRIPT - BANGALORE ICCR

Recent Cerenkov results from Samarkand (Alimov et al 1983, Kalmykov et al 1983) and Akeno (Inoue et al 1983) presented at the Bangalore conference are consistent with a mean depth of maximum of $\sim$600g cm^{-2} at 10^{16}eV. This disagrees with the values obtained by the earlier experiments discussed in this chapter which indicated that the depth of maximum at 10^{16}eV is $\lesssim$500g cm^{-2}. Inoue et al (1983) note that the interpretation of their results is uncertain due to selection effects related to the pulse height, pulse width interdependence. Alimov et al (1983) attribute the difference between their results and those of Thornton and Clay (1979b) to the types of biases discussed in this chapter.

In view of the examination of the data in this chapter and the general agreement with the results of lateral distribution experiments in which any bias would be toward downward fluctuating showers, the author feels that the results presented in this thesis are substantially correct.

CHAPTER SIX

DISCUSSION

6.1 INTRODUCTION

In chapters four and five the elongation rate and depth of maximum were derived from the Cerenkov pulse width for showers initiated by cosmic rays with primary energy (E_p) $\sim 10^{16}$eV. The results indicated a rapid variation of the depth of maximum with energy. In this chapter possible interpretations of this anomalously high elongation rate will be considered. To enable the situation to be examined in a wider context a compilation of depth of maximum data is shown in figure 6.1.

Three distinct energy ranges are apparent. Above 10^{17}eV the elongation rate (D_{10}) is about 70g cm^{-2} per decade, a value consistent with a constant composition and only slow changes in interaction parameters such as the proton-proton cross-section and the multiplicity. In the decade between 10^{16} and 10^{17}eV the depth of maximum changes rapidly, the difference over the decade being at least 100g cm^{-2} and possibly as high as 150g cm^{-2}. Just below 10^{16}eV the situation is less clear although an elongation rate of about 30g cm^{-2} down to 10^{13}eV would be the most simple fit.

Thus the large elongation rate measured in this experiment only persists over a limited energy range beginning at $\sim 10^{16}$eV.

Figure 6.1 Explanation of symbols

a Antonov et al 1981; high altitude size measurements.

A Akeno Cerenkov pulse widths; Inoue et al 1981.

C Mt. Chacaltaya constant intensity cuts;Kakimoto et al 1983.

G Gibson et al 1981; muon angles.

K Yakutsk Cerenkov pulse widths; Kalmykov et al 1979.

P Haverah Park pulse shapes; Hammond et al 1978 interpreted by Protheroe and Turver 1979.

T Tornabene 1979; lateral distributions interpreted by Durham (Andam et al 1981).

W Walker and Watson 1981; muon rise times.

X and ⊗ Dugway Cerenkov lateral distributions and pulse shapes respectively;Chantler et al 1983.

Solid points This thesis.

Solid line See text.

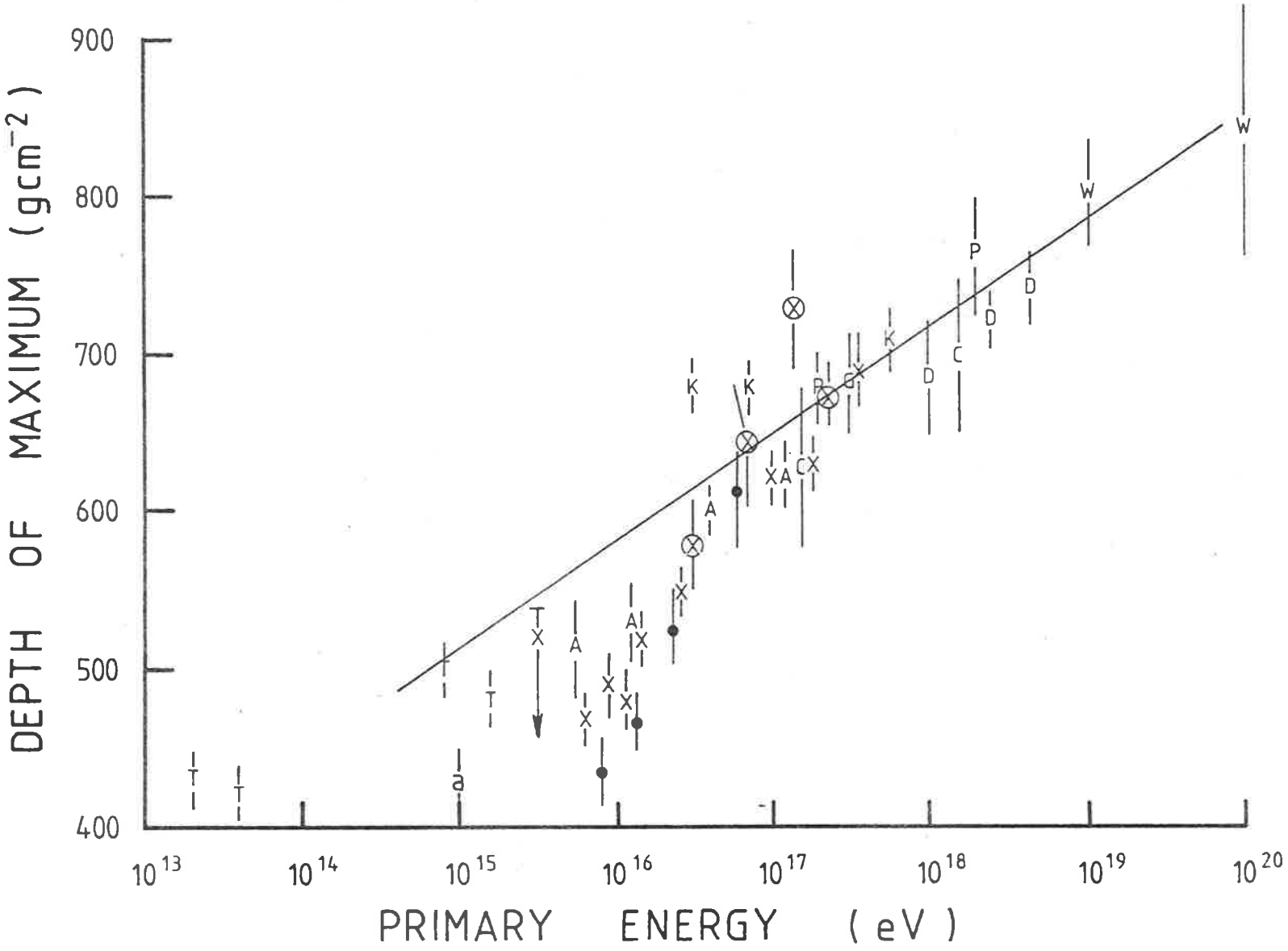

Fig 6.1 A compilation of depth of maximum data. The symbols are explained opposite

6.2 COMPOSITION CHANGE

The simplest explanation of an unusually large elongation rate is a change in composition from heavy to light nuclei. The extent of the required change can best be estimated from the difference between the depth of maximum extrapolated back from the region above 10^{17}eV and the actual value at 10^{16}eV.

Rearranging Eq. 2.8 to determine the relationship between the depth of maximum and the composition at a fixed energy, leads to

$$\Delta\overline{\ln A} = \Delta x_m/(1-B)X_o \qquad \text{Eq. 6.1}$$

The elongation rate above 10^{17}eV suggests a value of 70g cm^{-2} per decade for $(1-B)X_o$ at these energies while the extrapolation (the solid line in figure 6.1) produces $\Delta x_m \cong 80$g cm^{-2}. Thus

$$\Delta\overline{\log A} = 80/70 = 1.14 = \log 14.$$

Therefore, the change in composition required to account for the elongation rate just above 10^{16}eV would be from, say, CNO to H or from Fe to He in just over a decade of energy. (Of course the composition need not be pure, it could be mixed with the appropriate logarithmic mean mass.) If the mass change is estimated from the results of this thesis alone, a much larger change would be required. In fact, in that case it would be difficult to explain the result with anything less than a change from Fe to H.

Because the composition at low energies is known ($\overline{\log A} \cong 0.8$, see 1.4.2), the points near 2×10^{13}eV, although uncorroborated, might provide some indication of the actual composition at 10^{16}eV. Extrapolation from these points with an elongation rate of 70g cm^{-2} produces $x_m \cong 600$g cm^{-2} at 10^{16}eV suggesting that the composition at that energy is predominantly Fe. Further support for this interpretation can be obtained from the known development of low energy showers in water (Jones, 1979). From these measurements Linsley and Watson (1981) derive a mean depth of maximum for 10^{11}eV proton initiated air showers of 280±20g cm^{-2}.

Extrapolating from 10^{11} to 10^{16}eV is obviously fraught with danger, but cosmic ray physicists are a brave (foolish?) lot. Below $\sim 10^{12}$eV the elongation rate is less than at higher energies since the rest masses of the particles involved become significant in comparison with the centre of mass energy (see e.g. the simulated depth of maximum curves in Andam et al 1981). For this reason the extrapolation from 10^{11} to 10^{16}eV is assumed to be equivalent to only four and a half decades at the normal elongation rate. From Eq. 6.1 one has

$$\begin{aligned} \overline{\log A}(10^{16}\text{eV}) &= [x_m(\text{H}, 10^{16}\text{eV}) - x_m(10^{16}\text{eV})]D_{10} \\ &= [280 + 4.5D_{10} - 500]/D_{10} \\ &= 4.5 - 220/D_{10} \end{aligned}$$

Adopting the previously used value of $D_{10} = 70$g cm^{-2} leads to $\overline{\log A} = 1.4 = \log 25$ which suggests a heavy

enrichment at 10^{16}eV. (It is perhaps relevant to point out that the 20g cm^{-2} uncertainty at 10^{11}eV leads to an uncertainty of a factor of two in the mean mass. However, since the bulk of the data at 10^{16}eV favours x_m<500g cm^{-2}, the author feels that the mean mass cannot be much less than the calculated value.) A value of D_{10} greater than 80g cm^{-2}, as favoured by the results of many calculations (see 2.1.4), would imply almost total Fe at 10^{16}eV. The most recent calculations of the Durham group (Chantler et al 1983) also lead to that conclusion.

Thus the depth of maximum data indicate a predominantly Fe composition at 10^{16}eV, changing to a fairly light composition ($\bar{A}\lesssim 10$) above 10^{17}eV.

The low energy composition has been examined in chapter one. Below 10^{12}eV the Fe spectrum is not as steep as that for H but the highest energy Fe data (Abulova et al 1981, Sood 1983) suggest a steepening of the spectrum. Also the JACEE experiment finds no Fe nuclei in the small sample of events with $E_p > 10^{14}$eV (19 events, $\overline{\log A} = 0.6$, Burnett et al 1982).

On the other hand, the Maryland group (Goodman et al 1979a,c, 1982) find evidence for a high percentage of heavy nuclei ($\sim$40%Fe) in the energy range 10^{13}-10^{15}eV. Their experiment is not a direct measurement of the primary composition but examines the arrival time distribution of energetic hadrons near air shower cores.

Calculations show that hadrons with delays >15ns are mostly associated with heavy primaries, enabling the Maryland group to determine the fraction of heavy nuclei in the primary flux from a measurement of the fraction of delayed hadrons. They fit their data to two models. In the first the index is -2.68 for H and -2.39 for Fe in the range 10^{12}-10^{15}eV. This would seem to be at variance with the abovementioned direct measurements - it produces an Fe component about two to three times as great as those experiments. The second model has the same spectral index for all components and the spectra steepen by 0.5 at the same rigidity. The fit to this model has an index of -2.55 steepening at 10^{14}V/c. This model has the obvious advantages that it produces a knee in the spectrum and is easier to reconcile with the highest energy direct composition measurements.

The muon component of an air shower attenuates slowly, so the sea level flux is not sensitive to the shower development while the electron component is. Thus the muon to electron ratio should be an indicator of shower development and hence composition. The relationship between N_μ and N_e measured by Khristiansen et al (1971) has been interpreted in terms of an Fe composition over the whole size range $N_e = 10^5$-10^7 (Gaisser et al 1978). In other less direct measurements of the μ/e parameter, Bergamasco et al (1980) find $\bar{A}\sim(10\text{-}20)$ at $N_e = 10^6$ increasing to $\bar{A}\sim(20\text{-}30)$ at $N_e = 10^7$

while Acharya et al (1981) conclude that the composition is mixed at $N_e = 10^4$ but possibly becoming lighter above $N_e = 4 \times 10^5$. From the observed rate of multiple muons, Alessio et al (1979) find evidence for a significant abundance of heavy nuclei below about 10^{16}eV, diminishing at higher energies. Comparing the multiples rates from the Utah and Homestake detectors with a variety of primary compositions, Elbert et al (1983) are unable to find any composition that explains the whole set of experimental data, although the results seem to suggest a composition rich in heavy nuclei at 10^{14}eV/ nucleon and close to the low energy composition for higher energies.

Because fluctuations in shower development decrease with increasing A, fluctuations in the μ/e ratio can provide an indication of the primary composition. Unfortunately it requires only a small admixture of H to an otherwise pure Fe composition to produce the same fluctuations as a pure H composition. Thus, although fluctuation studies have rejected a pure Fe composition, the calculations of Elbert et al (1976) can fit the observed fluctuations with a composition of nearly pure H or one with $\sim$90% Fe. In a more recent study of the detailed shape of the fluctuation curve, Nikolsky et al (1981) find no change in composition between 10^{15} and 10^{16}eV with no more than 25% Fe.

Overall it is difficult to obtain a consistent picture from the muon data and they do not seem to place any serious constraints on the composition at 10^{16}-10^{17}eV although the results of Khristiansen et al (1971) seem difficult to reconcile with a lightening of the composition in that energy range.

Evidence for the composition above 10^{17}eV is scarce. Walker and Watson (1982) find a significant proportion of H ($\sim$40%) from muon fluctuations but the difficulty in deriving a composition by such techniques has already been mentioned. The measurement by Astley et al (1981) of an anisotropy out of the galactic plane above 2×10^{17}eV is suggestive of an extragalactic H composition but is not necessarily inconsistent with a heavy galactic compsition.

Thus, although there is some evidence against a change of composition from predominantly Fe at 10^{16}eV to a lighter composition above a few times 10^{17}eV, this interpretation of the depth of maximum data is not unreasonable. Figure 6.2 outlines two feasible scenarios capable of producing the required composition at 10^{16}eV and above from the known low energy composition. Case 1 is perhaps best described as a hybrid between the two Maryland models discussed earlier. Most species have an index at low energies of -1.7 except Fe with an index of -1.53, this being about as flat as the direct measurements would allow (c.f. figure 1.2). All indices steepen

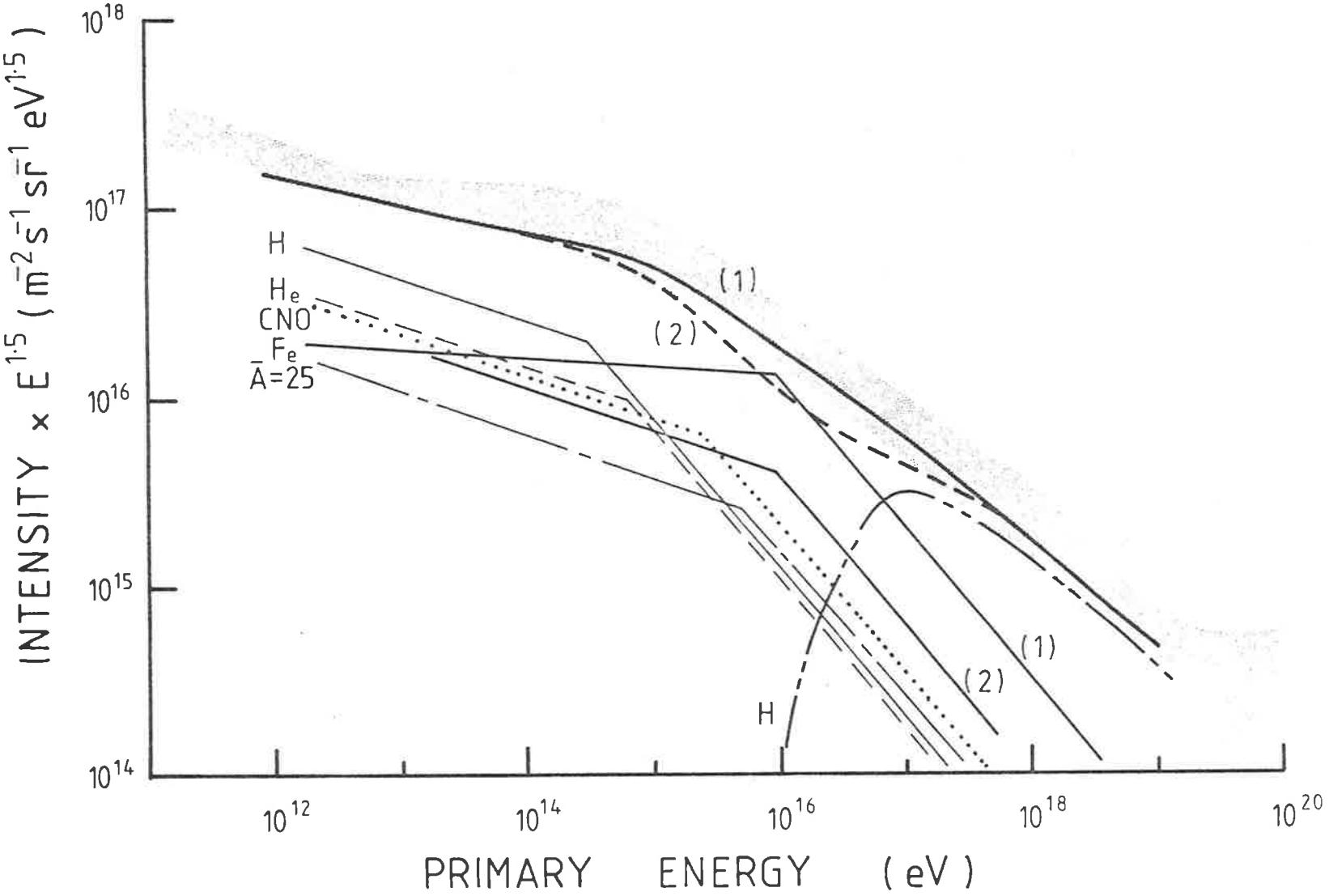

Fig 6.2 Two simplified scenarios that could produce the observed elongation rate by a change from a predominantly heavy composition at 10^{16}eV to a predominantly light composition above 10^{17}eV. The scenarios are described in the text. The shaded region is the measured all particles spectrum.

to -2.3 at a rigidity of 4×10^{14}V/c. The break in the spectrum was placed at that rigidity so that the Fe spectrum would steepen at 10^{16}eV, while the post break slope was chosen to ensure that the Fe component would not be a significant fraction of the all particles spectrum at a few times 10^{17}eV. An additional H component was then added in at high energies to produce the required change in mass, as well as providing a match to the all particles spectrum. Case 2 differs in that the Fe spectrum is assumed to steepen to the same slope as the other components above 10^{13}eV. The same high energy H component is used in this case because, although the fit to the total spectrum is not as good, the appropriately modified H spectrum does not produce the required mass change. There are, of course, sufficient free parameters that one could adjust to produce the desired result but the main purpose here is merely to indicate that a reasonable range of extrapolations from the low energy data can produce a sufficiently heavy composition at 10^{16}eV that a mass change above that energy can be consistent with the elongation rate. In case 1 the logarithmic mean mass changes from 1.5 at 10^{16}eV to 0.5 at 3×10^{17}, while in case 2 the change is from 1.3 to 0.3. Therefore these models would reproduce the observed features in the depth of maximum plot (figure 6.1) above 10^{16}eV.

As was discussed in chapter one, the increasing anisotropy above 10^{14}eV and the knee in the spectrum at $\sim 3\times10^{15}$eV are often interpreted as being associated with a rigidity dependent leakage of cosmic rays. This model also leads naturally to the predominantly heavy composition at 10^{16}eV deduced from the depth of maximum data. However, to explain the elongation rate above 10^{16}eV in terms of a mass change requires the *ad hoc* addition of a light component that becomes dominant above 10^{17}eV. The idea that the highest energy cosmic rays are extragalactic in origin is not new - it does not seem feasible that 10^{20}eV cosmic rays can be accelerated or confined within our galaxy - but the energy at which the changeover from galactic to extra-galactic sources occurs is open to debate (see e.g. Hillas 1982b). If the elongation rate measured here is the result of a mass change it would be evidence of a different, although not necessarily extra-galactic, source becoming dominant at $\sim 10^{17}$eV.

6.3 NEW INTERACTION PHENOMENA

Clearly one could alter the spectra in figure 6.2 to delay the need for an additional component until at least 10^{19}eV (e.g. case 2, but with a smaller change of slope). One would then require a change in particle interactions to produce the observed variation in depth of maximum with energy at 10^{16}-$10^{17.5}$eV. The

type of changes required are outside the scope of any reasonable extrapolation of current accelerator data and thus this line of argument is largely speculative.

However, there is evidence in the cosmic ray data that new phenomena may become important for $E_p \gtrsim 10^{14}$eV. For example, there are the previously mentioned Centauro events (Lattes et al 1973) in which little or no energy goes into the electromagnetic component, the Tien-Shan "long flying" component of slow attenuating hadrons (Yakovlev et al 1979) or the evidence of the Maryland group (Goodman et al 1979c) based on excessively delayed hadrons (>30ns) for the existence of relatively stable massive particles. Kakimoto et al (1983) also suggest the existence of a massive long-lived particle to reconcile the differences between the electron and muon developments measured at Mt. Chacaltaya. (The paper by Capdevielle et al 1982 is a useful reference to the evidence for, and possible interpretation of, these unusual phenomena.)

There are two ways to explain the depth of maximum change, depending on whether one considers the development at 10^{16}eV or above 10^{17}eV to be "normal". If the depth of maximum at 10^{16}eV is what one would expect from the composition at that energy and current interaction models, one could argue that these new phenomena, by delaying the transfer of energy from the

hadronic to the electromagnetic component, cause an increase in the depth of maximum as they become the dominant processes above 10^{16}eV. Alternately, one may consider the development at 10^{16}eV to be abnormally early. One would then require that just beyond the threshold for these new processes they absorb most of the primary energy and that the subsequent transfer of that energy to the electromangetic component is so slow as to be negligible. In this case, the development of the electromagnetic component would be similar to that of a shower of much lower primary energy.

A detailed knowledge of the depth of maximum data below 10^{16}eV would help make a choice between the two interaction possibilities. A smooth variation with energy would be consistent with the former (and also with the changing composition interpretation), while the latter should produce a downward step at the threshold for the new processes.

6.4 CONCLUSION

The energy variation of the depth of maximum determined in the current experiment for $E_p \sim 10^{16}$-10^{17}eV has been combined with other measurements to provide a consistent picture of the depth of maximum up to $\sim 10^{19}$eV. The large elongation rate measured between 10^{16} and 10^{17}eV is found not to persist beyond a few times 10^{17}eV. Two interpretations of this phenomenon were considered.

The first required a change of the primary composition from predominantly heavy nuclei at 10^{16}eV to a dominance of protons at a few times 10^{17}eV. The required composition at 10^{16}eV is not inconsistent with the known composition up to 10^{14}eV although it might require a flatter iron spectrum above 10^{13}eV than is generally expected. The change to a light composition would require a new source of cosmic rays to become dominant above 10^{17}eV. The second interpretation invokes new interaction phenomena for $E_p \sim 10^{16}$eV. Although evidence exists in the cosmic ray data for the existence of new processes that could alter the development of air showers, this possibility can only be considered in a qualitative manner. The true explanation may well involve both factors.

CHAPTER SEVEN

SINGLE DETECTOR DETERMINATION OF SHOWER SIZE

7.1 INTRODUCTION

Linsley (1983) has recently proposed a relatively low cost technique that could increase the collecting area of a simple particle array for high energy showers. The method involves measuring the particle density at essentially only one point per shower and determining the core distance, and hence shower size, from the pulse width. In practice several spaced detectors would be employed to obtain directional information as well. It was decided to use the data obtained in the experimental work of this thesis to investigate the use of the Cerenkov pulse in a similar way.

7.2 BASIC CONSIDERATIONS

Initially only large core distances, where the radial behaviour of the Cerenkov light can be described by simple functions, will be considered. The applicability of the technique at smaller core distances will be examined later.

At large core distances the radial behaviour of the FWHM can be represented by a power law. For a given experiment the exponent (n) will, to some extent,

be determined by the bandwidth of the system and the degree of compensation. For example, the observed pulses in this experiment have n∿1 and the reduced pulses have n = 1.5, while for unlimited bandwidth n will be even larger (see section 5.1). The FWHM is also dependent on the depth of maximum. The Kalmykov equation (Eq. 5.1) is

$$h_{max} = 17.05 - 9.17 \log\tau_{300} \text{ km}$$

Substituting this into an exponential atmosphere of the form

$$x = x_o \exp(-h/h_o)$$

with h_o = 8km gives

$$x_m \propto \exp(-9.17 \log\tau_{300}/8)$$

or $$x_m \propto (\tau_{300})^{1/2}$$

Thus, the dependence of τ on r and x_m can be written as

$$\tau \propto r^n x_m^2$$

The total flux (ϕ) at these core distances is approximately proportional to primary energy (E_p) and varies as r^{-2} (see section 5.4), so that

$$\phi \propto E_p r^{-2}$$

In principle, if ϕ and τ are both measured, one can eliminate the unknown core distance and obtain

$$E_p \propto \phi \tau^{2/n} x_m^{-4/n}$$

From the measurement of ϕ and τ at a single location, one

can derive a parameter (f) such that

$$f = \phi\tau^{2/n} E_p x_m^{-4/n} \qquad \text{Eq. 7.1}$$

With $n \sim 1.5$ and, for example, variations in x_m of 200g cm^{-2} about a mean of 600g cm^{-2}, the x_m dependence would introduce a factor of nearly two into the estimation of E_p from f (and a factor of $\sim$1.5 into any estimation of r from τ). Because the x_m dependence of f is in the same direction as the resultant variation in sea level shower size, it is useful to examine f in terms of N_e.

The expected dependence of N_e on x_m is of the form

$$N_e \propto E_p \exp(x_m/\lambda)$$

where λ is the typical shower attenuation length. Eq. 7.1 can then be rewritten as

$$f \sim N_e \exp(-x_m/\lambda) x_m^{4/n} \qquad \text{Eq. 7.2}$$

The minimum x_m dependence will occur for $\partial f/\partial x_m = 0$ which requires $n = 4\lambda/x_m$. Using λ = 185g cm^{-2} and $x_m \sim 500$g cm^{-2}, which is typical for the showers in the data sample, leads to $n \cong 1.5$. Thus, if the reduced FWHM, which has a radial exponent of 1.5, is used as τ in the determination of f the result should be a good measure of the shower size with only a minimal dependence on the depth of maximum.

The parameter f will also have some angular dependence. For a constant height of maximum (and hence τ) the increase in E_p (and hence ϕ) necessary to maintain

a constant N_e leads to

$$\frac{d\ln f}{d\cos\theta} = x_m(\sec\theta+h/h_o)/\lambda - x_o\sec^2\theta/\lambda \qquad \text{Eq. 7.3}$$

(In this chapter the only shower size referred to is the sea level size, i.e. N_e(s.l.) in the terminology of chapter four. For simplicity this size will be designated N_e throughout this chapter.) For values typical of this experiment ($x_m \sim 500$g cm^{-2}, x_o = 1030g cm^{-2}, $h \sim 6$km, $\sec\theta \sim 1.07$) Eq. 7.3 reduces to

$$\Delta \log f \simeq -0.6\Delta\cos\theta$$

which is clearly a small factor for the range of angles of the observed showers ($\sim 0°$-$40°$ so that $\cos\theta = 0.9 \pm 0.1$). The angular effect will be less for showers with greater x_m. Therefore, for convenience, the angular dependence will be ignored in the following section, although, since θ is an easily determined ground parameter, allowance can be made for it if warranted.

7.3 EXPERIMENTAL RESULTS

For comparison with the measured shower size, f was defined as

$$f = \phi\tau^{1.3}$$

The reduced FWHM, τ, is given by Eq. 3.5 except for observed FWHM<7ns in which case the observed FWHM is assumed to be 6ns. This is done because for values of the FWHM close to the system response value of 5.3ns, the FWHM is not very sensitive to core distance and because the rounding off in measuring to the nearest half nanosecond produces meaninglessly large variations.

in the reduced FWHM. Thus, if the FWHM was measured as 5.5, 6.0 or 6.5ns a value of 6ns was used in Eq.3.5. The flux $\emptyset$ was approximated as the product of the observed FWHM (in ns) and the pulse height (in mV) rather than by a proper integration.

In figure 7.1 f and N_e are shown as functions of each other for $r \geq 125$m. The difference between the two sets arises as a result of differences in the distributions of the data points with respect to the two variables. Nevertheless, in both cases, for large f or N_e the data are consistent with the expected slope of unity. The deviation at low values seems to be caused by the observational cutoff for both variables (at $\sim 10^5$ for N_e and $\sim 2 \times 10^2$ for f). The data were restricted to $r \geq 125$m rather than say, observed FWHM$\geq$7ns (which is similar), to minimize such effects. It is not surprising that the f binned data show a greater deviation since an extrapolation back from the high values would intercept the N_e cutoff much earlier than the f cutoff (i.e. the N_e cutoff is the dominant restriction).

Figure 7.2 shows the ratio f/N_e as a function of core distance. The shape inside 100 metres reflects the average lateral distribution function since the FWHM is insensitive to core distance in this range. Although f was derived from considerations appropriate to large core distances ($r \gtrsim 150$m) it is clear that in

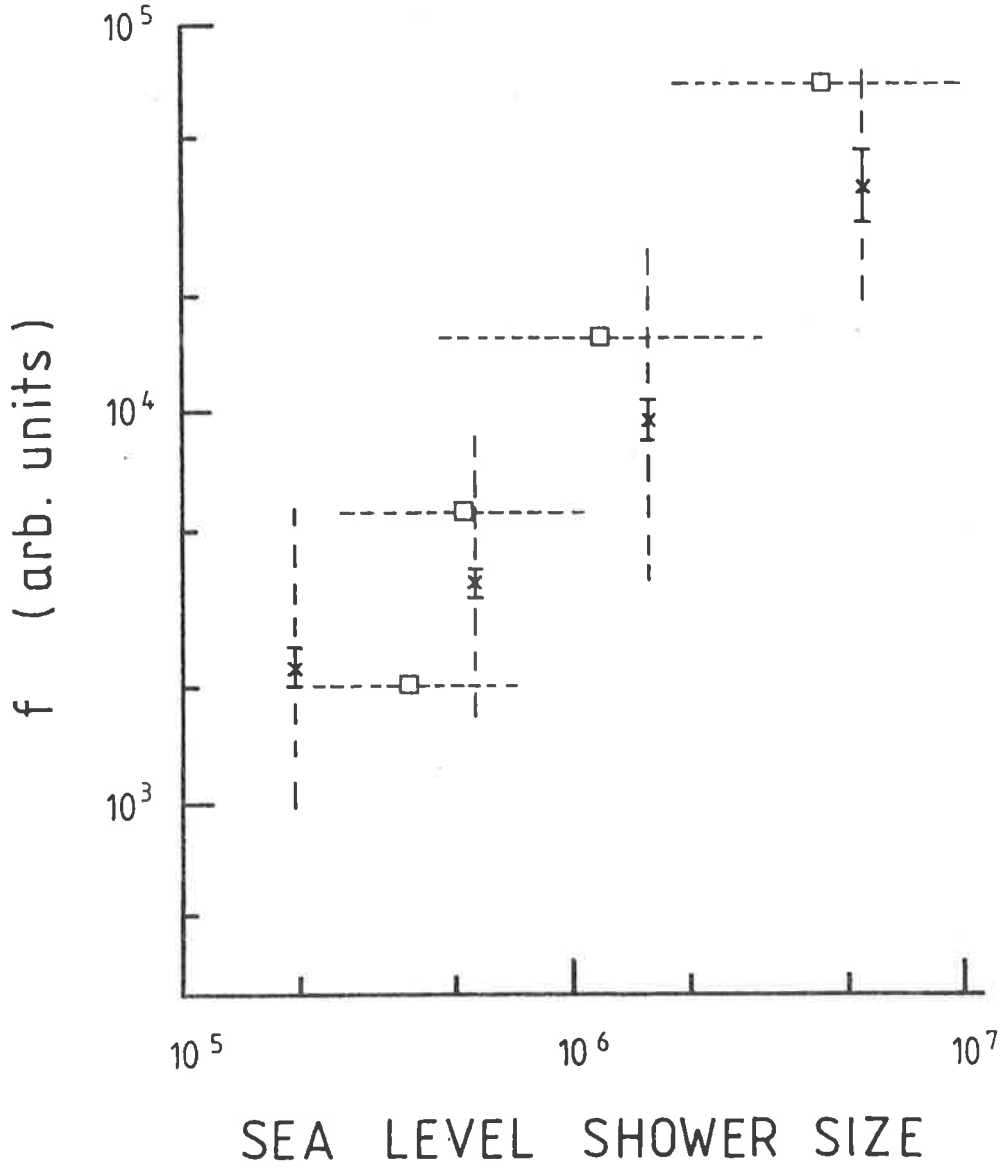

Fig 7.1 The relationship between the size parameter f and the measured shower size.

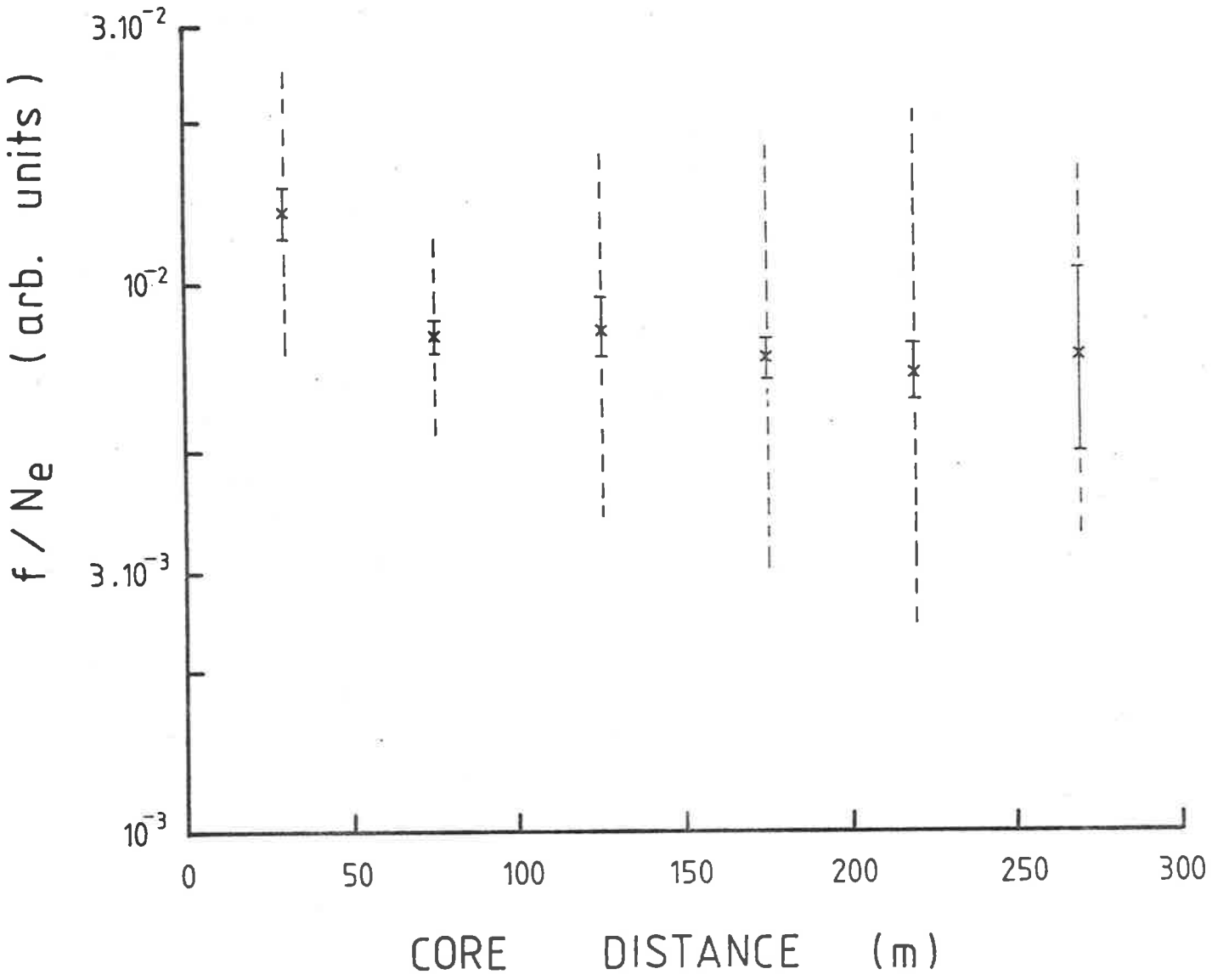

Fig 7.2 The radial dependence of the ratio of the size parameter f and the measured size N_e. The outer (broken) error bars are the standard deviation for the data as a whole while the inner (solid) error bars are the standard deviation of the mean values.

this case it can be used at smaller distances without modifications. Major discrepancies (compared to the inherent scatter of the data) only arise near the shower axis where the collecting area is minimal.

Sources of experimental error contributing to the scatter in f/N_e include variations in the system gain due to changes in the photomultiplier voltage and temperature ($\sim\pm30\%$), photoelectron statistics affecting both the measured pulse height ($\lesssim10\%$) and width ($\sim10\%$ in the observed width and $\sim20\%$ in the reduced width), differing pulse shapes not allowed for by the simple calculation of the flux (perhaps $\sim20\%$), zenith angle affects ($\sim10\%$) and the uncertainty in the measured size ($\sim10\%$). Since the total of all these would produce an error of a factor of about 1.5 in the ratio f/N_e, it seems that the observed scatter, typically a factor of 2-2½, indicates underlying physical uncertainties.

Thus, it is possible to determine the shower size from a single Cerenkov light pulse if both the pulse area and width are measured. For the showers examined here a standard deviation of about 2½ times was obtained but a higher degree of accuracy should be attainable if a less superficial examination of the relationship between the Cerenkov lateral distribution, the pulse width radial distribution and the shower size is made.

7.4 COLLECTING AREA

The collecting area of such a Cerenkov system will be determined by the minimum pulse height that can be clearly detected above the background sky noise. For a given shower size, the flux decreases as about r^{-2} while the pulse width increases as about r^2. (The measurements of Kalmykov et al 1977, 1979 show that these approximations are valid out to $\sim$1km.) The pulse height will then vary as r^{-4}, so that the limit of detection for showers will increase as $N_e^{1/4}$ and the collecting area as $N_e^{1/2}$.

The data indicate that, for the conditions of this experiment, showers with $N_e \sim 10^6$ can be comfortably detected out to $\sim$200 metres giving a collecting area $\sim 10^5 m^2$ at this size. Hence for $N_e \sim 10^{10}$ the collecting area should be $\sim 10 km^2$. This is similar to the collecting area Linsley expects to obtain at 10^{20}eV by using $4m^2$ of scintillator.

7.5 CONCLUSION

It has been shown that the shower size can be determined from a single Cerenkov light pulse. If, as seems likely, this technique can be extended to much larger shower sizes than were examined here, it would provide a simple method of obtaining a large collecting area for the highest energy showers. However, unless the collecting area estimated in section 7.4 is grossly

underestimated, the running time restrictions inherent in atmospheric Cerenkov measurements are likely to make such a system non-competitive with particle detection systems utilizing the same basic concepts.

CHAPTER EIGHT

CONCLUDING COMMENTS

8.1 THE DEPTH OF MAXIMUM

This thesis was based on an experiment to determine the depth of maximum of extensive air showers from the width of the associated Cerenkov light pulse. Early results established the sensitivity of the pulse width to shower development (Thornton and Clay 1978a,b, 1979a). The relationship between the pulse width and height of maximum then published by Kalmykov et al (1979) enabled the depth of maximum to be determined explicitly. The results showed that the depth of maximum changed rapidly with size near $N_e = 10^6$ (Thornton and Clay 1979b, 1981). Similar results were subsequently obtained by other research groups (Inoue et al 1981, Andam et al 1982, Chantler et al 1983) and by independent experiments at Buckland Park (Kuhlmann and Clay, 1981, Liebing 1983).

However, the situation below $N_e \sim 5 \times 10^5$ is not clear since such showers are near the lower threshold of the abovementioned experiments. Although it has been demonstrated in chapter five that the pulse width is sensitive to shower development at core distances as small as 120 metres, the extension of the Cerenkov technique to significantly smaller sizes will almost certainly be restricted to the measurement of its

lateral distribution. A knowledge of the variation of depth of maximum with energy to as low as 10^{14}eV, where the composition is known, might give some indication as to whether the features near 10^{16}eV are due to a change in composition or to the onset of new interaction phenomena.

8.2 SINGLE DETECTOR SIZE DETERMINATION

The data were also used to investigate a technique of determining the shower size from measurements made with a single detector. Although the results were interesting, it was not clear that Cerenkov light measurements would have advantages over particle measurements using a similar technique. However, a more thorough examination of the technique (its accuracy, collecting area and cost) at energies much higher than available in this experiment would be required to determine the relative merits of the Cerenkov light and particle systems.

APPENDIX 1

DATA TABLES FOR CHAPTERS FOUR AND FIVE

Figure 4.1 $5.10^5 \leq N_e < 2.10^6$

$\bar{r}$	21	39	63	88	115	138	161	186	211	233
$\overline{FWHM}$	2.2	2.0	1.5	2.0	3.0	3.9	4.8	5.7	7.4	10.6
$\Delta FWHM$	0.6	0.1	0.1	0.3	0.3	0.2	0.2	0.3	0.6	1.6
$\bar{N}_e/10^6$	0.5	1.0	0.8	0.9	1.0	0.9	1.0	0.9	1.1	1.0
EVENTS	4	15	14	13	17	51	57	49	36	11

Figure 4.2 $5.10^5 \leq n_e < 2.10^6$

$r^2/10^4$	0.2	0.7	1.3	1.7	2.2	2.7	3.3	3.7	4.2	4.7	5.2	5.8
$\overline{FWHM}$	1.9	1.9	3.0	3.6	4.4	4.8	5.5	6.1	7.2	7.1	9.5	13.1
$\Delta FWHM$	0.1	0.2	0.4	0.2	0.2	0.3	0.4	0.5	0.8	1.0	1.5	2.6
$\bar{N}_e/10^5$	0.9	0.8	1.0	0.9	1.0	0.9	0.9	0.9	1.0	1.2	1.0	1.2
EVENTS	28	16	12	33	47	31	31	20	20	14	9	4

Figure 4.3a $N_e < 7.10^5$

$\bar{r}$	162	185	208
FWHM	4.0±0.2	4.7±0.3	5.5±0.4
$\bar{N}_e/10^5$	3.3	4.3	4.3
EVENTS	56	32	17

$7.10^5 \leq N_e < 3.10^6$

$\bar{r}$	161	186	211	232
FWHM	5.0±0.3	6.3±0.4	7.5±0.5	10.3±1.3
$\bar{N}_e/10^6$	1.3	1.4	1.4	1.4
EVENTS	55	52	38	14

$3.10^6 \leq N_e < 10^7$

$\bar{r}$	168	189	210	237	266
FWHM	6.6±1.0	9.8±1.1	11.0±2.0	18.2±1.9	15.5±1.7
$\bar{N}_e/10^6$	4.1	4.7	4.2	5.7	4.8
EVENTS	7	10	7	6	5

Figure 4.3b $3.10^5 \leq N_e < 3.10^6$

$\theta \leq 20°$ $\overline{\sec\theta} = 1.03$

$\bar{r}$	161	186	210	234
FWHM	5.2±0.3	6.6±0.4	8.1±0.7	11.7±1.3
$\bar{N}_e/10^6$	0.8	0.9	1.0	1.1
EVENTS	50	43	26	12

$\theta > 20°$ $\overline{\sec\theta} = 1.14$

$\bar{r}$	162	185	211	228
FWHM	4.1±0.3	4.8±0.3	5.8±0.4	6.0±0.6
$\bar{N}_e/10^6$	1.0	1.1	0.9	1.7
EVENTS	40	37	28	4

Figure 5.2

$\log N_e$	5.30	5.77	6.23	6.67	7.24
(i)	406±11	439±6	524±7	602±19	662±34
x_m (ii)	382±14	427±7	527±10	621±21	672±38
(iii)	335±16	376±8	487±11	594±22	641±40
EVENTS	29	130	109	34	10

Figure 5.3a $\theta<20°$ $\overline{\sec\theta} = 1.03$

$\log N_e$	5.29	5.76	6.21	6.67	7.23
x_m	393±11	432±7	530±13	575±18	578±11
EVENTS	17	70	47	19	3

$\theta<20°$ $\overline{\sec\theta} = 1.13$

$\log N_e$	5.30	5.79	6.25	6.68	7.25
x_m	423±21	448±8	519±9	636±34	697±41
EVENTS	12	58	62	15	7

Figure 5.3b $120 \leq r < 150m$ $\bar{r} = 137m$

$\log N_e$	5.31	5.75	6.21	6.73
x_m	437±24	460±10	558±13	606±46
EVENTS	10	50	36	5

$150 \leq r < 185m$ $\bar{r} = 167m$

$\log N_e$	5.30	5.76	6.23	6.62	7.21
x_m	410±13	438±7	531±10	521±24	592±15
EVENTS	25	77	53	9	2

Figure 5.3b $r \geq 185m$ $\bar{r} = 212$

$\log N_e$	5.31	5.79	6.23	6.69	7.25
x_m	376±14	441±9	517±11	631±21	679±40
EVENTS	4	51	56	25	8

Figure 5.5

$\log[N_e(x_m+550)]$	5.35	5.80	6.21	6.68	6.10
x_m	458±19	479±9	499±8	553±24	627±28
EVENTS	20	136	130	24	2

Figure 5.6a $\theta < 20°$ $\overline{\sec\theta} = 1.03$

$\log[N_e(x_m+550)]$	5.37	5.80	6.24	6.69
x_m	448±29	466±11	491±12	480±41
EVENTS	11	77	59	9

$20° \leq \theta < 40°$ $\overline{\sec\theta} = 1.12$

$\log[N_e(x_m+550)]$	5.32	5.80	6.18	6.66
x_m	470±23	495±14	501±12	536±40
EVENTS	9	60	66	15

Figure 5.6b $150 \leq r < 185$m $\quad \bar{r} = 167$m

$\log[N_e(x_m+550)]$	5.33	5.80	6.19	6.66
x_m	450±17	463±10	480±10	505±21
EVENTS	17	85	55	9

$\bar{r} \geq 185$m $\quad \bar{r} = 212$m

$\log[N_e(x_m+550)]$	5.79	6.22	6.69
x_m	505±17	513±11	581±35
EVENTS	51	75	15

Figure 5.10

$\log[N_e(x_m+550)]$	5.91	6.11	6.38	6.12	6.37	6.78±0.11
x_m	436±23	472±18	590±24	468±17	527±24	613±33
EVENTS	19	30	8	33	14	6

APPENDIX 2

DERIVATIONS USED IN CHAPTER FOUR

1. DETERMINATION OF THE ER FROM α AND β

Assume that the FWHM, τ, is just a function of the height of maximum, h, but can also be represented as a function of N_e and $\cos\theta$ as discussed in section 4.2. That is

$$\tau(h) \sim (\cos\theta)^{\alpha} N_e^{\beta}$$

Thus $(\partial\tau/\partial\cos\theta) = (\partial\tau/\partial h)(\partial h/\partial\cos\theta)$

and $(\partial\tau/\partial N_e) = (\partial\tau/\partial h)(\partial h/\partial N_e)$

Therefore

$$(\partial\tau/\partial h) = \alpha\tau(\partial h/\partial\cos\theta)^{-1}/\cos\theta = \beta\tau(\partial h/\partial N_e)^{-1}/N_e$$

so that $\alpha(\partial h/\partial\cos\theta)^{-1}/\cos\theta = \beta(\partial h/\partial N_e)^{-1}/N_e$ Eq.A

Now $h = -h_o \ln(x\cos\theta/x_o)/\cos\theta$

and $(\partial h/\partial\cos\theta) = h_o \ln(x\cos\theta/x_o)/(\cos\theta)^2 - h_o/(\cos\theta)^2$ Eq.B

and $(\partial h/\partial N_e) = (\partial h/\partial x)(\partial x/\partial \ln N_e)(\partial \ln N_e/\partial N_e)$

$$= [-h_o/(x\cos\theta)](\partial x/\partial \ln N_e)/N_e \quad \text{Eq.C}$$

Substituting Eq.B and C into Eq.A leads to

$$x_n = (\partial x/\partial \ln N_e) = x(\ln(x_o/x\cos\theta)+1)\beta/\alpha \quad \text{Eq.4.1}$$

From Eq.2.10 $N_e \sim E_p^{1+D_e/\lambda}$

so $x_n = (\partial x/\partial \ln N_e) = (\partial x/\partial \ln E_p)(\partial \ln E_p/\partial \ln N_e)$

$$= D_e/(1+D_e/\lambda)$$

or $$1/x_n = 1/D_e + 1/\lambda$$

Therefore $$D_{10} = 2.3/(1/x_n - 1/\lambda) \quad \text{Eq.4.2}$$

2. ZENITH ANGLE DEPENDENCE FOR N_e AND $N_e(sl)$

The value of α obtained using the measured shower size, $N_e(sl)$, differs from that obtained using the size extrapolated to a fixed depth. For clarity call the former α^1. Then

$$FWHM \sim (\cos\theta)^{\alpha} N_e^{\beta} \sim (\cos\theta)^{\alpha^1} N_e(sl)^{\beta}$$

and $$N_e(sl) \sim N_e \exp(-x_o/\lambda\cos\theta)$$

$$(\partial\tau/\partial\cos\theta) = \alpha\tau/\cos\theta = \alpha^1\tau/\cos\theta + (\cos\theta)^{\alpha^1}(\partial N_e(sl)^{\beta}/\partial\cos\theta)$$

$$= \alpha^1\tau/\cos\theta + \beta x_o/\lambda\cos\theta$$

so $$\alpha = \alpha^1 + \beta x_o/\lambda\cos\theta$$

APPENDIX 3 and

APPENDIX 4

(see pocket on the back cover of the thesis)

REFERENCES

(The abbreviation Xth ICCR refers to the Proceedings of the Xth International Conference on Cosmic Rays.)

Abulova V.G., Dezhurko M.D., Mandritskaya K.V., Rakobolskaya I.V., Sazhina G.P., Zamchalova E.A. and Zatsepin V.I., 1981, 17th ICCR, 2, 114.

Acharya B.S., Naranan S., Rao M.V.S., Sivaprasad K. and Sreekantan B.V., 1981, 17th ICCR, 11, 385.

Aguirre C., Kakimoto F., Kamata K., Kameko T., MacKeown P.K., Mizumoto Y., Murakami K., Nagano M., Nakatani H., Nishi K., Suga K., Toyoda Y., Trepp A. and Yoshii H., 1979, J.Phys.G, 5, 139.

Alessio S., Bilokon H., D'Ettore Piazzoli B. and Mannocchi G., 1979, 16th ICCR, 8, 298.

Alimov T.A., Aliev N.A., Efimov N.N., Grigoriev V.M., Kakhkharov M.K., Mackhmudov B.M., Prosin V.V., Rakhimova N.R., Tashpulatov R.T., Khakimov N.Kh. and Khristiansen G.B., 1983, 18th ICCR, Late papers, EA4-3.

Allan H.R., 1971, Prog.Elem.Part.Cos.Ray Phys., 10, 169.

Amaldi V., Cocconi G., Diddens A.N., Dobinson R.W., Dorenbosch J., Duinker W., Gustavson D., Meyer J., Potter K., Wetherell A.M., Baroncelli A. and Bosio C., 1977, Phys.Lett. B66, 390.

Andam A.A., Chantler M.P., Craig M.A.B., McComb T.J.L., Orford K.J., Turver K.E. and Walley G.M.,
1981, 17th ICCR, 11, 281
1982, Phys.Rev. D 26, 23

Antonov R.A., Kuzmin V.A, and Fateeva I.M., 1981, 17th ICCR, 6, 229.

Arons J., 1980, I.A.U. Symposium 94, 175.

Ashton F., Nasri A. and Ward I.A., 1977, 15th ICCR, 8, 6.

Ashton F. and Nejabat J., 1981, 17th ICCR, 6, 172.

Astley S.M., Cunningham G., Lloyd-Evans J., Reid R.J.O. and Watson A.A., 1981, 17th ICCR, 2, 156.

Axford W.I., 1980, I.A.U. Symposium 94, 339.

Bell A.R., 1978, Mon.Nat.Roy.Ast.Soc., 182, 147.

Benecke J., Chou T.T., Yang C.N. and Yen E., 1969, Phys.Rev., 188, 2159.

Bergamasco L., D'Ettore Piazzoli B. and Mannocchi G., 1980, Lett.Nuo.Cim., 27, 71.

Bevington P.R., 1969, "Data Reduction and Error Analysis for the Physical Sciences", McGraw-Hill, New York.

Blackett P.M.S., 1948, Phys.Soc. Gassiot Comm.Rep, 34.

Blandford R.D. and Ostriker J.P., 1978, Ap.J.Lett., 221, L29.

Bohm E., Holtrup G., Bosia G., Navarra G., Saavedra O. and Cachon A., 1975, 14th ICCR, 8, 3046.

Boley, F.I., Baum J.H., Palsedge J.A. and Pereue J.H., 1961, Phys.Rev., 124, 1205.

Boley F.I., Palsedge J.A. and Baum J.H., 1962, Phys.Rev., 126, 734.

Boley F.I., 1964, Rev.Mod.Phys., 36, 792.

Bosia G., Castagnoli C., Marangoni G., Navarra G. and Saavedra O., 1970a, Lett.Nuo.Cim., 3, 373.

Bosia G., Castagnoli C., Dardo M. and Marangoni G., 1970b, Nature, 225, 532.

Bosia G., Maringelli M. and Navarra G., 1972a, Nuo.Cim., 9B, 201.

Bosia G., Castagnoli C., Marangoni G., Navarra G., Raspollini G. and Saavedra O., 1972b, Nuo.Cim., 9B, 177.

Bosia G., Navarra G., Saavedra O., Bohm E. and Cachon A., 1973, 13th ICCR, 4, 2375.
1975, 14th ICCR, 8, 3052.

Burnett, T.H., Dake, S., Fuki M., Gregory J.C., Hayashi T., Holynski R., Iwai J., Jones W.V., Jurak A., Lord J.J., Miyamura O., Ogato T., Parnell T.A., Saito T., Tabuki T., Takahashi Y., Tominaga T., Watts J., Wilkes R.J., Wolter W. and Wosiek B., 1982, Workshop on Very High Energy Cosmic Ray Interactions, 220 (M.L. Cherry, K. Lande and R.I. Steinberg eds., University of Pennsylvania).

Capdevielle J.N. and Gawin J., 1982, J.Phys.G, 8, 1317.

Capdevielle J.N., Gawin J., Grochalska B. and Wdowczyk J., 1982, Nuo.Cim., 5C, 672.

Casse M., 1981, 17th ICCR, 13, 111.

Castagnoli C., Locci M.A., Picchi P. and Verri G., 1967a, Nuc.Phys.B., 2, 369.

Castagnoli C., Dardo M. and Penengo P., 1967b, Phys.Rev., 160, 1186.

Cerenkov P.A., 1934, Dokl.Akad.Nauk S.S.S.R., 2, 451.
1937, Dokl.Akad.Nauk S.S.S.R., 14, 101.

Cesarsky C.J. and Lagage P.O., 1981, 17th ICCR, 9, 250.

Chantler M.P., Craig M.A.B., McComb T.J.L., Orford K.J., Turver K.E. and Walley G.M., 1982, J.Phys.G., 8, L51.
1983, J.Phys.G., 9, L26.

Clay R.W., Gerhardy P.R., Liebing D.F., Thornton G.J. and Patterson J.R., 1981, Nuo.Cim. 4C, 668.

Clay R.W. and Gerhardy P.R., 1981, Nuo.Cim. 4C, 26.
1982a, Aust.J.Phys., 35, 59.
1982b, Aust.J.Phys., 35, 441.

Colgate S.A. and Johnson M.H., 1960, Phys.Rev.Lett., 5, 235.

Cowsik R. and Wilson L.W., 1973, 13th ICCR, 1, 500.

Cowsik R., 1980, I.A.U. Symposium 94, 93.

Crouch P.C., Gerhardy P.R., Patterson J.R., Clay R.W. and Gregory A.G., 1981, Nuc.Inst.Meth., 179, 467.

Cunningham G., Lloyd-Evans J., Pollock A.M.T., Reid R.J.O. and Watson A.A., 1980, Ap.J., 236, L71.

Daniel R.R. and Dugaprasad N., 1962, Nuo.Cim., 23, Suppl.82.

Danilova T.V., Kabanova N.V., Nesterova N.M., Nikolskaya N.M., Nikolsky S.I., Katsarky L.M., Kirov I.N., Stamenov J.N. and Janminchev V.D., 1977, 15th ICCR, 8, 129.

Eichler D., 1980, Ap.J., 237, 809.

Efimov N.N., and Sokurov V.F., 1979, 16th ICCR, 8, 52.

Elbert J.W., Mason G.W., Morrison J.L. and Narasimham V.S., 1976, J.Phys.G., 2, 971.

Elbert J.W., Gaisser T.K. and Todor Stanev, 1983, Phys.Rev.D., 27, 1448.

Ellsworth R.W. and Yodh G.B., 1981, 17th ICCR, 11, 390.

Erlykin A.D., 1981, 17th ICCR, 13, 273.

Feinberg E.L., 1972, Physics Reports 5C, 237.

Fermi E., 1949, Phys.Rev., 75, 1169.
1951, Phys.Rev., 81, 683.

Feynman R.P., 1969, Phys.Rev.Lett., 23, 1415.

Fomin Yu.A. and Khristiansen G.B., 1972, Sov.J.Nuc.Phys., 14, 360.

Frank I.M. and Tamm Ig., 1937, Dokl. Akad.Nauk S.S.S.R., 14, 109.

Gaisser T.K., Protheroe R.J., Turver K.E. and McComb T.J.L., 1978, Rev.Mod.Phys., 50, 859.

Gaisser T.K., McComb T.J.L. and Turver K.E., 1979, 16th ICCR, 9, 275.

Gaisser T.K. and Yodh G.B., 1980 Ann.Rev.Nuc.Part.Sci., 30, 475.

Galbraith W. and Jelley J.V., 1953, Nature, 171, 350.

Garcia-Munoz M., Simpson J.A. and Wefel J.P., 1981, 17th ICCR, 2, 72.

Gibson A.I., McComb T.J.L., and Turver K.E., 1981, 17th ICCR, 6, 16.

Goodman J.A., Ellsworth R.W., Ito A.S., MacFall J.R., Siohan F., Streitmatter R.E., Tonwar S.C., Vishwanath P.R. and Yodh G.B.,
1979a, Phys.Rev.Lett., 42, 854.
1979b, 16th ICCR, 6, 64.
1979c, Phys.Rev.D., 19, 2572.
1982, Phys.Rev.D., 26, 1043.

Gregory J.C., Ogata T., Saito T., Holynski R., Jurak A., Wolter W., Wosiek B., Dake S., Fuki M., Tominaga T., Friedlander E.M., Heckman H.H., Hugget, R.W., Hunter S., Jones W.V., Takahashi Y., Parnell T.A., Watts J., Miyamura O., Burnett T.H., Lord J.J., Wilkes R.J., Hayashi T., Iwai J. and Tabaki T., 1981, 17th ICCR, 9, 154.

Greisen K., 1956, Prog.Cos.Ray Phys., 3, 1.
1960, Ann.Rev.Nuc.Sci., 10, 63.

Grigor'ev V.M., Efimov N.N., Kalmykov N.N., Nechin Yu.A., Prosin V.V. and Khristiansen G.B., 1978, Sov.J.Nuc.Phys., 27, 225.
1979, J.E.T.P.Lett., 30, 708.

Grigorov N.L., Rapoport I.D., Savenko I.A., Nesterov V.E. and Prokhin V.L., 1971, 12th ICCR, 5, 1746.

Grindlay J.E., 1971, Nuo.Cim. 2B, 119.

Hammond R.T., Protheroe R.J., Orford K.J., Shearer J.A.L., Turver K.E., Waddoup W.D. and Wellby D.W., 1977, 15th ICCR, 8, 287.

Hammond R.T., Orford K.J., Protheroe R.J., Shearer J.A.L., Turver K.E., Waddoup W.D. and Wellby D.W., 1978, Nuo.Cim., 1C, 315.

Hara T., Hatano Y., Hayashida N., Kamata K., Kifune T., Mizumoto Y., Nagano M., Tan Y.J., Kawaguchi S., Daigo M. and Hasabe N., 1981, 17th ICCR, 11, 250.

Heiles C., 1979, Ap.J., 229, 533.

Hillas A.M., 1975, Physics Reports, 20C, 59.
1979, 16th ICCR, 8, 7.
1981, 17th ICCR, 13, 69.
1982a, J. Phys.G., 8, 1475.
1982b, "Composition and Origin of Cosmic Rays", (M.M. Shapiro ed.) D. Reidel Publishing Company, Dordrecht,Holland.

Inoue N., Sugawa N., Tamura T., Kakimoto F., Inaba T., Matsumoto Y., Suga K. and Nishi K., 1981, 17th ICCR, 11, 270.

Inoue N., Sugawa S., Tamura T., Enoki T., Miyazaki Y., Kakimoto F., Suga K. and Nishi K., 1983, 18th ICCR, Late Papers EA4-8.

Ivanenko I.P., and Makarov V.V., 1977, 15th ICCR, 8, 303.

Jelley J.V. and Galbraith W., 1955, J.A.T.P., 6, 304.

Jelley J.V., 1958, Nuo.Cim., 8, Suppl.578.
1967, Prog.Elem.Part.Cos.Ray Phys., 9, 139.

Jones W.V., 1979, Proc.1978 Dumand Summer Workshop, 1, 313, (A. Roberts ed.) Fermilab, Batavia, Illinois.

Juliusson E., 1975, 14th ICCR, 8, 2689.

Kafatos M., Bruhweiler F. and Sofia S., 1981, 17th ICCR, 2, 222.

Kakimoto F., Kaneko T., Mizumoto Y., Suga K., Inoue N., nishi K., Yamada Y., Tajima N., Gotoh E., Nakatani H., Yoshii H., Anda R., Aquirre C., MacKeown P.K., Murakama K., Hara T., Toyoda Y. and Maeda T., 1983, J.Phys.G., 9, 339.

Kalmykov N.N., Khristiansen G.B., Nechin Yu.A., Prosin V.V., Grigoriev V.M. and Efimov N.N., 1977, 15th ICCR, 8, 244.

Kalmykov N.N., Nechin Yu.A., Prosin V.V., Tomin Yu.A., Khristiansen G.B., Berezhko I.A., Grigoriev V.M. and Efimov N.N., 1979, 16th ICCR, 9, 73.

Kalmykov N.N., Prosin V.V., Silaev A.A., Khristiansen G.B., Alimov T.A., Aliev N.A., Kakhkharov M.K., Makhmudov B.M., Rakhimova N.R., Tashpulatov R.T. and Khakimov N.Kh., 1983, 18th ICCR, Late Papers EA4-2.

Kamata K. and Nishimura J., 1958, Prog.Theor.Phys., Suppl. 6, 93.

Khristiansen G.B., Vedeneev O.V., Kulukov G.V., Nazarov V.I. and Solovjeva V.I., 1971, 12th ICCR, 6, 2097.

Kiraly P., Kota J., Osborne J.L., Stapley N.R. and Wolfendale A.W., 1979, Rivista Nuo.Cim., 2, No.7.

Kuhlmann J.D. and Clay R.W., 1981, J.Phys.G., 7, L183.

Landau L.D., 1953, Izv.Akad.Nauk S.S.S.R., 17, 51. (Translated in "Collected Papers of L.D. Landau", 1965, D.Ter Haar ed., Gordon and Breach, New York.)

Lattes C.M.G., Mantovani M.S.M., Santos C., Shibuya E.H., Turtelli A., Amato N.M., Fujimoto Y., Hasegawa S., Shibata T. and Yokoi K., 1973, 13th ICCR, 4, 2671.

Liebing D.F., 1983, Ph.D. Thesis, University of Adelaide.

Linsley J., 1977, 15th ICCR, 12, 89.
1979, 16th ICCR, 9, 274.

Linsley J. and Watson A.A., 1981, Phys.Rev.Lett., 46, 459.

Linsley J., 1983, University of New Mexico preprint.

Longair M.S., 1981, "High Energy Astrophysics", Cambridge University Press.

McComb T.J.L. and Turver K.E., 1981a, 17th ICCR, 6, 234.
1981b, 17th ICCR, 6, 130.

McCubbin N.A., 1981, Rep.Prog.Phys., 44, 1027.

McCusker C.B.A., Peak L.S. and Rathgeber M.H., 1969, Phys.Rev., 177, 1902.

Mewaldt R.A., 1981, 17th ICCR, 13, 49.

Mewaldt R.A., Spalding J.D., Stone E.C. and Vogt R.E., 1981, 17th ICCR, 2, 68.

Miesowicz M., 1971, Prog.Elem.Part.Cos.Ray Phys., 10, 101.

Nikolsky S.I., Nikolskaja N.M., Stamenov I.N. and Ushez S.Z., 1981, 17th ICCR, 2, 129.

Orford K.J. and Turver K.E., 1976, Nature, 264, 727.
1980, Phys.Rev.Lett., 44, 959.

Ostriker J.P. and Gunn J.E., 1969, Ap.J., 157, 1395.

Patterson J.R. and Hillas A.M., 1983, J.Phys.G., 9, 323.

Pomeranchuk I.Ya., 1951, Dokl.Akad.Nauk S.S.S.R., 78, 889.

Protheroe R.J. and Turver K.E., 1977, 15th ICCR, 8, 275.
1979, Nuo.Cim., 51A, 277.

Rieke G.H., 1969, Smithsonian Ap.Obs.Spec.Rep., 301.

Roberg J. and Nordheim L.W., 1949, Phys.Rev., 75, 444.

Simon M., Spiegelhauer H., Schmidt W.K.H., Siohan F., Ormes J.R., Balasubrahmanyan V.K. and Arens J.F., 1980, Ap.J., 239, 712.

Sitte K., 1962, Nuo.Cim., 25, 86.
1970, Acta Physica, 29, Suppl.3, 389.

Sood R., 1983, Nature, 301, 44.

Stephens S.A., 1981, 17th ICCR, 13, 89.

Streitmatter R.E., Balasubrahmanyan V.K., Ormes J.F. and Protheroe R.J., 1983, 18th ICCR, 2, 183.

Thornton G.J. and Clay R.W., 1978a, J.Phys.G., 4, L193.
1978b, J.Phys.G., 4, L251.
1979a, J.Phys.G., 5, L137.
1979b, Phys.Rev.Lett., 43, 1622 (and Erratum 45, 1463).

Thornton G.J., Kuhlmann J.D., Liebing D.F., Clay R.W., Gregory A.G., Patterson J.R. and Prescott J.R., 1979, 16th ICCR, 9, 103.

Thornton G. and Clay R., 1981, Phys.Rev.D., 23, 2090.

Tornabene H., 1979, 16th ICCR, 9, 99.

Walker R. and Watson A.A., 1981, J.Phys.G., 7, 1297.
1982, J.Phys.G., 8, 1131.

Watson A.A., 1981, Proc.16th Recontre de Moriond Astrophysics Meeting, "Cosmology and Particles", J. Audouze et al eds.

Webber W.R., 1982, Ap.J., 252, 386.

Wiedenbeck M.E. and Greiner D.E., 1981, 17th ICCR, 2, 76.

Woidneck C.P. and Bohm E., 1975, J.Phys.A., 8, 997.

Yakovlev V.I., Nikolsky S.I., Pavluchenko V.P., Golubnichy P.I., Efimenko L.A. and Savchenko R.T., 1979, 16th ICCR, 6, 59.

Yodh G.B., Yash Pal and Trefil J.S., 1972, Phys.Rev.Lett., 28, 1005.

Zatsepin V.I. and Chudakov A.E., 1962, J.E.T.P., 15, 1126.

Development of Atmospheric Cosmic-Ray Showers

Greg Thornton and Roger Clay
Physics Department, University of Adelaide, Adelaide, South Australia 5000, Australia
(Received 19 June 1979)

The depths of shower maximum of cosmic-ray showers have been determined in the sea-level size range $10^5 < N_e < 10^7$ with use of atmospheric Cherenkov techniques. The mean depth has been found to increase rapidly in the middle of this range, suggesting a change in the mean primary composition from heavy to light nuclei.

Studies of the longitudinal development of cosmic-ray extensive air showers can give information on the energy spectrum and composition of the primary particles and also enable us to investigate some of the basic parameters of particle interactions at energies not yet available at accelerators. Unfortunately, in interpreting the outcome of any experiment there is often uncertainty in separating out the effects of all the poorly known parameters. However, these difficulties are less critical near the shower maximum, and the most basic and useful shower measurements are then those which aim to determine and interpret the electron number at shower maximum and the atmospheric depth at which it occurs. We therefore wish to discuss the way in which interesting astrophysical and particle properties influence the depth of electron maximum observed in our experiments.

Early stages of air-shower development depend critically on the initial primary-particle interaction mean free path, the interaction inelasticity, and secondary-particle multiplicity. Also, the inelasticity and multiplicity of the secondary-pion (etc.) interactions and the development of the electromagnetic cascades[1] are important. Exceptionally early shower development can be caused by a short initial mean free path, a high inelasticity, or a high multiplicity. It can also be associated with a high-atomic-number primary particle which is expected to have a short mean free path and a relatively high initial multiplicity.[2] These early stages are difficult to observe and their interaction parameters are often studied by interpreting observations of the depth in the atmosphere of shower maximum as a function of shower size. Ideally, this is measured by the elongation rate (rate change in depth of shower maximum for a factor-of-e change in primary-particle energy) and the absolute depth of shower maximum for one given primary energy. Linsley[3] has shown that, with general arguments and few assumptions about particle physics, for a constant primary-particle composition the elongation rate (X_e) is bounded from above by the characteristic length of cascade theory, X_c

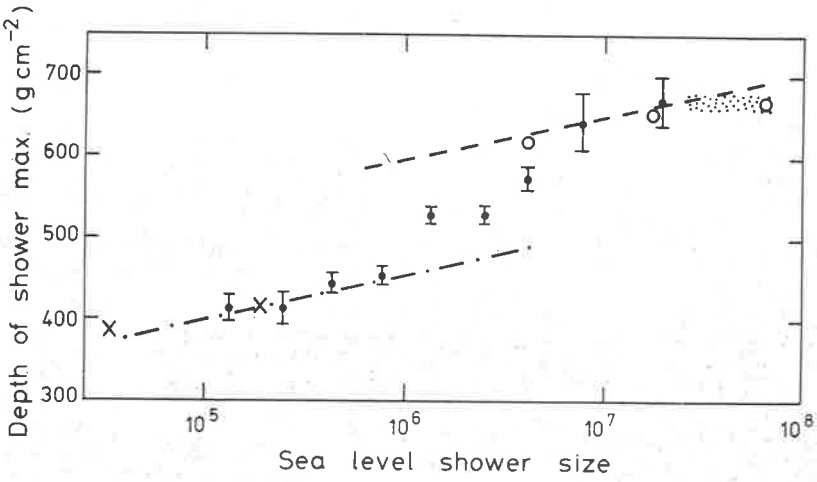

FIG. 1. The measured relationship between the depth of air-shower maximum and sea-level shower size. The filled circles are our data. Open circles are Cherenkov observations of Ref. 8. The stippled band is a Cherenkov result from Ref. 12. The crosses are direct airplane observations of Ref. 13. The lines correspond to simple model relationships for proton primaries (dashed line) and iron primaries (dot-dashed line) as described in the text.

38 g cm^{-2} in air), and is most probably ~ (1 B)X_c, where B is the exponent of the pion mul-)licity formula [multiplicity $\propto$ (energy)^B, with $\lesssim 0.5$; scaling models predict multiplicity $\ln E$, with a low effective value for B].

We have demonstrated[4,5] that the full width at lf maximum (FWHM) of the atmospheric Cher-kov-light pulse from extensive air showers is rongly dependent on the sea-level size (N_e) for ~ 10^6 showers. We have also shown[6,7] that cal-lations relating FWHM to the height of shower aximum indicate a rapid increase in depth of ower maximum [X_m (g cm^{-2})] with N_e's over r range of observation ($10^5 \lesssim N_e \lesssim 10^7$). The rresponding elongation rate is ~ 60 g cm^{-2}. Be-use this is significantly greater than the maxi-um expected from any conventional shower mod- we are led to examine the possibility of a ange in chemical composition over our observed ze range.

Let us consider in a simple way the shower de-lopments for different primary nuclei using e cosmologically significant nuclei of iron and otons as two species to be compared. We wish examine their variation of depths of shower aximum with observed sea-level size. We as-me an increase in X_m of 75 g cm^{-2} (X_e) per cade of primary energy for both species (see, g., Kalmykov *et al.*)[8]. The mean free path of 10^{16}-eV primary iron nucleus in air[9] is taken be 14 g cm^{-2} and that of a 10^{16}-eV proton[8] is ten to be 55 g cm^{-2}. The shower attenuation ngth (λ) is assumed to be 200 g cm^{-2} (see, e.g., hton *et al.*[10]). With the understanding that the del is crude, we use the common approxima-n that the iron-induced shower develops at 56 lependent showers after the first interaction. is also assumed that, to a first approximation, ower size at maximum is proportional to the imary energy. For a 10^{16}-eV iron nucleus,

$$X_m = X_0 + 14 + 75 \log_{10}(10^6/56)$$
$$= X_0 + 333 \text{ g cm}^{-2};$$

a 10^{16}-eV proton,

$$X_m = X_0 + 55 + 75 \log_{10}(10^6)$$
$$= X_0 + 505 \text{ g cm}^{-2}.$$

r the purposes of this calculation, X_0 is an bitrary constant and will depend critically on eraction multiplicities, etc. The assumption a common X_0 is similar to assuming independ-nucleon interactions after the first nucleus eraction.

The proton shower has its maximum ~ 170 g cm^{-2} closer to sea level than the iron shower, and hence will have a sea-level size greater by

$$\frac{N_e(10^{16}\ p)}{N_e(10^{16}\ \text{Fe})} = \exp(170/200) \simeq 2.3.$$

Thus we know the relationship between the sea-level sizes and also between the depths of maximum for the two showers. It can be shown that the change of X_m with a factor of e in N_e for a particular primary species is

$$X_e' = \left(\frac{1}{X_e} + \frac{1}{\lambda}\right)^{-1}.$$

As with Linsley,[3] this should be $\lesssim 32$ g cm^{-2}/ change in N_e by a factor of e. We will now compare these changes in X_m with N_e to those obtained when X_m is derived from the Cherenkov FWHM.

The data were recorded during 1978 and 1979 at the sea-level Buckland Park air-shower array[11] with use of a Mullard XP2040 photomultiplier and a Tektronix 7912 transient recorder in the non-store mode. The system FWHM of 5.3 ns was removed from the data under the assumption that the system FWHM and the signal FWHM add in quadrature.[7] A total of 317 events in the core distance range $150 < R < 350$ m, and with N_e from ~ 10^5 to ~ 10^7, were used. The FWHM at 300 m from the core [τ_{300}(ns)] was calculated for each shower with the assumption that[6] FWHM ~ $R^{1.4}$, and the distance of shower maximum from the observer (H_m) was derived with use of[8]

$$H_m = 17.05 - 19.17 \log_{10}(\tau_{300}) \text{ km}.$$

The depth of shower maximum was calculated from H_m and the shower zenith angle for an exponential atmosphere of scale height 7.1 km and a vertical depth of 1000 g cm^{-2}. The results are shown in Fig. 1 along with three points from Cherenkov observations of Kalmykov *et al.*,[8] a stippled band corresponding to observations of Hammond *et al.*,[12] and direct airplane observations of Antonov and Ivanenko.[13] Near $N_e = 10^6$, we find $X_e' \sim 60$ g cm^{-2}, which is much greater than the 32 g cm^{-2}, derived above, implying[3] that more is probably needed than merely a change in the particle-interaction mechanism.

The two lines in Fig. 1 are from the above calculations with use of $X_0 = 100$ g cm^{-2} under the assumption and that for a 10^{16}-eV primary proton shower $N_e = 1.5 \times 10^6$. These are in reasonable agreement with calculations presented by Dixon and Turver.[14] It can be seen that the experimen-

tal data match the iron line at $N_e \sim 10^5$, but at $N_e \sim 10^7$ they fit the proton line much better. Although X_m is changing rapidly with N_e near $N_e \sim 10^6$, the data of Kalmykov *et al.*[8] indicate that this trend does not continue past a few times 10^6. For small shower sizes there is some suggestion that the rate again decreases and the direct airplane observations of Antonov and Ivanenko[13] tend to confirm this opinion. We therefore believe that the experimental results are consistent with a changing primary composition with increasing energy from "iron" to "protons" for showers with sea-level sizes $\sim 10^6$ particles.

Experiments by other workers[15] are in the main consistent with early development at $\sim 10^{15}$ eV primary energy. However, interpretations of the observations in terms of composition are not consistent. The observations usually cited as the strongest evidence of a nonheavy nuclear composition at the lower energies are those concerning fluctuations in the muon- to electron-shower size ratio at sea level.[16] These fluctuations should mirror large fluctuations in the depth of shower maximum such as those associated with large-interaction-mean-free-path proton primaries. However, these experimental observations are mainly for showers with sizes above $N_e \sim 10^6$ and the observations may be consistent with fluctuations due to a composition change in this sea-level size range. Vernov *et al.*[15] have demonstrated that the observed muon- to electron-shower size ratio at $N_e \sim 10^5$ is compatible with iron primaries in that size range even with the slowly developing showers derived with use of the scaling model of nuclear interactions but they also claim that complete agreement with experiment is not possible at any energy with a scaling model since high interaction multiplicities are needed if observations of high-energy hadrons are to be explained. Ouldridge and Hillas[1] have disputed the latter suggestion and shown that a development of a scaling model for shower development and a mainly proton composition with energy-dependent hadron cross sections can explain most observations above $\sim 10^{16}$ eV. The remaining problem has been that the observations of Antonov and Ivanenko[13] have not been fitted into an accepted scheme of shower development.

Our data, together with those of Antonov and Ivanenko,[13] strongly suggest that development is early for showers with sea-level sizes of $\sim 10^5$ and that the development becomes "normal" for showers above $\sim 5 \times 10^6$ thus suggesting that a corresponding composition change occurs in this size region from predominantly heavy (iron) primaries to mainly proton primaries. This change occurs at the same sea-level size as the well-known break in the sea-level shower-size spectrum[17] which has speculatively been associated by Karakula, Osborne, and Wdowczyk[18] with an end to a primary component associated with pulsar acceleration.

This work was supported by the Australian Research Grants Committee.

[1]M. Ouldridge and A. M. Hillas, J. Phys. G 4, L35 (1978).

[2]P. Freier and C. J. Waddington, in *Proceedings of the the Thirteenth International Conference on Cosmic Rays, Denver, Colorado, 1973* (University of Denver, Denver, Colo., 1973), Vol. 4, p. 2449.

[3]J. Linsley, in *Proceedings of the Fifteenth International Conference on Cosmic Rays, Plovdiv, Bulgaria, 1977* (Bulgarian Academy of Sciences, Plovdiv, Bulgaria, 1977).

[4]G. J. Thornton and R. W. Clay, J. Phys. G 3, L193 (1978).

[5]G. J. Thornton and R. W. Clay, J. Phys. G 4, L251 (1978).

[6]G. J. Thornton and R. W. Clay, to be published.

[7]G. J. Thornton, J. D. Kuhlmann, D. F. Liebing, R. W. Clay, A. G. Gregory, J. R. Patterson, and J. R. Prescott, in Proceedings of the Sixteenth International Conference on Cosmic Rays, Kyoto, Japan, 1979 (University of Tokyo, Tokyo, Japan, to be published).

[8]N. N. Kalmykov, Yu. A. Nechin, V. V. Prosin, Yu A. Fomin, G. B. Khristiansen, I. A. Bereshko, V. M. Grigoryev, and N. N. Efimov, in Proceedings of the European Conference on Cosmic Rays, Kiel, 1978 (unpublished).

[9]R. R. Daniel and N. Durgaprasad, Nuovo Cimento Suppl. 23, 82 (1962).

[10]F. Ashton, A. Parvaresh, and A. J. Saleh, in *Proceedings of the Fourteenth International Conference on Cosmic Rays, Munich, West Germany, 1975* (Max-Planck-Institut für Extraterrestrische Physik, Garching, West Germany, 1975), Vol. 8, p. 2831.

[11]P. C. Crouch, J. D. Kuhlmann, R. W. Clay, A. G. Gregory, J. R. Patterson, and G. J. Thornton, in *Proceedings of the Fifteenth International Conference on Cosmic Rays, Plovdiv, Bulgaria, 1977* (Bulgarian Academy of Sciences, Plovdiv, Bulgaria, 1977).

[12]R. T. Hammond, R. J. Protheroe, K. J. Orford, J. A. L. Shearer, K. E. Turver, W. D. Waddup, and D. W. Wellby, in *Proceedings of the Fifteenth International Conference on Cosmic Rays, Plovdiv, Bulgaria, 1977* (Bulgarian Academy of Sciences, Plovdiv, Bulgaria, 1977), Vol. 8, p. 287.

[13]R. A. Antonov and I. P. Ivanenko, in *Proceedings of the Fourteenth International Conference on Cosmic Rays, Munich, West Germany, 1975* (Max-Planck-Institut für Extraterrestrische Physik, Garching, West Germany,

1975), Vol. 8, p. 2708.
[14]H. D. Dixon and K. E. Turver, Proc. Roy. Soc. London, Ser. A 339, 171 (1974).
[15]S. N. Vernov, G. B. Khristiansen, A. T. Abrosimov, N. N. Kalmykov, G. V. Kulikov, V. I. Solovieva, Yu. A. Fomin, and B. A. Khrenov, J. Phys. G 3, 1601 (1977).
[16]S. N. Vernov, G. B. Khristiansen, A. T. Abrosimov, V. B. Atrashkevitch, I. F. Belijaeva, G. V. Kulikov, K. V. Mandritskaya, V. I. Solovjeva, and B. A. Khrenov, Can. J. Phys. 46, S197 (1968).
[17]A. M. Hillas, Acta Phys. Acad. Sci. Hung. 29, Suppl. 3, 355 (1970).
[18]S. Karakula, J. L. Osborne, and J. Wdowczyk, J. Phys. A 7, 437 (1974).

ERRATA

DEVELOPMENT OF ATMOSPHERIC COSMIC-RAY SHOWERS. Greg Thornton and Roger Clay [Phys. Rev. Lett. 43, 1622 (1979)].

The data in Fig. 1 were analyzed using an atmospheric scale height which was too low. The corrected figure (analyzed with a scale height of 8.0 km) is given below.

This scale-height revision was made in response to criticism by K. J. Orford and K. E. Turver [Phys. Rev. Lett. 44, 959 (1980)]. A full response will be published elsewhere.

The new Refs. 19–24 given below should be appended to the original list of references.

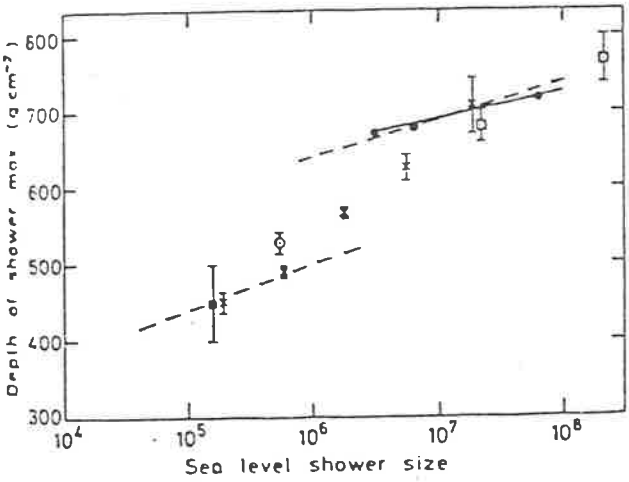

FIG. 1. The measured relationship between the depth of air-shower maximum and sea-level shower size. Where results have been given in terms of primary energy, the relationship

$$\text{sea-level size} = (\text{primary energy}) \times 10^{-16}$$

has been used. This is derived from our measured shower-size spectra and primary-energy (Ref. 19) spectra. Crosses, our present Cherenkov observations; solid circles, data from the Cherenkov observations of Kalmykov *et al.* (Ref. 20); open squares, data from the Cherenkov observations of Hammond *et al.* (Ref. 21). The solid square, airplane particle datum of Antonov *et al.* (Ref. 22) interpreted by Watson and Linsley (Ref. 23). Open circle, a mean value derived from our early Cherenkov data (Ref. 24).

[19]R. J. Protheroe, Ph.D. thesis, University of Durham 1977 (unpublished).

[20]N. N. Kalmykov, Yu. A. Nechin, V. V. Prosin, Yu. A. Fomin, G. B. Khristiansen, I. A. Berezhko, V. M. Grigoryev, and N. N. Efimov, in Proceedings of the Sixteenth International Conference on Cosmic Rays, Kyoto, Japan, 1979 (University of Tokyo, Tokyo, Japan, to be published), Vol. 9, p. 73.

[21]R. T. Hammond, K. J. Orford, R. J. Protheroe, J. A. L. Shearer, K. E. Turver, W. D. Waddoup, and D. W. Wellby, Nuovo Cimento 1C, 315 (1978).

[22]R. A. Antonov, I. P. Ivanenko, and V. A. Kuzmin, in Proceedings of the Sixteenth International Conference on Cosmic Rays, Kyoto, Japan, 1979 (University of Tokyo, Tokyo, Japan, to be published), Vol. 9, p. 263.

[23]A. A. Watson and J. Linsley, unpublished.

[24]G. J. Thornton and R. W. Clay, J. Phys. G 4, L137 (1979).

PHYSICAL REVIEW D VOLUME 23, NUMBER 9 1 MAY 1981

Development of atmospheric cosmic-ray showers. II

Greg Thornton and Roger Clay
Physics Department, University of Adelaide, Adelaide, South Australia 5000, Australia
(Received 18 August 1980)

In a recent paper Orford and Turver criticized one of our previous papers which had concluded that a change in cosmic-ray primary mass composition was required in the energy range 10^{15} to 10^{17} eV. It is suggested here, in reply, that the inconsistencies and shortcomings claimed by Orford and Turver are largely not substantiated in the light of available information and that, in the absence of new ideas, the original conclusions are valid.

In a recent paper[1] we offered evidence for a change in the primary cosmic-ray chemical composition between 10^{15} and 10^{17} eV per nucleus. The basis for our claim was the variation with sea-level shower size of the depths of cosmic-ray extensive-air-shower (EAS) maxima inferred from the measured time full width at half maximum (FWHM) of the atmospheric Čerenkov radiation signal in individual showers measured with a single detector. The depths of maxima of EAS's are expected to depend on the nuclear physics of the shower cascade process and also on the composition of the initiating particle. It is thought that progressive changes in the nuclear physics, combined with changes in total shower energy, cause the depth of maximum to increase progressively with increasing initiating particle energy for a fixed composition. However, if the depth of maximum changes rapidly with increasing shower energy (often measured by the number of particles at sea level, the shower size), the preferred explanation is probably a change in primary composition. This change in depth with energy (the elongation rate) appears consistent with a fixed composition above sea-level shower sizes of ~10^7 particles (about 10^{17} eV primary energy) but we offered evidence for a very rapid change in the two size decades below this. Orford and Turver[2] of the Durham group have recently suggested that this conclusion is invalidated by inconsistencies and errors in that work.

The criticisms of Orford and Turver are in four broad categories: They regard our assumptions on the form of the dependence of the Čerenkov FWHM with distance from the shower core as incorrect. They believe it is hard to do our experiment. They feel we have used an inadequate model of the atmosphere. They believe the data we presented are in conflict with a datum previously published by ourselves. We feel their points are interesting and believe there is substance in their criticism of our atmospheric model, a criticism that we have previously made ourselves.

The problem of the dependence of the FWHM on shower-core distance (r) is of central importance in the use of Čerenkov FWHM techniques in air-shower physics. The reason for this is that, in the data-analysis process, experimental data usually have to be standardized to a convenient reference core distance. Theory can be developed with most confidence at the larger core distances and a distance of 300 m from the core is now normally[3] chosen as a useful compromise for standardizing data and also comparison with theory. The problem for the experimentalist is then to determine a proper method of standardizing the data to a core distance of 300 m. This problem is particularly important to us since we have chosen to study the interesting energy region around 10^{16} eV primary particle energy where the air showers are small and consequently we have little data at such large core distances. Extrapolation is therefore necessary. It is usual to assume a functional form for the dependence of FWHM on core distance and two forms have been used by ourselves and others. These are either

$$\mathrm{FWHM} = cr^n \tag{1}$$

or

$$\mathrm{FWHM} = a + br^2 . \tag{2}$$

Either of these expressions can be an adequate

epresentation of the same theoretical or experiental data, depending on the range of the variables being considered and the uncertainties in em.

The former functional form has been used mainly ourselves and the Moscow[3] group and the latter ainly by the Durham[4] group. Here the values of b, c, and n are to be determined. The usual ssumption is that a, b, and n are functions of ower development through dependence on H_m, e shower height of maximum (usually expressed in km above the observer). The appropriate value of n is clearly important and is the subject of much of the criticism made by Orford and Turver. The Soviet group[5] find a value of 1.6 [later revised to 1.7 (Ref. 6)] as a useful experimentally based value for them at larger core distances and shower energies. We[7] find that a value of 1.4 ± 0.2. fits our data as a best estimator for the FWHM at 300 m (from a multiple regression analysis). It is difficult to compare our data with Durham experiments since both we and the Soviet group use an estimate of the value of the measured FWHM after removal of the instrumental impulse response (by assuming that instrumental response and light pulse shape had added in quadrature[3,7,8]) and the Durham group display their data without any such subtraction. We have, however, taken some recent Durham data[9] (measured at their Dugway field station) and subtracted (in quadrature) their published impulse response to produce the data (with error bars) in Fig. 1. A power-law form appears reasonable with a value of n of ~0.9 being appropriate. This is of interest in demonstrating the reasonableness of a power-law form but the value of n cannot be directly compared with the other data since the Dugway array is at a different altitude from the others. Figure 1 also includes data presented by Hammond *et al.*[4] from a sea-level experiment with a system FWHM of 18 ns.[11] Again we have removed the system FWHM in the standard way. A value of n of ~1.1 seems appropriate to these data. We have demonstrated that the quadratic subtraction of the system impulse response works reasonably for our data[8] and the Soviet group uses a similar technique. It is clearly possible that this may not work well for the Durham data. Nonetheless, if the data is handled *consistently* and an experimentally derived relation used for n then the experimental best estimator of the FWHM at 300 m should be appropriate and at this core distance the effect of most system FWHM's is small.

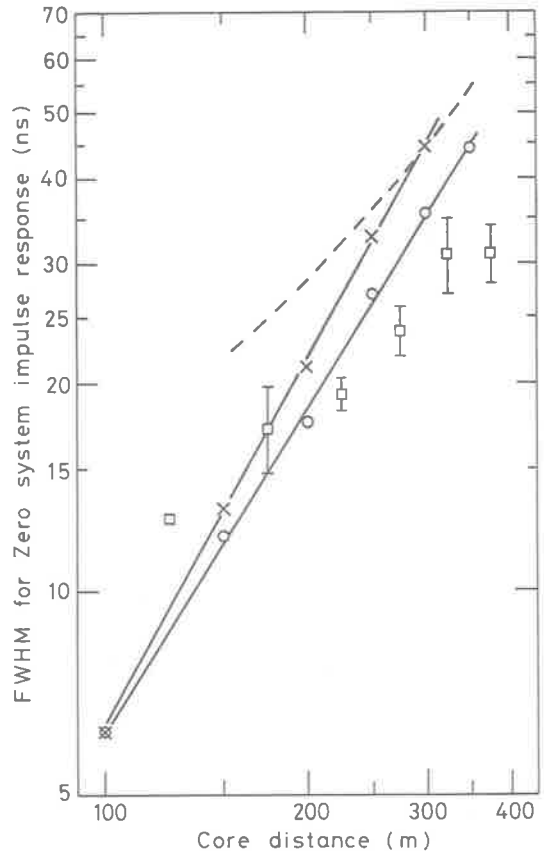

FIG. 1. Some representative data showing the dependence (theoretical and experimental) of the atmospheric erenkov pulse FWHM for a system with an ideal response on shower-core distance over the core-distance nge relevant to the Adelaide observations. Crosses: lculations by Gaisser *et al.* (Ref. 10) for a 5×10^{18}-eV on primary observed at sea level. Open circles: Calations by Gaisser *et al.* (Ref. 10) for a 10^{17}-eV iron imary observed at sea level. Open squares: Observaons by Andam *et al.* (Ref. 9) made at a high altitude te. The system FWHM (6.7 ns) has been removed on e assumption that it had added in quadrature with the gnal. Dashed line: Experimental relationship obtained r large sea-level showers by Hammond *et al.* (Ref. 4). ıe system FWHM (Ref. 11) (18 ns) has been removed ı the assumption that it had added in quadrature with e signal. Solid lines are added to open circles and osses for clarity.

Computer simulations of shower development can help and Fig. 1 also includes two relations calculated at Durham[10,12] for different shower developments observed at sea level. Values of n of ~1.8 and ~1.6 are found with the larger value corresponding to the lower value of H_m. Again, the power-law form seems entirely appropriate. Orford and Turver claim that Durham calculations[11] show a value of $n \sim 2.0$. We were unable to confirm this from their reference. The Soviet group[3] has also made calculations on cascades and Orford and Turver quote a value of $n = 2.0$ from this work. We have reservations about this result since there appears to us to be an inconsistency in this paper. This is currently the subject of correspondence

between ourselves and the Soviet workers.

It appears therefore that experimental results in our range of core distances give values of n in the range of ~1.0 to 1.7 and theory fits $n \lesssim 1.8$. A value of n below 1.6 (the smaller of the Durham[10,12] theoretical values) seems appropriate to showers which develop somewhat higher than those discussed in the calculations. It is our opinion therefore that the value of 1.4 ± 0.2 found and used by us is probably about right. We have, however, previously conceded that a problem exists due to uncertainties in n and for purposes of comparison have also used formula (2) for analyzing our data.[8] We showed (Fig. 1, Ref. 8) that our data can be analyzed using either formula (1) *or* (2) and essentially the *same* result is produced. It appears to us therefore that while it is right to examine the core-distance dependence critically, the dependences we have employed are both reasonable and produce consistent results. We note that if we reanalyze our data with $n = 1.8$ (we regard this as an extreme case) the effect is to increase *all* our deduced depths of maxima by ~45 g cm^{-2}.

Orford and Turver next make a few comments on the technical difficulty of measuring useful FWHM's at core distances below 300 m. It is well known[8,11,13] that at ~70–100 m from the shower core FWHM's are practically invariant with depth of maximum and the ease of determining shower development (in terms of system time resolution) improves with core distance away from this region. On the other hand, signals have greater amplitudes at smaller core distances and there is much physical interest in the showers of smaller size which are difficult to detect at core distances ≥ 300 m. It is with this in mind that we set up a system with good time response. Our 5.3 ns system FWHM was the best of any in the field until recently when we ourselves have set up an improved second system. The Durham workers currently have an impulse response FWHM of 6.7 ns but digitize at 10 ns intervals and have in the past used an impulse FWHM of 18 ns. We would certainly regard our data as being at least as well measured in terms of physically useful parameters as theirs; compare for instance, Ref. 14, p. 45 with Ref. 8, p. 107. We, of course, do not use data from showers with core distances close to 100 m. Contrary to the assertion of Orford and Turver, with a system FWHM of 5.3 ns, it is not too difficult to extract a useful *averaged* height of maximum data on variations of less than 100 g cm^{-2} with a sensitivity of ~3.5 ns per 100 g cm^{-2}. In fact, they have, for an extended period, used a system FWHM of 18 ns with a sensitivity at their core distance of 10 ns per 100 g cm^{-2}. In a sense, the consistency of the variation of the data in Fig. 1 of Ref. 1 would lead one to conclude that in our core-distance range, measurements of useful sensitivity certainly can be made. Any problems in the data definitely are not *statistical* uncertainties. We note that our errors as shown are reasonable for the spread in the data and are quite small enough to show trends in the data. An examination of the figure in our paper[1] makes this obvious.

Since we wish to determine the development of EAS in the atmosphere in terms of atmospheric depth in g cm^{-2} from the top of the atmosphere and since the Čerenkov FWHM gives us the height of that development above the observer, it is necessary to have a model for the atmosphere with which one can relate absorber depth to altitude. This problem is not trivial and it seems to us that it should be brought explicitly to the attention of EAS workers although we know it has been discussed privately many times. It is customary to approximate the atmosphere to one having exponential properties with a characteristic scale height. This is the crudest of models and Orford and Turver were correct to criticize us for using an atmospheric pressure scale height of 7.1 km. We have mentioned this problem in an earlier paper[15] in which we ourselves pointed out that at

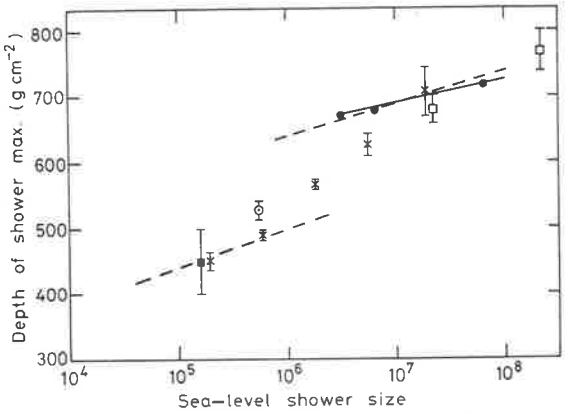

FIG. 2. The measured relationship between the depth of air-shower maximum and sea-level shower size. Where results have been given in terms of primary energy, the relationship sea-level size = primary energy $\times 10^{-10}$ has been used. This is derived from our measured shower-size spectra and primary energy (Ref. 12) spectra. Crosses are our Čerenkov observations (Ref. 1). Filled circles and the solid line are data from the Soviet Čerenkov observations (Ref. 3). Open squares are data from the Durham Čerenkov observations (Ref. 4). The filled square is from airplane particle data of Antonov (Ref. 16) interpreted by Watson and Linsley. Open circle, a mean value derived from early Čerenkov data of Thornton and Clay (Ref. 7).

ur observing site, the appropriate scale height is .0 km. We therefore present here, in Fig. 2, a evised version of the figure in our previous aper[1] which displays our current FWHM data an-lyzed using the appropriate pressure scale height. Ve wish to make a more general comment here lso, however. The value of 8.0 km we use is de-ived from local measurements (S. Young, private ommunication). We have found this local infor-nation most beneficial. As far as we know, some ther EAS sites have not been so fortunate as to ave this information although it is of most prac-ical interest. The atmosphere is not isothermal, nd although for many practical purposes (such s ours) an exponential *form* is adequate and seful, the scale height is not unique. The pres-ure and density scale heights are *not* the same nd can be very discrepant. We make this point ince this problem is related to both Čerenkov heory and experiment. Some EAS parameters epend on local pressure (e.g., the relationship etween atmospheric depth in g cm^{-2} and height n the atmosphere) and others on local density e.g., Coulomb scattering, Čerenkov production hreshold). It appears that these differences are ot always taken into account in theory (see, e.g., tef. 12, p. 150) and we have always had difficulty n deciding the best procedure for interpreting our wn data. The Soviet[3] calculations, for instance, se a scale height of ~7 km (appropriate to their bservation site) and hence will use Čerenkov hresholds, scattering functions, etc., as functions f altitude which are slightly inappropriate to our eeds. All observers have to contend with this roblem to some extent (even particle EAS work-rs) since the scale heights are meteorological unctions and vary by relatively large amounts at ixed geographical locations.

The criticism of our paper concerning inconsis-ency with previous work seems to merit little omment. It has been suggested that a value of 86 ± 13 g cm^{-2} is not consistent with our data at mean size of 5.5×10^5. We would suggest that he concerned reader might plot this point on our ig. 1 in Ref. 1. Alternatively, the point is in-luded in Fig. 2 here with the depth appropriate o an 8-km scale height. The point with its errors s not statistically inconsistent with a reasonable ine which one might draw through the total of our ata and one would in any case expect a slightly igh value since the derivation of this mean in-ludes a group of larger showers with, as we how, rather larger depths of maxima than one night have expected. We should add that, despite he contrary assertion by Orford and Turver,[2] it s our understanding that a depth of maximum of 500 g cm^{-2} for showers from iron primaries is quite appropriate in our size range.[10] This is not a conventional composition. In our first paper we displayed an interpretation of data derived from measurement by Antonov *et al.* at airplane alti-tudes on the height of maxima of small EAS. Wat-son and Linsley[16] have used more recent work of Antonov[17] and his collaborators to derive a depth of maximum for small showers. This point is included in Fig. 2 and appears to us to add strength to our conclusions.

To summarize, the criticisms of our work by Orford and Turver were fourfold.

(1) They were critical of our choice of techniques for deriving depths of maxima, particularly in the way we determine the estimated FWHM at 300 m. We have demonstrated here that a power-law form for the dependence of FWHM on r fits a broad class of published data including data from all three major groups in the field. Also, the power-law index we find is not by any means extreme and is consistent with Soviet experiment, internally consistent in our own data, and fits Durham calculations. In any case, alternative analysis procedures produce essentially the same final results.

(2) They pointed out that estimates of depth of maximum based on measurements closer to the core than 300 m are less sensitive than those made further out. This is obvious since the FWHM increases faster than $r^{1.0}$ with increasing core distance and it is the reason why we use equipment which gives us a very short system FWHM.

(3) We did not choose the best atmospheric mo-del. This is true and we had already published material to this effect and revised our results.[15] We also note that as far as we know, other EAS workers have similar problems when their de-tailed procedures (theoretical and experimental) are examined.

(4) They thought there was an inconsistency with our previous work. The simple procedure of plot-ting the result they derived from our previous work on our figure should have demonstrated to them the considerable degree of agreement be-tween early data and later analysis.

We conclude that Orford and Turver[2] have aired some interesting points and as a result we have revised our previously published results which are now shown in Fig. 2. The essential conclu-sions remain, viz, there is broad agreement with other observations for sea-level shower sizes of ~10^7. Considering known errors in depths of maxima for experiments on showers of sea-level size ~10^5, there is still good agreement. The elongation rate for showers with sea-level sizes of ~10^6 is still too high to be explained simply by a progressive change of nuclear physics with en-

ergy and can most simply be explained by a composition change.

There is perhaps a further point to be made on the subject of atmospheric Čerenkov measurements of the smaller air showers. We agree that difficult problems are encountered due to the generally small signals to be detected and that to overcome some of these problems it is necessary to work at core distances which make extrapolation necessary for comparison with theory. We do believe, however, that with sufficient accumulation of data it has become possible to disentangle the variables in the data and produce physically useful results. At the very least, Orford and Turver have conceded that our mean height of maximum for showers of mean size below $\sim 10^6$ is high. Even taking this datum and those of Protheroe and Turver[11] for primary energies of $\sim 10^{17}$ and 10^{18} eV (we convert shower size to primary energy through the shower-size and primary energy spectra), there is a clear need for a very high elongation rate (>100 g cm^{-2}/decade in Ne). The paper they criticize says little *in principle* in addition to this except that details of the change in depth of maxima with energy are added.

This work was supported by the Australian Research Grants Committee. We are grateful for comments on this manuscript made by members of the Adelaide Cosmic Ray Group.

[1]G. Thornton and R. Clay, Phys. Rev. Lett. 43, 1622 (1979).
[2]K. J. Orford and K. E. Turver, Phys. Rev. Lett. 44, 959 (1980).
[3]N. N. Kalmykov, Yu. A. Nechin, V. V. Prosin, Yu. A. Fomin, G. B. Khristiansen, I. A. Berezhko, V. M. Grigor'ev, and N. N. Efimov, in *Sixteenth International Cosmic Ray Conference, Kyoto, 1979, Conference Papers* (Institute of Cosmic Ray Research, University of Tokyo, 1979), Vol. 9, p. 73.
[4]R. T. Hammond, K. J. Orford, R. J. Protheroe, J. A. L. Shearer, K. E. Turver, W. D. Waddoup, and D. W. Wellby, Nuovo Cimento 1C, 315 (1978).
[5]V. M. Grigor'ev, N. N. Efimov, N. N. Kalmykov, Yu. A. Nechin, V. V. Prosin, and G. B. Khristiansen, Yad. Fiz. 27, 418 (1978) [Sov. J. Nucl. Phys. 27, 225 (1978)].
[6]N. N. Kalmykov, G. B. Khristiansen, Yu. A. Nechin, V. V. Prosin, V. M. Grigor'ev, and N. N. Efimov, in *Proceedings of the Fifteenth International Conference on Cosmic Rays, Plovdiv, 1977*, edited by S. Betev (Bulgarian Academy of Sciences, Sofia, 1977), Vol. 8, p. 244.
[7]G. J. Thornton and R. W. Clay, J. Phys. G 4, L137 (1979).
[8]G. J. Thornton, J. D. Kuhlmann, D. F. Liebing, R. W. Clay, A. G. Gregory, J. R. Patterson, and J. R. Prescott, in *Sixteenth International Cosmic Ray Conference, Kyoto, 1979, Conference Papers* (Ref. 3), Vol. 9, p. 103.
[9]A. Andam, M. C. Chantler, M. A. B. Craig, K. J. Orford, J. A. L. Shearer, K. E. Turver, and G. M. Walley, in *Sixteenth International Cosmic Ray Conference, Kyoto, 1979, Conference Papers* (Ref. 3), Vol. 9, p. 48.
[10]T. K. Gaisser, R. J. Protheroe, K. E. Turver, and T. J. L. McComb, Rev. Mod. Phys. 50, 859 (1978).
[11]R. J. Protheroe and K. E. Turver, Nuovo Cimento 51A, 277 (1979).
[12]R. J. Protheroe, Ph.D. thesis, University of Durham, 1977 (unpublished).
[13]V. I. Galkin, I. P. Ivanenko, and V. V. Makarov, in *Sixteenth International Cosmic Ray Conference, Kyoto, 1979, Conference Papers* (Ref. 3), Vol. 9, p. 79.
[14]M. Chantler, K. J. Orford, J. A. L. Shearer, K. E. Turver, and G. M. Walley, in *Sixteenth International Cosmic Ray Conference, Kyoto, 1979, Conference Papers* (Ref. 3), Vol. 9, p. 42.
[15]R. W. Clay and G. J. Thornton, Aust. J. Phys. 33, 607 (1980).
[16]J. Linsley and A. A. Watson, Phys. Rev. Lett. 46, 459 (1981).
[17]R. A. Antonov, I. P. Ivanenko, and V. A. Kuzmin, in *Sixteenth International Cosmic Ray Conference, Kyoto, 1979, Conference Papers* (Ref. 3), Vol. 9, p. 263.